

TA7
106
CER-88/89-4

COPY 2

DOWNWIND AND LATERAL WAKE EFFECTS ON WIND TURBINE PERFORMANCE

Prepared by
David E. Neff
Robert N. Meroney

LIBRARIES
MAR 21 1989
COLORADO STATE UNIVERSITY

Final Report
(October 1987 - October 1988)

for
U.S Windpower, Inc.
6952 Preston Avenue
Livermore, California 94550

FLUID MECHANICS AND WIND ENGINEERING PROGRAM



CSU Contract No. 2-97210

CER88-89DEN-RNM-4

**DOWNWIND AND LATERAL WAKE
EFFECTS ON WIND TURBINE PERFORMANCE**

by

D. E. Neff

and

R. N. Meroney

Fluid Mechanics and Wind Engineering Program
Department of Civil Engineering
Colorado State University
Fort Collins, Colorado 80523

Prepared for
U.S Windpower, Inc.
6952 Preston Avenue
Livermore, California 94550

CSU Contract No. 2-97210

October 1988

EXECUTIVE SUMMARY

Title: Downwind and Lateral Wake Effects
on Wind Turbine Performance

Contractors: Civil Engineering Department
Colorado State University
Fort Collins, Colorado 80523

Principal

Investigators: D.E. Neff and R.N. Meroney

Report Period: October 1987 - October 1988

Objective: The objective of the fluid modeling measurement program was to determine how arrays of the US Model 56-100 wind-turbine rotors and towers interact with the flow. These multiple turbine arrays produce perturbed wind environments which consequently effect rotor power performance and rotor loading. The measurement program was to produce design and spacing information which can be used to improve wind-energy conversion performance. Measurements were also to be taken of the velocity deficits downwind of multiple turbine arrays.

Results: The test program was split into six different tasks. These were:

- 1) The potential for a passive model turbine design to simulate the wake of adjacent turbine structures was evaluated. This study involved the construction of a 1:50 scale model of the USW 56-100 wind turbine, geometrically scale rotor blades for the active turbine and a passive rotor disk. Wind tunnel tests showed that the geometrically scaled wind turbine rotor produced no power; thus, it could not be used to provide data for a passive design. A commercial Graupner model helicopter blade was found to produce finite power; hence, comparisons between active and passive turbine wake behavior were made.
- 2) The decision was made to model the turbine arrays with only active turbines. A new model blade design was sought which reproduced the performance and thrust characteristics of the USW 56-100 wind turbine. Power performance, thrust and wake measurements were obtained for various rotor designs. A modified TNO blade design was found to operate satisfactorily.
- 3) Five additional TNO style rotors were produced. Three 1:50 scale models of the 60 foot tower design and two models of the 140 foot tower design were prepared.

Rotors were placed on all five towers, and each turbine was attached to a generator load and a tachometer mounted on the tower base plate.

- 4) Velocity measurements were made at 28 locations upwind and to the side of a single model 60 foot tower-turbine. The turbine had very little influence on the flow field at upwind or lateral positions.
- 5) Velocity measurements were made at 96 locations in the wake of a five turbine array for six different turbine spacing combinations. For closely spaced turbines the velocity deficit in the wake is persistent.
- 6) Power performance measurements on a single turbine within a multiple turbine array were obtained for 49 different run conditions. These tests demonstrated that:
 - a) When a 140 foot tower with the turbine off is placed upwind of the 60 foot tower-turbine the power output decreases by 15 percent. For an active 140 foot tower-turbine this loss in power performance is less severe.
 - b) Placing the three active 60 foot turbines upwind of a 140 foot test turbine causes a power increase of 14 percent.
 - c) Two 60 foot tower-turbines adjacent to another 60 foot tower-turbine improved its power performance by 3 to 4 percent.
 - d) Under some approach flow conditions, when two 140 foot turbines are placed downwind of the 60 foot tower-turbine a power loss of 2 to 4 percent occur.
 - e) The results obtained for the 140 foot tower-turbines are very similar to those obtained with 130 foot tower-turbines.

TABLE OF CONTENTS

EXECUTIVE SUMMARY	i
LIST OF TABLES	v
LIST OF FIGURES	vi
1. INTRODUCTION	1
2. MODELING OF WIND TURBINES	2
2.1. <u>Wind Turbine Wakes</u>	2
2.1.1. <i>Dynamic Modeling</i>	2
2.1.2. <i>Static Modeling</i>	3
2.2. <u>Wind Turbine Rotor Performance</u>	4
2.2.1. <i>Power Coefficient</i>	4
2.2.2. <i>Thrust Coefficient</i>	5
3. DATA ACQUISITION AND ANALYSIS	7
3.1. <u>Wind Tunnel Facilities</u>	7
3.2. <u>Flow Visualization Techniques</u>	7
3.3. <u>Wind Velocity Measurements</u>	7
3.3.1. <i>Pitot-Static Probes</i>	8
3.3.2. <i>Hot-film Probes</i>	8
3.4. <u>Turbine Power Measurements</u>	9
3.4.1. <i>Dynamometer Measurements</i>	9
3.4.2. <i>Turbine Loading Technique</i>	10
3.5. <u>Turbine Thrust Measurements</u>	10
3.5.1. <i>Momentum Balance Technique</i>	10
3.5.2. <i>Direct Measurement Technique</i>	10
4. TEST PROGRAM AND DATA	12
4.1. <u>Passive and Dynamic Turbine Wakes (TASK 1)</u>	12
4.1.1. <i>USWP Sixty Foot Tower Model</i>	12
4.1.2. <i>USWP Scaled Rotor</i>	13
4.1.3. <i>Graupner Rotor Tests</i>	13
4.1.4. <i>Passive Design and Test Data</i>	14
4.2. <u>Dynamic Turbine Model Development (TASK 2)</u>	14
4.2.1. <i>Graupner Rotor Test Series</i>	14
4.2.2. <i>USWP Type Blade Design Test Series</i>	15
4.2.3. <i>TNO Type Blade Design Test Series</i>	15
4.3. <u>Multiple Turbine Construction (TASK 3)</u>	16
4.4. <u>Single Turbine Disturbed Flow Tests (TASK 4)</u>	17
4.5. <u>Multi-Turbine Far Wake Tests (TASK 5)</u>	17
4.6. <u>Multi-Turbine Power Performance Tests (TASK 6)</u>	18
4.6.1. <i>First Test Series</i>	18
4.6.2. <i>Second Test Series</i>	18
4.6.3. <i>Third Test Series</i>	18

5.	DISCUSSION OF RESULTS	20
5.1.	<u>Single Wind Turbine Wake Behavior</u>	20
5.2.	<u>Model Turbine Dynamic Performance</u>	21
5.3.	<u>Multiple Wind Turbine Wake Behavior</u>	22
5.4.	<u>Multiple Wind Turbine Power Performance Interaction</u>	23
5.4.1.	<i>First Test Series</i>	24
5.4.2.	<i>Second Test Series</i>	24
5.4.3.	<i>Third Test Series</i>	26
REFERENCES		27
TABLES		30
FIGURES		49

LIST OF TABLES

Table 1	TASK 1 Sixty Foot Tower Wake Data	31
Table 2	TASK 1 Rotor # 2 Loaded Wake Data	31
Table 3	TASK 1 Rotor # 2 Unloaded Wake Data	31
Table 4	TASK 1 Passive Device Wake Data	32
Table 5	TASK 2 Rotor # 6 Loaded Wake Data	32
Table 6	TASK 2 Graupner and USWP 10-20 Rotor Thrust Data	33
Table 7	TASK 2 TNO 10 and TNO 6 Rotor Thrust Data	33
Table 8	TASK 2 Rotors # 2, 6, 8, 10 Thrust Coefficient Data	33
Table 9	TASK 1 Rotor # 2 Power Test with Pulley Drive	34
Table 10	TASK 2 Rotor # 2 Power Test with Chain Drive	34
Table 11	TASK 2 Rotor # 6 Power Performance Data	35
Table 12	TASK 2 Rotor # 7 Power Performance Data	35
Table 13	TASK 2 Rotor # 8 Power Performance Data	36
Table 14	TASK 2 Rotor # 9 Power Performance Data	36
Table 15	TASK 2 Rotor # 10 Power Performance Data	36
Table 16	TASK 3 Rotor # 11 Power Performance Data	37
Table 17	TASK 3 Rotor # 12 Power Performance Data	37
Table 18	TASK 3 Rotor # 13 Power Performance Data	37
Table 19	TASK 3 Rotor # 14 Power Performance Data	38
Table 20	TASK 3 Rotor # 15 Power Performance Data	38
Table 21	TASK 3 Rotor # 16 Power Performance Data	38
Table 22	TASK 4 Disturbed Flow Test Locations	39
Table 23	TASK 4 Disturb Flow Normalized Data	39
Table 24	TASK 5 Far Wake Test Program	40
Table 25	TASK 5 Far Wake Test Positions	40
Table 26	TASK 5 Tunnel Only Velocity Data	41
Table 27	TASK 5 Tower Wake Deficits, Test 2a	41
Table 28	TASK 5 Wake Deficits for Test 2	41
Table 29	TASK 5 Wake Deficits for Test 3	42
Table 30	TASK 5 Wake Deficits for Test 4	42
Table 31	TASK 5 Wake Deficits for Test 5	42
Table 32	TASK 5 Wake Deficits for Test 6	43
Table 33	TASK 5 Wake Deficits for Test 7	43
Table 34	TASK 6 Series 1 Test Program	44
Table 35	TASK 6 Series 2 Test Program	44
Table 36	TASK 6 Series 3 Test Program	44
Table 37	TASK 6 Series 1 Data Summary	45
Table 38	TASK 6 Series 2 Data Summary	46
Table 39	TASK 6 Series 3 Data Summary	47
Table 40	TASK 6 Series 3 Test Program (cont.)	48
Table 41	TASK 6 Series 3 Data Summary (cont.)	48

LIST OF FIGURES

Figure 1	U.S. Windpower 60 ft Field Wind Turbine Array	50
Figure 2	Environmental Wind Tunnel (EWT)	51
Figure 3	Industrial Wind Tunnel (IWT)	51
Figure 4	EWT Entrance Grid No. 1	52
Figure 5	EWT Entrance Grids No. 2A and 2B	52
Figure 6	Power Measurement Schematic	53
Figure 7	Turbine Loading Schematic	53
Figure 8	Clifton Motor Efficiency	54
Figure 9	CSU Force Balance	54
Figure 10	USW Model 56-100 Wind Turbine Generator	55
Figure 11	USW 56-100 Turbine on 60 foot Tower	56
Figure 12	140 Foot Tower Design	56
Figure 13	Model 60 foot Wind Turbine Picture	57
Figure 14	Model Wind Turbine Array Picture	57
Figure 15	Model Shaft Bearing Housing	58
Figure 16	Passive Wake Device	58
Figure 17	Geometrically Scaled USW Turbine Rotor Design	59
Figure 18	Graupner Rotor Design	59
Figure 19	USWP Blade Design	60
Figure 20	TNO Type Blade Design	60
Figure 21	Graupner Power Performance Curve	61
Figure 22	TASK 2 Pulley and Chain Drive Comparison	61
Figure 23	USWP Type Rotor Power Performance Comparisons	62
Figure 24	TNO Type Rotor Power Performance Comparisons	62
Figure 25	Power Performance Curves for Rotors 11 to 15	63
Figure 26	Power Performance Curve for Rotor 16	63
Figure 27	Single Turbine Wakes : Velocity Deficit vs. Height at X/D=1 for Rotors #2, #3, #6	64
Figure 28	Single Turbine Wakes : Velocity Deficit vs. Height at X/D=1.5 for Rotors #2, #3, #6	64
Figure 29	Single Turbine Wakes : Velocity Deficit vs. Height at X/D=2 for Rotors #2, #3, #6	65
Figure 30	Single Turbine Wakes : Velocity Deficit vs. Height at X/D=4 for Rotors #2, #3, #6	65
Figure 31	Single Turbine Wakes : Velocity Deficit vs. Height at X/D=6 for Rotors #2, #3	66
Figure 32	Single Turbine Wakes : Velocity Deficit vs. Height at X/D=10 for Rotors #2, #3	66
Figure 33	Single Turbine Wakes : Velocity Deficit vs. Height for Rotor # 2	67
Figure 34	Single Turbine Wakes : Velocity Deficit vs. Height for Rotor # 3 (Passive)	67
Figure 35	Single Turbine Wakes : Velocity Deficit vs. Downwind Distance for Rotors #2, #3, #6	68
Figure 36	Power Performance Curves for Rotors 2, 6, 8 and 10	68
Figure 37	Single Turbine Wakes : Velocity Deficit vs. Radial Distance at X/D=1 for Rotors #2, #6, #8, #10 Unloaded	69

Figure 38	Single Turbine Wakes : Velocity Deficit vs. Radial Distance at $X/D=1$ for Rotors #2, #6, #8, #10 Loaded	69
Figure 39	Single Turbine Wakes : Static Pressure vs. Radial Distance at $X/D=1$ for Rotors #2, #6, #8, #10 Unloaded	70
Figure 40	Single Turbine Wakes : Static Pressure vs. Radial Distance at $X/D=1$ for Rotors #2, #6, #8, #10 Loaded	70
Figure 41	Multiple Turbine Wakes: Velocity Deficit vs. Height at Different Downwind Distances for Run 2 ($Y/D=0$)	71
Figure 42	Multiple Turbine Wakes: Velocity Deficit vs. Height at Different Downwind Distances for Run 3 ($Y/D=0$)	71
Figure 43	Multiple Turbine Wakes: Velocity Deficit vs. Height at Different Downwind Distances for Run 4 ($Y/D=0$)	72
Figure 44	Multiple Turbine Wakes: Velocity Deficit vs. Height at Different Downwind Distances for Run 5 ($Y/D=0$)	72
Figure 45	Multiple Turbine Wakes: Velocity Deficit vs. Height at Different Downwind Distances for Run 6 ($Y/D=0$)	73
Figure 46	Multiple Turbine Wakes: Velocity Deficit vs. Height at Different Downwind Distances for Run 7 ($Y/D=0$)	73
Figure 47	Multiple Turbine Wakes: Velocity Deficit vs. Downwind Distance for Runs 2,4,5,6,7 at Height $Z/D = 1$ ($Y/D=0$)	74
Figure 48	Multiple Turbine Wakes: Velocity Deficit vs. Downwind Distance for Runs 3,4,5,6,7 at Height $Z/D = 2.25$ ($Y/D=0$)	74
Figure 49	Multiple Turbine Wakes: Velocity Deficit vs. Height for all Runs at Downwind Distance $X/D = 6.67$ ($Y/D=0$)	75
Figure 50	Multiple Turbine Wakes: Velocity Deficit vs. Height for all Runs at Downwind Distance $X/D = 15$ ($Y/D=0$)	75
Figure 51	Multiple Turbine Wakes: Velocity Deficit vs. Height for all Runs at Downwind Distance $X/D = 30$ ($Y/D=0$)	76
Figure 52	Multiple Turbine Wakes: Velocity Deficit vs. Height at Different Lateral Positions for Run 2 ($X/D=20$)	76
Figure 53	Multiple Turbine Wakes: Velocity Deficit vs. Height at Different Lateral Positions for Run 3 ($X/D=20$)	77
Figure 54	Multiple Turbine Wakes: Velocity Deficit vs. Height at Different Lateral Positions for Run 4 ($X/D=20$)	77

Figure 55	Multiple Turbine Wakes: Velocity Deficit vs. Height at Different Lateral Positions for Run 5 (X/D=20)	78
Figure 56	Multiple Turbine Wakes: Velocity Deficit vs. Height at Different Lateral Positions for Run 6 (X/D=20)	78
Figure 57	Multiple Turbine Wakes: Velocity Deficit vs. Height at Different Lateral Positions for Run 7 (X/D=20)	79
Figure 58	Multiple Turbine Power Interaction : Power Coefficient vs. Tip Speed Ratio for Run Numbers 1, 2, 3, 4, 5, 6	79
Figure 59	Multiple Turbine Power Interaction : Power Coefficient vs. Tip Speed Ratio for Run Numbers 7, 8, 9, 10	80
Figure 60	Multiple Turbine Power Interaction : Power Coefficient vs. Tip Speed Ratio for Run Numbers 19, 20, 21, 22, 1, 4	80
Figure 61	Multiple Turbine Power Interaction : Power Coefficient vs. Tip Speed Ratio for Run Numbers 23, 24, 25, 26, 7, 10	81
Figure 62	Multiple Turbine Power Interaction : Power Coefficient vs. Tip Speed Ratio for Run Numbers 19, 27, 28	81
Figure 63	Multiple Turbine Power Interaction : Power Coefficient vs. Tip Speed Ratio for Run Numbers 29, 30	82
Figure 64	Multiple Turbine Power Interaction: Power Coefficient vs. Tip Speed Ratio for Run Numbers 31, 32	82
Figure 65	Multiple Turbine Power Interaction: Power Coefficient vs. Tip Speed Ratio for Run Numbers 33, 34	83
Figure 66	Multiple Turbine Power Interaction: Power Coefficient vs. Tip Speed Ratio for Run Numbers 35, 36	83
Figure 67	Multiple Turbine Power Interaction: Power Coefficient vs. Tip Speed Ratio for Run Numbers 37, 38	84
Figure 68	Multiple Turbine Power Interaction: Power Coefficient vs. Tip Speed Ratio for Run Numbers 39, 40	84
Figure 69	Multiple Turbine Power Interaction: Power Coefficient vs. Tip Speed Ratio for Run Numbers 42, 43	85
Figure 70	Multiple Turbine Power Interaction: Power Coefficient vs. Tip Speed Ratio for Run Numbers 44, 45	85
Figure 71	Multiple Turbine Power Interaction : Power Coefficient vs. Tip Speed Ratio for Run Numbers 46, 47	86

Figure 72 Multiple Turbine Power Interaction : Power
Coefficient vs. Tip Speed Ratio for Run Numbers
48, 49 86

1. INTRODUCTION

Wind turbine aerodynamics research is concerned with the dynamic interaction between atmospheric flow and the turbine's rotor. Design extrapolation from propeller, helicopter blade and airplane aerodynamics to the response of wind turbine blades in steady, uniform, low-turbulence wind flows is felt to be understood. The wind-turbine rotor, however, operates in the atmospheric surface layer, where wind shear, gustiness and upwind rotors change the operating environment. In particular upwind rotors perturb the approach winds resulting in localized flow accelerations, decelerations and secondary motions. These perturbations result in wind turbine performance and loading changes of un-resolved magnitude.

During early design studies of the efficacy of multiple wind turbine arrays engineers considered the actual availability of energy in the wind. Templin (1974) estimated the effective power reduction in a wind-turbine array due to the removal of upwind wind energy; however, the estimates were based on tenuous estimates of the restoration of wind energy from the surrounding atmosphere. A number of analytic and numeric programs have been developed to predict multiple array wind turbine wake effects (Taylor, 1980; Bate et al, 1981; Vermeulen and Builtjes, 1981) by studying the flow field over model arrays represented by disks of wire and filter paper (Builtjes, 1978; Faxen, 1978; Riley et al, 1980). None of these model exercises actually used dynamic model wind-turbines; hence, they might represent some momentum characteristics of wind-turbines, but they did not actually remove kinetic energy or induce the appropriate vortex wakes. These studies resulted in recommendations for turbine separation ranging from 3 to 30 diameters.

Corrections for the influence of buildings, trees, and vegetation were recommended by Meroney (1968, 1977, 1982). These numbers were based on experience with wake effects on vegetative canopy flows and air pollution problems. Again they can only approximately reflect the response of a wind turbine on energy and aerodynamic loads.

Subsequently, various researchers have measured the wakes downstream of MOD-OA, and MOD-2 wind turbines (Connell, 1984; Hadley and Tenne, 1983). Although valuable, these data are difficult to interpret due to the non-stationarity of the wind fields sampled. In addition the wake separations, turbine/turbine and turbine/obstacle configurations studied are very limited.

It is the purpose of this report to provide experimental model data on the simulation of wind-turbine performance in perturbed flow fields through the science of fluid-modeling and physical simulation. Scaled models of horizontal-axis wind turbines, having rotor diameters of about 34 cm would represent turbines equivalent to the US Windpower 56-100 kw turbine (see Figure 1) at a scale of 1:50. An array of five side-by-side model rotor diameters can be accommodated in the FDDL Environmental Wind Tunnel without undue blockage.

2. MODELING OF WIND TURBINES

Physical modeling of wind turbine wakes can be classified into two general categories: approximately scaled dynamic models of wind turbines, and greatly simplified static models (e.g. porous disks). Accurate simulation of field conditions at laboratory scales can be attained if the proper geometric, kinematic and dynamic similarity is maintained. These similarity requirements can be conveniently summarized by dimensionless similarity parameters that should be equal for both the field and the laboratory situations.

Geometric similarity requires that all geometric objects be scaled up or down proportionally. Kinematic similarity requires that the path lines of fluid particles move in geometrically similar patterns. This will occur if velocities and accelerations at geometrically similar points are scaled proportionally. For example, the tip speed ratio (turbine blade tip speed divided by free stream wind speed) should be the same in both the laboratory and the field. Dynamic similarity requires that all forces acting on fluid particles or turbine be scaled proportionally. For example, the thrust coefficient (the drag force on the turbine rotor divided by the characteristic wind momentum) or the power coefficient (the power extracted from the wind divided by the potential power in the incoming wind) should be the same in the laboratory as in the field. If geometric and dynamic similitude are attained, then kinematic similarity is generally assured as a result of Newton's laws of motion.

The following sections first discuss dynamic (rotating) models for wind turbines, next static (non-rotating) models, and, finally, specific aspects of the power and thrust coefficients.

2.1. Wind Turbine Wakes

2.1.1. *Dynamic Modeling*

The wake characteristics of full-size wind turbines are often predicted by examining the performance of intermediate size or miniature turbines. Reliable results require consideration of the simulation of both the flow characteristics of the approach wind and the response of the wind turbine. Simulation of the atmospheric boundary approach wind characteristics is extensively discussed by Snyder (1981) and Meroney (1986). Riley et al. (1980) and Milborrow (1980) review studies which consider the dynamic simulation of both horizontal and vertical axis wind turbines.

Dimensional or inspectional analysis suggest that the important kinematic and dynamic parameters which control wake behavior are:

Tip Speed Ratio - (Rotor tip speed)/(Wind speed) - $(R\Omega)/U$,

Reynolds Number - (Inertial forces)/(Viscous forces) - $(UL)/\nu$,

Thrust Coefficient = (Rotor load)/(Inertial forces) = $F/(\frac{1}{2}\rho AU^2)$,

Power Coefficient = (Turbine power)/(Potential Power) = $P/(\frac{1}{2}\rho AU^3)$.

Many full-scale wind turbines produce power most efficiently when they are operated at a Tip Speed Ratio between four to eight. Since full-scale rotational speeds are usually from 50 to 100 rpm, then a model turbine constructed to a 1/50 scale would operate at 2500 to 5000 rpm for equivalent wind speeds. Thus, care must be taken that dynamic models are sufficiently strong to resist very high centrifugal forces.

A Reynolds number for a model turbine based on chord length is often several orders of magnitude below the full-scale value. Yet the effect of Reynolds number on the turbine blade lift curve is indeed profound and often quite unpredictable. Unfortunately most "modern" wind turbine airfoils will yield embarrassingly poor results at low Reynolds numbers. In some cases perfectly satisfactory blade shapes at high Reynolds numbers will produce at low Reynolds numbers extremely wiggly lift curves and drag curves showing less drag at finite angles of attack than at zero angle (Rae and Pope, 1984). These variations result from the tendency for flow to separate from the blade surface when operated at low Reynolds number.

The Reynolds number magnitude may also affect flow around the turbine support tower. Savino and Wagner (1976) and Bureley et al. (1979) studied the tower shadow of the DOE/NASA Mod 0 wind turbine tower, but did not include the influence of turbine rotors. Care should be taken to use sharp-edged structural elements for model tower members, and, if possible, run the wind tunnel at "large" velocities to assure constant drag coefficients.

Power and thrust coefficients are directly related to the lift and drag performance of a rotor blade. Previous attempts to study geometrically scaled blade shapes have always resulted in reduced power coefficients compared to full-scale performance data (Riley et al., 1980; Cao and Wentz, 1987). Indeed, in some cases the torque produced by the model wind turbines were so small that they could not overcome bearing friction! Many researchers did not attempt to geometrically scale blade shape, but they chose to work with blades redesigned to reduce stall (Vermeulen, 1978, 1979; Neff and Meroney, 1985). It is generally conceded that wind turbine wake characteristics are strongly dependent upon the thrust perceived by the rotor disk; thus, an acceptable wake simulation approach would be to utilize a modified model rotor design in the laboratory experiment which produces an equivalent magnitude thrust coefficient.

2.1.2. *Static Modeling*

As noted above there is strong evidence for scaling problems when modeling full-scale wind turbines dynamically in a wind tunnel. Model turbines must run at large revolution speeds (circa 2000 to 5000 rpm), and blade performance at lower Reynolds numbers is not well known. Past experience suggests model blades stall more frequently resulting in lower

performance characteristics. Furthermore the construction of dynamic models at the small scales (1:100 to 1:500) necessary to include significant downwind terrain distances would be extremely expensive, if not impossible. Thus, although a dynamic model would be desirable, the additional measurement difficulties and potential mismatch of performance characteristics may not justify the effort.

A number of researchers have used simplified static models to represent wind-mill wake performance during model tests (Troller, 1940; Builtjes, 1979; Milborrow, 1979; Vermuelen, 1979). Combinations of wire mesh, fliter paper, perforated disks, and wire screens have been used. Builtjes (1979) used a tea-strainer shaped mesh and gauze combination to reproduce initial velocity deficit profiles (and hence drag) behind a dynamic model. Simulation of the drag is expected to assure simulation of the wake behavior to the first order.

Of course these models only reproduce the momentum deficit characteristics of a wind turbine, they do not extract power or energy from the wind. Therefore, the velocity deficit must be produced not by an extraction of energy but by a conversion of orderly (mean flow) energy into disorderly energy (turbulence). Hopefully, the wire screens produce small scale turbulence which decays rapidly, leaving the larger scale turbulence produced by the bulk of the disk. In that case the wake characteristics could be very similar to a wind turbine. However, there is no assurance that such a proposition is correct. We do not know what differences exist between such statically and dynamically produced wakes. Remember, these static models do not induce wake swirl, and they do not pass any ambient turbulence through the disk area, possibly affecting the wake growth and the influence on downstream turbines.

The strength of static models is, of course, their simplicity. It is impractical to work with large arrays of dynamically scaled miniature turbines. Small static models can be cheaply constructed and are safer to work around (no high rpm and related centrifugal forces). A physicial model incorporating such static models, even given the deficiencies, is often a better model of full-scale behavior than a theoretical or numerical model.

2.2. Wind Turbine Rotor Performance

2.2.1. *Power Coefficient*

The maximum performance expected from a wind turbine according to the idealized one-dimensional model developed by Betz is $C_p = 16/27 = 0.59$. This upper limit has never been achieved because of losses associated with flow separation, tip vortices, and swirl. Nonetheless, it is not uncommon for full-scale turbines to achieve performance levels from 0.4 to 0.45. Most laboratory studies of scaled turbine blades produce coefficients between 0.2 to 0.3, and few exceed 0.36. The reasons for this loss in performance are discussed in the preceeding report sections.

Theoretically, the power coefficient and thrust coefficient of a wind turbine are directly related, and specification of one parameter would be sufficient to assure similarity. Actually, the thrust coefficient on a turbine is also a function of pressure difference over the rotor disk, turbulent momentum flux, flow separation over the rotor blade, and tip vortex loads. Hence, the relative performance of a model turbine can be used to evaluate the influence of an upwind rotor, but equivalence in thrust coefficient should be used to assure similarity in wake characteristics to the first order.

2.2.2. Thrust Coefficient

Using simple momentum and energy considerations a Betz limit for the thrust coefficient is $8/9 = 0.89$. Experimental measurements of rotor disk loads reveals that numbers in excess of 0.8 can occur for full-scale turbines and in excess of 1.75 can occur for dynamic model turbines (Vermeulen, 1978; Baker and Walker, 1982). A momentum balance for the axial direction behind a wind turbine shows that the thrust coefficient, C_T , instead of the power coefficient, C_p , controls the value of the velocity defect in the wake.

The value of the trust coefficient can be determined directly by measuring forces on the actuator disk with a force balance. Its value can also be obtained by integrating the momentum deficit in the wake at larger distances. Close to the wind turbine the pressure disturbance and turbulence contribute to the momentum balance. Vermeulen (1979) measured static pressures, mean and turbulence profiles behind a model turbine and the turbine drag using a force balance. Terms in the momentum balance equation are:

At a distance of $X/D = 1.67$ conditions were measured for a tips speed ratio of 6.6. He found that the integrated terms in the momentum equation were:

momentum flux:	0.58
pressure :	0.19
turbulence :	-0.02

$$C_T = \frac{\quad}{0.75}$$

$$\begin{aligned} C_T = & - 4 \int U/U_\infty (U/U_\infty - 1) r' dr' \\ & - 2 \int \Delta P / (\frac{1}{2} \rho U_\infty^2) r' dr' \\ & - 4 \int \Delta u'^2 / (U_\infty^2) r' dr' \end{aligned}$$

Equation 2-1

This value was very close to the $C_T = 0.74$ value measured with the force balance. At larger distances the pressure disturbances diminished and the integrated momentum flux equals drag (thrust).

Although the thrust coefficient is believed to assure similarity in wake characteristics, there is some evidence that wake behavior may not be very sensitive to the type of turbine or the absolute magnitude of the thrust parameter. Baker et al. (1984) report measurements of full-scale wakes behind horizontal and vertical axis turbines whose coefficients of thrust were 0.53 and 0.70, respectively, yet the magnitudes and decay rate

of the measured centerline wake velocity deficits beyond $X/D = 4$ were nearly identical. Vermeulen (1979) made similar measurements behind model vertical and horizontal axis turbines. He found similar wake behavior behind the two different type turbines.

3. DATA ACQUISITION AND ANALYSIS

Laboratory equipment and measurement techniques are discussed in this section. Many of the methods employed are conventional and require limited explanation.

3.1. Wind Tunnel Facilities

The Environmental Wind Tunnel (EWT) shown in Figure 2 was used for all experiments except the drag force measurements. The EWT is an open circuit test facility powered by a 50 hp variable speed drive. The test section is about 2.5 m tall by 3.7 m wide and 18 m long. Mean wind speeds ranging from 0.2 m/s to 15 m/s can be obtained in the EWT. The flexible test section roof on the EWT is adjustable in height to permit the longitudinal pressure gradient to be set to zero.

For the early tests in this project the models were located over the middle turntable and the tunnel entrance grid number 1 (see Figure 4) was used to increase the turbulence level. For the latter tests the model were located over the upwind turntable and the tunnel entrance grid number 2 (see Figure 5) was used.

The Industrial Aerodynamics Wind Tunnel (IWT) shown in Figure 3 was used for all drag force measurements. This wind tunnel is a closed circuit facility powered by a 75 hp AC motor driving a variable-pitch fan. The test section is about 1.8 m tall by 1.8 m wide and 18 m long. Mean wind speeds ranging from 0.5 m/s to 20 m/s can be obtained in the IWT. The flexible test section roof on the IWT is adjustable in height to permit the longitudinal pressure gradient to be set to zero. For measurements in this tunnel the model wind turbine was placed over the downwind turntable. A turbulence grid similar to the shown in Figure 4 but 1.8 meters wide was installed upwind of the testing site.

3.2. Flow Visualization Techniques

A visible gas produced by a Rosco Fog/Smoke Machine was introduced into the wind tunnel upwind of the turbine array via a 0.5 inch diameter brass tube. The path of this plume was recorded on VHS video cassettes with a Panasonic Omnivision II camera/recorder system. A Sage Action Inc. Model 3 helium bubble generator was also used to visualize the flow patterns. It introduced small neutrally buoyant bubbles at locations upwind of the turbine array. Polaroid color prints and 35 mm color slides were used to document the model wind turbines and the test site setup.

3.3. Wind Velocity Measurements

Pitot-static probe measurements documented the mean longitudinal wind velocities upwind and downwind of the model wind turbines. Typically one probe was located upwind of the turbines for an approach flow reference and a rake of seven other probes was moved to the different measurement locations. All eight pitot probe signals were digitized by a Data Translations DT2818 board within an IBM AT computer for sixty

seconds and the mean velocities were reported. A detailed explanation of the usage of pitot probes is provided in Section 3.3.1.

The longitudinal turbulence levels downwind of the different approach flow conditions were documented. These measurements were made with a Thermo-Systems Inc. (TSI) 1050 hot-film anemometer system capable of responding to the highest frequency velocity fluctuations present in the wind tunnel. A detailed explanation of the experimental technique is provided in Section 3.3.2.

3.3.1. Pitot-Static Probes

Pitot-static probe measurements are an accurate and reliable method for obtaining mean velocity within a wind tunnel. These probes measure the static and total pressure at a point within a flowing fluid. The static and total pressure difference is related to the local fluid velocity via the general equation :

$$V = \sqrt{2g(P_t - P_s)/d}$$

where V is velocity,
 g is gravitational const.,
 P_t is total pressure,
 P_s is static pressure,
 d is local fluid density.

The accuracy of a pitot-static probes measurement of mean velocity is dependent on the pitot-static probes ability to respond to the true static and total pressure and the pressure transducer's differential pressure measurement accuracy. The pitot-static probe response is generally within $\pm 1\%$ provided that the probe Reynolds number is greater than 30 ($V > 0.5\text{m/s}$), that the velocity is below a compressible flow range (Mach number < 0.7), and that the yaw and pitch angles are within ± 5 degrees of the mean velocity vector. All differential pressure transducers (Setra Model 237, MicroSwitch Model PK 8772 and Datametrics C-1018) used were calibrated against an N.B.S. traceable Micro-manometer (Dwyer model no. 1430). These calibrations indicate that the pressure measurements were accurate to within $\pm 1\%$ over the current range of measurements. Accumulating the various sources of error for pitot-static probe velocity measurements yields a mean velocity measure in the range of 4 to 12 m/s accurate to ± 1 percent.

3.3.2. Hot-film Probes

The hot-film probe (TSI model 1210) was calibrated inside the wind tunnel, upwind of the entrance grid, against a pitot-static probe. During calibration single-film probe anemometer voltages were digitized for several velocities covering the range of interest. These voltage-velocity (E,U) pairs were then regressed to the equation $E^2 = A + BU^c$ via a least squares approach for assumed values of exponent c . Convergence to the minimum square was accelerated by using the secant method to find the best new estimate for c .

During a measurement sequence the anemometer response voltage was digitized and stored on a disk file within an IBM AT computer. This voltage time series was then converted to a velocity time series using the inverse of the calibration equation $U = [(E^2 - A)/B]^{1/c}$. This velocity time series could then be analyzed for pertinent statistical quantities, such as mean, root-mean-square, etc. and tabulated at the computer.

The calibration curve yielded hot-film anemometer velocities that were always within two percent of the known pitot-static probe velocity. The accuracy of a single-hot-film probe during the measurement of turbulent flow quantities is dependent upon the flow regime being measured. During the present study the single-film probe was used in the favorable conditions of approximately isotropic turbulence. Considering the method of calibration and data reduction used the model velocity time series should be accurate to within five percent.

3.4. Turbine Power Measurements

A survey of small DC generators and their power generation capabilities indicated that a generator capable of properly loading the model rotor would be two to three times larger than a properly scaled nacelle. To circumvent these difficulties a flexible belt drive was attached to the rear of the rotor shaft on all five model wind turbines. This belt drive was connected to either a dynamometer located under the tunnel floor for accurate power measurements (see Figure 6) or to a small DC generator located on the model base plate for approximate loading capabilities (see Figure 7). Whenever multiple turbine arrays were tested one of the towers was connected to the dynamometer and all the others were loaded by their DC generators.

3.4.1. *Dynamometer Measurements*

The dynamometer, a Magtrol Model HO-400-2, allowed one to adjust the torque from 0.2 to 32 inch ounces and monitor angular velocity (rpm). The power developed at the dynamometer is the product of the torque setting and angular velocity. The power developed at the rotor is the power measured at the dynamometer divided by the drive train efficiency. To measure the drive train efficiency (power in divided by power out) the following step were performed:

- 1) A Clifton Precision Products Model DH-2250-AB-1 permanent magnet DC motor was connected to the dynamometer and a mapping (see Figure 8) of the motors efficiency at different angular velocities and applied torques was obtained. Note that power into the motor is voltage times amperage.
- 2) The Clifton motor was coupled to the shaft on the wind turbine model where the rotor would normally be mounted. The dynamometer was connected to the belt drive under the tunnel. In this configuration known values of power into the drive train (power into motor divided by motor efficiency) were applied and the dynamometer measured the power out of the drive train.

In this manner the drive train efficiency for a variety of drive speeds, loads and belt tensions were calculated. The initial tests used a notched v-belt. It's efficiency varied from 0.35 at low loads to 0.65 at high loads and was somewhat independent of speed. A majority of the tests used a Flex-E-Gear cable drive. It's efficiency varied from 0.88 to 0.92 for all speeds, loads and tensions tested.

3.4.2. *Turbine Loading Technique*

Each model wind turbine was connected to a Pittman 9414B589 permanent magnet DC motor mounted on the tower base plate. The motor was operated as a generator to load the model turbine, and, thus, to insure that proper wake interaction occurred with the turbine that was connected directly to the dynamometer. Each generator was electrically connected to a variable power resistor and ammeter. The loading on the rotor was equal to the no load generator voltage times the ammeter reading divided by the drive train efficiency. The no load generator voltage versus generator speed was measured for each of the five Pittman generators. Two different methods were employed to measure the generator's speed. During the early tests a laser light passing through the spinning rotor blades fell upon a photodiode which registered pulses on a digital oscilloscope. The time between pulses, number of rotor blades and drive train gear ratio yielded generator speed. During later tests a very small tachometer was connected directly to each generator.

3.5. Turbine Thrust Measurements

Two different approaches were employed to obtain turbine thrust estimates. The first and the least accurate of the methods performed a momentum balance on a control volume that encapsulated the turbine rotor. The second method was to measure the drag force on the turbine rotor directly.

3.5.1. *Momentum Balance Technique*

The wind speed approaching the rotor was measured with a single pitot-static probe at an unperturbed location upwind of the turbine. The approach profile was assumed to be uniform. The wind speed and static pressure downwind of the rotor were measured with pitot-static probes placed at several radial distances from the rotor's centerline. The mean longitudinal flow downwind of the rotor was assumed to be axisymmetric and the turbulent contribution to momentum was neglected. Evaluating the momentum difference between these two sections (equation 2-1, see section 2.2.2) yields the drag force on the air induced by the turbine rotor. The thrust coefficient is this drag force divided by total momentum in the wind approaching the rotor.

3.5.2. *Direct Measurement Technique*

The wind turbine was mounted on a Colorado State University designed force balance located in the IWT. A diagram of this balance is shown in Figure 9. This strain-gage force-balance system can measure the three

major forces and moments that act on the wind turbine model. The drag force on the rotor was obtained by subtracting the tower only drag force from the tower and rotor drag force. The thrust coefficient is this drag force divided by total momentum in the wind approaching the rotor.

4. TEST PROGRAM AND DATA

The test program consisted of many different developmental phases and measurement tasks. During these phases and tasks the experimental methodology was often updated to reflect improved modeling capabilities. To provide a comprehensive summary of the test program this section has been organized chronologically. TASK 1 compared the wake behavior of both passive and dynamic wind turbine models. TASK 2 involved the development of a dynamic wind turbine model that reproduced field scale performance characteristics. TASK 3 entailed the construction of five model-scale dynamic wind turbines, three mounted on scaled sixty foot towers and two mounted on scaled 140 foot towers. TASK 4 measured the disturbed flow field upwind and to the side of a single dynamic wind turbine model mounted on a scaled 60 foot tower. TASK 5 measured the wake behavior of multiple turbine arrays for a variety of spacings. TASK 6 investigated power performance changes relative to multiple turbine spacing specifications.

TASKS 1 and most of TASK 2 were performed in the EWT over the middle turntable with entrance grid 1 (see Figure 2 and Figure 4). The force balance measurements in TASK 2 were taken in the IWT (see Figure 3). TASKS 4 and 5 were performed in the EWT at an upwind location with entrance grid 2A. TASK 6 series 1 and 3 were performed in the EWT at an upwind location with entrance grid 2A. TASK 6 series 2 was performed in the EWT at an upwind location with entrance grid 2B. These six tasks and associated data are described in the following sections.

4.1. Passive and Dynamic Turbine Wakes (TASK 1)

The initial objective of Task 1 was to geometrically model a 60 foot USWP wind turbine at a scale of 1:50, measure its mean wake behavior and then design a passive device which would produce a similar wake. Since the predominate effect of a turbine wake is simply a velocity deficit, it was presumed possible to simulate a wake similar to that produced by an active turbine with a passive device. Preliminary testing of the geometrically scaled rotor blade revealed significant performance differences due to loss of Reynolds number equality between the model and field rotor blades. A model helicopter rotor was purchased from a hobby shop. This three bladed rotors performance and wake characteristics were measured and compared to different passive rotor disk designs. The following sub-sections detail the TASK 1 experimental program and present the data results.

4.1.1. *USWP Sixty Foot Tower Model*

A model length scale ratio of 1 to 50 was selected to accommodate the testing of the interaction between five USW Model 56-100 wind turbines, three mounted on 60 foot towers and two mounted on 140 foot towers. Figure 10 summarizes information about the USW Model 56-100 wind turbine generator. Figure 11 illustrates the 60 foot tower design. The model 60 foot tower was 14.4 inches tall and was made of 0.2 inch diameter brass rods brazed together. A top plate was attached to this rod frame

and a shaft-bearing housing (see Figure 15) scaled to nacelle size was bolted to the top plate. The tower was mounted on an aluminum base plate. Figure 13 pictures the model 60 foot tower, nacelle, and geometrically scaled rotor.

4.1.2. *USWP Scaled Rotor*

A 1 to 12 scale model of the USWP 56-100 wind turbine rotor blade was provided by USWP to assist in the fabrication of a 1 to 50 scale model. Measurements of blade profile shape, outline, chord and twist variation with radius from this 1:12 model were entered into a computer aided design package (CAD). The CAD package scaled the 1:12 design down to a 1:50 scale and generated properly scaled drawings to assist in the reproduction of a 1:50 scale blade. From these drawings a prototype blade was constructed out of balsa wood. This prototype blade was used to produce a silicone mold, and twenty identical plastic rotor blades were produced. A threaded rod connected the plastic rotor blades to a small hub that mounted on the shaft extending out of the modeled nacelle. Figure 17 shows the rotors shape and details blade profile, chord, and twist.

When this geometrically scaled rotor (Rotor # 1) was tested at a wind speed of 9.2 meters per second (mps) it turned slowly at less than 400 revolutions per minute (rpm) and produced very little power. These results were not entirely unexpected as performance characteristics of an airfoil can be strongly dependent on the Reynolds number. The Reynolds number in these model tests was approximately fifty times smaller than the field situation.

4.1.3. *Graupner Rotor Tests*

A Graupner Model 36-18 model helicopter rotor (Rotor # 2) was purchased from a local hobby shop. This three-bladed rotor, detailed in Figure 18, had the proper model blade length and was known to produce significant thrust over the appropriate operating range. Its dynamic performance was tested and its wake character was measured to provide some insight into passive device design. Table 9 and Figure 21 show the results from the power performance tests. Figure 21 also displays the power performance curve for the prototype variable pitch USW 56-100 wind turbine.

During the wake measurements three different conditions were tested; one with the rotor fully loaded, one with no load on the rotor and one with only the model tower present. These tests were performed to bracket possible variations in wake behavior. Table 1 presents normalized velocity values measured in the absence of a turbine at 54 locations downwind of the modeled sixty foot tower. Table 2 and Table 3 display the percent velocity deficit normalized by the tower-only data in Table 1 for the loaded and unloaded Graupner rotor. This normalization by the tower-only data serves to remove wind perturbations produced by the tower and wind tunnel's measurement location, thus focusing attention on the true deficit caused by the spinning rotor.

4.1.4. *Passive Design and Test Data*

The passive rotor design (Rotor # 3) was a scaled version of the "tea strainer" design used by Vermeulen (1979). The passive rotor device shown in Figure 16 was a conic section made of rolled brass brazed to cross braces. This device was mounted to the rotor shaft at the top of the model 60 foot tower. Several different types of screen were placed across the upwind (smaller) opening. Comparisons of the measured wake velocity profile produced by the different screens to the profile measured behind the dynamic Graupner rotor revealed that conventional window screen has the most suitable open area character. Table 4 displays the percent velocity deficit normalized by the tower-only data in Table 1 for the passive device wake measurement data.

4.2. Dynamic Turbine Model Development (TASK 2)

The USW 56-100 wind turbine has variable pitch rotor blades. The ability to vary the rotor's pitch allows one to optimize the power performance of the wind turbine over a range of wind speeds. The model rotors studied were limited to a specific operating condition. USWP personnel specified that the performance region of most interest was 30 mph. At this wind speed the USW 56-100 wind turbine attains a tip speed ratio of 5.0, a power coefficient of 0.36. The thrust coefficient for the USW 56-100 wind turbine varied from 0.4 to 0.9 at tip speed ratios 3.5 to 10.8. At the design wind speed of 30 mph the thrust coefficient was approximately 0.6. A good model turbine rotor should reproduce all three of these dimensionless numbers (tip speed ratio, thrust and power coefficients). To produce conservative estimates of multiple turbine power performance interactions it was decided to find a model rotor that, 1) produced sufficient power performance to discern changes due to adjacent turbines, and 2) produced a thrust coefficient that was greater than the design value of 0.6.

Figure 21 indicates a very poor comparison in power performance exists between the Graupner rotor (model wind speed of 9.1 m/s) and the USW 56-100 wind turbine. A thrust coefficient (neglecting the pressure and turbulent terms; see section 3.5.1) calculated from the $X/D = 1$ wake data (Table 2) for the loaded Graupner rotor yielded a value of 0.36. To identify a better model blade configuration a series of different model turbine blade designs were constructed and tested. Two different basic blade patterns were tested. For each basic blade pattern a series of modifications to the twist angle and/or profile shape was studied. The first blade pattern tested was suggested by USWP staff. The second design selected was similar to that used by Vermeulen (1979), and it is hereafter referred to as the TNO design.

4.2.1. *Graupner Rotor Test Series*

A more efficient cable-chain drive system was installed prior to the testing of these new blade designs. Both of these drive systems are described in section 3.4.1. Additional power performance tests were

performed on the Graupner rotor with this new drive system. Table 10 lists this new data and Figure 22 provides a comparison between data obtained by each of these drive systems. The chain system reduced pulley friction considerably. Static pressure and velocity profiles were obtained downwind of the Graupner rotor at a distance of $X/D = 1$ for unloaded and loaded rotor conditions (see Table 6). The thrust coefficients were calculated from the data in Table 6 and are presented in Table 8. Table 8 also presents the thrust coefficients for an unloaded and loaded rotor obtained from direct measurements with a force balance in the IWT.

4.2.2. USWP Type Blade Design Test Series

Figure 19 describes the rotor design (Rotor # 4) suggested by the USWP staff. Rotor # 4 was made of aluminum, and it had

- 1) A blade chord variation similar to a 1:50 scaled field blade,
- 2) A linear blade twist angle of 0° at the tip and 10° at the base,
- 3) A flat profile shape that was rounded at the leading edge and tapered at the trailing edge, and
- 4) A constant thickness of $1/8"$.

Rotor # 4 was attached to the model 60 tower assembly and tested. It rotated slowly and produced negligible power. Rotor # 5 was similar to Rotor # 4 but it was made of steel and had a thickness of $1/16"$. Again this rotor's performance was poor.

Rotor # 6 was similar to Rotor # 5, but the blade twist angle was changed to 10° at the tip and 20° at the base. This rotor design could withstand loading, so it was fully tested. Table 11 lists the power performance data. Table 5 presents the wake data at 42 downwind locations as percent velocity deficit with respect to the tower-only data presented in Table 1. Table 6 displays the static pressure and normalized velocity profile data at the downwind centerline stations of $X/D = 1$ and $X/D = 2$ for a loaded turbine condition. From the data in Table 6 the thrust coefficients were calculated and are presented in Table 8. Rotor # 6's power performance (see Figure 23) was still unsatisfactory; thus, further blade modifications were considered.

Rotor # 7 was similar to Rotor # 6 except that the blade twist was changed to vary radially from the base at 40° to the tip at 5° . Table 12 lists the power performance data for this rotor. This power performance data is graphically presented as one of the curves in Figure 23. Rotor # 7 produced more power than any of the other USWP type designs, but, unfortunately, the hub-blade connection fatigued, and it flew apart before any wake measurements could be made. Since modifications to the USWP model blade did not yield significant improvement in turbine performance, the USWP model blade design was abandoned, and a new blade design similar to a TNO design was constructed.

4.2.3. TNO Type Blade Design Test Series

Figure 20 describes the TNO rotor design. The first rotor similar to this design, Rotor # 8, made of steel, had

- 1) A constant blade chord,

- 2) A constant blade twist angle of 10° ,
- 3) A curved profile shape that was rounded at the leading edge and tapered at the trailing edge, and
- 4) A constant thickness of $1/8"$.

Rotor # 8 was attached to the model 60 tower assembly and tested. Table 13 lists the power performance data for this rotor. This power performance data is graphically presented as one of the curves in Figure 24. Figure 24 shows that Rotor # 8 produced peak power performance at low tip speed ratios. It's character was similar to the Graupner rotor (Rotor # 2). Table 7 displays the static pressure and normalized velocity profile data at the downwind centerline station of $X/D = 1$ for unloaded and loaded conditions. From the data in Table 7 the thrust coefficients were calculated and are presented in Table 8. Also presented in Table 8 is the thrust coefficient for the unloaded rotor obtained from direct measurements with a force balance in the IWT.

Rotor # 9 was similar to Rotor # 8 except that there was a little less curvature in the profile shape and the twist was set at 6° . Table 14 lists the power performance data for this rotor. This power performance data is graphically presented as one of the curves in Figure 24. Figure 24 shows that Rotor # 9 produced a power coefficient at a tip speed ratio of 5 similar to the USW 56-100 wind turbine. Unfortunately during the pressure and velocity profile measurements this rotor slammed into the support tower and was destroyed. Thus no thrust coefficient data for this rotor was obtained.

Rotor # 10 was similar to Rotor # 9 except that a sharper taper on the trailing edge was incorporated to make the blade profile similar to that used by Vermeulen (1979). Table 15 lists the power performance data for this rotor. This power performance data is graphically presented as one of the curves in Figure 24. Table 7 displays the static pressure and normalized velocity profile data at the downwind centerline station of $X/D = 1$ for unloaded and loaded conditions. From the data in Table 7 the thrust coefficients were calculated and are presented in Table 8. Direct measurements with a force balance in the IWT found the unloaded and loaded rotor thrust coefficient were equal to 1.12 and 0.93 (see Table 8).

Figure 24 shows that Rotor # 9 produces power coefficient performance similar to the full scale USWP rotor at a tip speed ratio of 5, $C_p = 0.36$. The loaded model (tip speed ratio ≈ 5) thrust coefficient of 0.93 was sufficiently larger than the field value of 0.6 to insure conservative model estimates.

4.3. Multiple Turbine Construction (TASK 3)

Three new model 60 foot towers and two new model 140 foot towers were constructed at a model length scale ratio of 1 to 50. Figure 10 details information about the USW Model 56-100 wind turbine generator and Figure 11 displays the sixty foot tower design. Figure 12 depicts the 140 foot tower design. The model 60 foot towers were 14.4 inches tall and were made of 0.2 inch diameter brass rods brazed together. The model 140 foot towers were 33.6 inches tall and were made of square brass rods brazed

together. A top plate was attached to these rod frames and a shaft-bearing housing (see Figure 15) scaled to nacelle size was bolted to each top plate. Each tower had a belt drive that connected the rotor shaft to a small generator on the tower base plate for loading purposes (see section 3.4.1 for a more complete description). Figure 14 is a picture of the five wind turbine models mounted in the wind tunnel.

Five model turbine rotors (Rotors # 11 to # 15) similar to that described in section 4.2.3 were constructed and mounted on the towers. Table 16 through Table 20 presents the power performance test data for Rotors # 11 through # 15. Figure 25 shows the power performance curves for each of these five rotors. All rotors performed quite similarly, but not quite as well as the rotor constructed earlier for the rotor test program (see section 4.2.3). This demonstrates that small differences in blade shape can lead to significant differences in performance. Early in the test program one of these five rotor blades slammed into the tower structure. When this rotor (Rotor # 16) was reconstructed its power performance changed (see Table 21). Figure 26 shows the new curve for this rotor. This rotor was never used for power measurement tests and was always placed in a position where it would have the least effect on the measured turbine power interaction.

4.4. Single Turbine Disturbed Flow Tests (TASK 4)

In these tests mean velocity profiles were obtained at several locations upwind and to the side of a single model turbine mounted on a 60 foot tower with both the turbine on and off. Table 22 summarizes the velocity measurement locations. Table 23 lists the turbine-on data normalized by the turbine-off data. This table shows that at the locations measured there is very little mean velocity change due to the wind turbine.

4.5. Multi-Turbine Far Wake Tests (TASK 5)

In this task mean velocity profiles were measured at several locations downwind of five model wind turbines for a variety of different turbine spacings. There were three scaled sixty foot towers and two scaled 140 foot towers. The measurement locations were between 6 to 30 rotor diameters downwind. Table 24 lists the tower spacings for all the tests, and Table 25 shows the different profile positions that were measured in each test.

A velocity profile was obtained at each measurement location with both the turbines removed from the tunnel and with the turbines in the tunnel but not operating. Table 26 provides the velocity data for the no-turbines-in-the-tunnel case, test number 1. Table 27 presents the turbines off data for test number 2 normalized by the no towers in tunnel case. Table 28 through Table 33 present percent velocity deficits for each of the loaded turbine tests. These values were normalized by their turbine-off condition to remove wind tunnel spacial velocity variations from the data set. When the turbines were running they were always fully loaded by the small generators at the base of the towers.

4.6. Multi-Turbine Power Performance Tests (TASK 6)

The purpose of these tests was to measure the magnitude of turbine performance changes due to the proximity of other operating turbines. The turbine of central interest was connected to the dynamometer for accurate power performance measurements. For each turbine spacing arrangement power performance data was measured both when all other turbines were off and when they were fully loaded. The coordinate system used was right-handed with the origin at ground level under the data turbine and the positive X axis pointing downwind. This task was accomplished in three different test series performed in chronological order. During each test series somewhat different techniques were employed during the data acquisition. The following sub-sections elaborate on these differences and present the data.

4.6.1. *First Test Series*

In this test series the turbines were located over the upwind turntable in the EWT and grid number 2A (see Figure 4) was mounted at the tunnel entrance. The average rotational speed of the main turbine was the average of the values recorded every ten seconds for three minutes. The average wind speed was obtained from a reference pitot-static probe connected to a voltmeter with a ten second averaging time. The voltmeters reading was written down four to five times in the three minute test period.

Table 34 summarizes the different turbine spacings tested in this series. Table 37 summarizes the data results obtained.

4.6.2. *Second Test Series*

In this test series the same tunnel location and entrance grid were used, but the entrance grid was placed in the tunnel upside down. Similar power performance measurements were also performed.

Table 35 summarizes the different turbine spacings tested in this series. Table 38 summarizes the data results obtained.

4.6.3. *Third Test Series*

In this test series the same tunnel location and entrance grid were used as in the first test series. The measurement of mean revolutionary turbine speed and mean approach velocity were improved for this test series. A frequency to voltage converter was incorporated to convert the dynamometer rotational speed output to an analog voltage that was subsequently digitized and stored in an IBM AT computer. The rpm time series was then digitally averaged over the test period. The pitot-static probe transducer signal was also digitized over the test period, and the mean velocity was computed. To take advantage of the improved accuracy and ease of data collection several of the conditions tested in the previous test series were reexamined.

Table 36 and Table 40 summarize the different turbine spacings tested in this series. Table 39 and Table 41 summarize the data results obtained.

5. DISCUSSION OF RESULTS

This test program produced documentation on model wind turbine behavior for four different descriptive categories. These were single active or passive model wind turbine wakes, multi-turbine wakes, model turbine rotors dynamic performance and multi-turbine power performance interactions. Each of these four topics are discussed in the following sub-sections.

5.1. Single Wind Turbine Wake Behavior

In task 1 and 2 measurements of velocity deficits were obtained for a variety of different model wind turbines. Table 2 through Table 7 present this data set. The data from these tables is graphically summarized in Figure 27 through Figure 38. Figure 27 shows centerline vertical velocity deficit profiles at the downwind distance $X/D = 1$ for rotors 2, 3 and 6. Figure 28 through Figure 32 display similar information but at $X/D = 1.5, 2, 4, 6, 10$ respectively. Rotors # 2, 3 and 6 were the Graupner, the passive and the USWP design with a linear twist variation from base to tip of 20 to 10 degrees, respectively. Figure 33 and Figure 34 show centerline vertical velocity deficit profiles at downwind distances $X/D = 1, 1.5, 2, 4, 6, 10$ for Rotor # 2 (loaded) and Rotor # 3 respectively. Figure 35 displays the centerline downwind velocity deficit decay for rotors 2, 3 and 6.

The passive rotor's (# 3) screen was selected to produce the same centerline velocity deficit at $X/D = 1$ as the loaded Graupner rotor (# 2); thus, agreement between these data was expected at this distance. The figures show that the passive rotor tended to produce larger centerline wake deficits at about $X/D = 2$. This is a feature of passive devices also noted by Riley et. al. (1980). The agreement of centerline wake deficits for the passive rotor and the active rotors at downwind distances of $X/D = 6$ to 10 was quite good. The passive device tended to produce a larger wake deficit on the ground side of the rotor but performed well above hub height at most downwind distances. One potential modification to the passive rotor design that would reduce it's velocity deficit at lateral points would be to use a perforated plate for the conic section (see Figure 16). The wake behavior of the loaded and the unloaded Graupner rotor were very similar.

Figure 37 and Figure 38 present the radial velocity deficit profiles at the downwind distance $X/D = 1$ for rotors 2, 6, 8, 10 under unloaded and loaded conditions respectively. These data are tabulated in Table 6 and Table 7. These repeat measurements at a finer spacial resolution for rotors 2 and 6 produced similar results as noted in the previous paragraph. Rotors 8 (10 degree twist) and 10 (6 degree twist) based on the TNO type design behaved somewhat differently than other rotors. Both of these rotors showed a greater velocity deficit when unloaded as compared to a loaded condition. This result is most likely due in part to the greater tip speed ratio when the rotor is unloaded. The loaded Rotor # 10 produced the greatest velocity deficit at all radial distances.

The passive rotor would have to be redesigned to produce a greater initial deficit if it were to be used to predict this rotor's wake decay behavior.

5.2. Model Turbine Dynamic Performance

The objective of this portion of the study was to develop a 1:50 scale model wind turbine rotor that reproduced field turbine behavior well enough to simulate multiple turbine wake and power interactions. The USWP wind turbine being modeled was a variable pitch rotor that optimized power output at different approach wind speeds. Attention was focused on a field wind speed of 30 mph. At this wind speed the USWP wind turbine has a tip speed ratio of 5, a power coefficient of 0.36 and a thrust coefficient of 0.6. To produce conservative estimates of multiple turbine power performance interactions it was decided to find a model rotor that, 1) produced sufficient power performance to discern changes due to adjacent turbines, and 2) produced a thrust coefficient that was greater than the design value of 0.6.

Ten different model turbines were constructed and tested before a satisfactory design was obtained. The details of each turbine model were presented in section 4.2 and only rotors 2, 6, 8 and 10 will be discussed here.

The power performance data for these four rotors are listed in Table 10, Table 11, Table 13 and Table 15. The data in these tables are graphically presented in Figure 36. Also shown in Figure 36 is the USWP wind turbine operational point of modeling interest; ie. a power coefficient of 0.36 at a tip speed ratio of 5.0. Rotor # 10 satisfactorily replicated field turbine power behavior at the design wind speed of 30 mph.

The thrust coefficient for these model rotors was obtained by two different methods. The first was via integration of radial velocity and pressure profiles in the turbine wake at $X/D = 1$ and the second was via direct measurement on a force balance. The velocity and pressure profile data for these rotors were presented in Table 6 and Table 7. Figure 37 and Figure 38 show the velocity deficit profiles for unloaded and loaded conditions. Figure 39 and Figure 40 show the static pressure profiles for unloaded and loaded conditions. In these figures it is seen that both the velocity deficit and the pressure deficit increase with decreasing load on the rotors 8 and 10. Since both these terms are additive in the calculation of the thrust coefficient, a decreased load caused a larger rotor thrust. Table 8 provides a summary of the thrust coefficient calculations for both the wake integration technique and the direct measurement technique. The direct measurement technique was the more difficult but more accurate technique for finding the turbines thrust coefficient. The direct measurement value of the thrust coefficient for a loaded Rotor # 10 was 0.93.

The Power Performance and Thust Coefficients (0.36 and 0.93, respectively) measured for Rotor # 10 at a tip speed ratio of 5 are very similar to the rotor performance characteristics found by earlier

researchers (Vermueulen, 1978; Cao and Wentz, 1987). Fortunately, although the thrust coefficients are not the same as those expected for the USWP rotor, measurements by Baker et. al. (1984) show that the average centerline wake velocity deficits measured behind a turbine are not sensitive to even a 50% variation in thrust coefficient magnitude.

5.3. Multiple Wind Turbine Wake Behavior

During task 5 measurements of velocity deficits were obtained for six different multiple wind turbine spacings. Table 24 describes these spacing arrangements. Table 27 through Table 33 present this data set. The data from these tables is graphically summarized in Figure 41 through Figure 53.

Figure 41 through Figure 46 display for each run respectively the centerline ($Y/D = 0$) vertical velocity deficit profiles at downwind distances $X/D = 6.67, 10, 15, 20, 30$. Figure 41 displays these profiles for Run 2 which had three sixty foot turbines spaced eighty feet apart symmetric to tunnel centerline. The velocity deficit at $Z/D = 1$ decreases with increasing downwind distance, X/D , and the wake expands (look at 0 % crossing) in height with increasing X/D . Continuity of mass requires that the low speed wake region immediately downwind of the rotor disk induces a narrowing of streamlines and an acceleration of velocity at larger radial distances from the turbine axis. Thus, negative deficits (larger velocities) of -2 to -3 % exist at $Z/D = 3$ at all downwind distances. The deficit near the ground at $Z/D = 0.5$ was greater at all downwind stations than the deficit at $Z/D = 1.5$.

Figure 42 displays the profiles for Run 3 which had two 140 foot tower-turbines spaced eighty feet apart symmetric to tunnel centerline. This figure shows a similar decay pattern as the three 60 foot tower-turbines in Run 2, which indicates that the two off-center 140 foot tower-turbine wakes must have merged together by the first downwind measurement position, $X/D = 6.67$.

Run 4 (shown in Figure 43) also had eighty foot lateral spacing but two 140 foot towers were placed 50 foot downwind of the three 60 foot tower-turbines. The wake deficit of the two off-centerline 140 foot tower ($Z/D = 2.25$) turbines is as strong as the on-centerline 60 foot tower ($Z/D = 1$) turbine at a downwind distance $X/D = 6.67$. The wakes from the 60 foot and 140 foot tower-turbines have fully merged losing the double peak profile shape by the downwind distance of $X/D = 15$. Figure 44, Figure 45 and Figure 46 display runs 5, 6 and 7 where lateral spacing for the five turbines was increased to 100, 120 and 160 feet respectively. These figures show a progressive decline in the magnitude of the two 140 foot tower-turbines influence on centerline velocity deficits with increasing turbine spacing in the near field. Also seen is a progressive decline in the maximum velocity deficit at $X/D = 30$ from 15 % with 80 foot spacing to 5 % with 160 foot spacing.

Figure 47 and Figure 48 display the centerline ($Y/D = 0$) downwind velocity deficit decay for each run at heights $Z/D = 1$ and $Z/D = 2.25$

respectively. From Figure 47 it is seen that in run 2 the two 60 foot tower-turbines 80 feet to the side of the center turbine must be increasing the magnitude of the wake since lateral spacings of 100 feet and greater show an initial deficit of 15 % as compared to 20 % at $X/D = 6.67$. The velocity deficits increasing at between $X/D = 6.67$ and 15 indicates the 60 foot and 140 foot tower-turbine wake are merging at this point. Figure 48 shows that with the 80 foot turbine spacing the wakes at height $Z/D = 2.25$ have merged by $X/D = 6.67$, and larger turbine spacings result in wakes which merge at points further downwind ($X/D = 10$). The 60 foot tower-turbine wakes appear to have merge into the 140 foot tower-turbine wakes near the downwind distance $X/D = 15$.

Figure 49, Figure 50 and Figure 51 show the centerline vertical velocity deficit profiles for all runs at the downwind distance $X/D = 6.67$, 15 and 30 respectively. Figure 49 for $X/D = 6.67$ clearly shows the combining of the 60 and the 140 foot tower-turbine wakes. Separations of greater than 80 feet for the two 140 foot tower-turbines show a marked decrease in the centerline velocity deficit. Figure 50 shows that by the downwind distance $X/D = 15$ the wake of the 60 foot and the 140 foot tower-turbines have fully merged. There is a progressive decline in the velocity deficit with increasing turbine spacing. The data for Run 4 in Figure 51 appears abnormally high. This result remains unexplained.

Figure 52 through Figure 57 display for each run the vertical velocity profiles at lateral positions $Y/D = -1.67, 0, 1.67$ (-100, 0, 100 feet) at downwind position $X/D = 20$. Figure 52 displays an asymmetric wake for Run 2, three 60 foot tower-turbines with 80 foot lateral spacing. This asymmetry is most prominent in Run 4, Figure 54, where all five turbines with 80 foot spacings are on. The asymmetry declines with the 100 foot spacing in Run 5, see Figure 55, and is gone with 120 and 160 foot spacings in runs 6 and 7 (see Figure 56 and Figure 57). This asymmetry is not seen in Run 3, Figure 53, where only the two 140 foot tower-turbines at 80 foot spacing were operating. It is felt that the pattern of this asymmetric behavior is too consistent to be an error in the experimental program. This behavior is possibly due to the interaction between the rotating turbine wakes and a developing boundary layer in the wind tunnel.

5.4. Multiple Wind Turbine Power Performance Interaction

In Task 6 three different test series were performed. The test programs for these test series are shown in Table 34, Table 35, Table 36 and Table 40. The data for the first and second test series are listed in Table 37 and Table 38. The data for the third test series are listed in Table 39 and Table 41. The homogeneity of the wind tunnel mean turbulent velocity field approaching the wind turbines was approximately ± 4 percent. Thus when comparing power coefficients in and between these different data sets it should be remembered that a 3.3 percent error in the measurement of mean turbulent velocity would cause a 10 percent error in the power coefficient. The data results for these test series are graphically summarized as power coefficient versus tip speed ratio in Figure 58 through Figure 72.

5.4.1. *First Test Series*

The data results for the first test series are shown in Figure 58 and Figure 59. Figure 58 compares the power performance data for runs 1 through 6. This sequence of tests was designed to look at the effect of two upwind 140 foot tower-turbine structures on the performance of a downwind 60 foot tower-turbine. Runs 1 and 2 are reference data points for the cases of 3-60 foot tower-turbines with only the middle turbine on and 3-60 foot tower-turbines all on. Runs 3 and 5 show the influence of the 140 foot tower with the turbine off for positions 50 foot directly upwind and 50 foot upwind but offset laterally 20 feet. These data points show a marked decrease (-15 %) in performance due to the presence of the upwind 140 foot tower structure. Runs 4 and 6 show the influence of these same two positions but with the upwind turbines on. They show that the downwind 60 foot tower-turbines gain a benefit from flow accelerations around and below the 140 foot tower-turbines but only for the 20 foot laterally offset case is this benefit enough to compensate for losses due to the tower's wake. The offset lateral position produced about a 5 to 6 % better power performance than the directly upwind case.

Figure 59 compares the power performance data for runs 7 through 10. This sequence of tests was designed to look at the effect of three upwind 60 foot tower-turbine structures on the power performance of a downwind 140 foot tower-turbine. Run 7 is a reference data point for the case of 2-140 foot tower-turbines with only one on and no 60 foot tower-turbines in the tunnel. In runs 8, 9 and 10 all five turbines were operating, but different upwind positions of the three 60 foot tower-turbines were employed. There wasn't much difference in power performance between the three positions of the upwind 60 foot tower-turbines. In all cases flow accelerations over the 60 foot array improved the power performance of the downwind 140 foot tower-turbines by 14 percent.

Runs 11 through 18 were designed to look at the power performance changes at the center 60 foot tower-turbine as the result of different lateral spacings of the adjacent 60 foot tower-turbines. Since only single data points were obtained for each of these tests no figures are presented. The reader should refer back to the data summary in Table 37 for this discussion. Runs 11, 13, 15 and 17 were for lateral spacings of 80, 100, 120 and 160 feet, but only the center turbine was operating. Runs 12, 14, 16 and 18 were for the lateral spacings with all three turbines operating. The percent improvement in power performance between the lateral turbines on and off conditions for each of these spacings was 4.3 %, 3 %, 3.5 % and 2.6-3.5 % respectively.

5.4.2. *Second Test Series*

During the second test series the turbulence generating entrance grid was inadvertently inserted upside down. This resulted in an inconsistent reference mean velocity with respect to the data in test series one and three. Since power is proportional to the cube of velocity large comparative errors may exist between this data set and the others.

The data results for the second test series are show in Figure 60, Figure 61 and Figure 62.

Figure 60 compares the power performance data for runs 19 through 22 and includes the data from the first test series for runs 1 and 4. This sequence of tests was designed to look at the effect of two upwind 130 foot tower-turbine structures on the performance of a downwind 60 foot tower-turbine. Runs 19 and 1 provide data for the case of 3-60 foot tower-turbines with only the middle turbine on. Run 20 shows the influence on the 60 foot tower-turbine (one of three on) of a non-operating 130 foot tower for a position 50 foot directly upwind. Run 21 shows the influence on the 60 foot tower-turbine (three of three on) of a non-operating 130 foot tower for a position 50 feet directly upwind . Run 22 and 4 show the influence at the same position but with the upwind, 130 or 140 foot tower-turbines on respectively. Examination of the data in this figure leads one to similar conclusions to those noted for Figure 58 and the 140 foot towers. There is little observable difference between the 130 and 140 foot high tower data. That is:

- 1) There is a marked decrease in performance due to the presents of the upwind 130 foot tower structure,
- 2) The downwind 60 foot tower-turbines gain a benefit from flow accelerations around and below the 130 foot tower-turbines, and
- 3) With the 130 foot tower-turbine directly upwind of the 60 foot tower-turbine the increased performance due to flow accelerations does not overcome the losses due to the tower wake.

Flow channeling resulting from the presence of two operating lateral 60 foot tower-turbines helps to overcome the loss of performance due to the upwind 140 foot tower wake.

Figure 61 compares the power performance data for runs 23, 24, 25, 26 and runs 7 and 10 from the first test series. This sequence of tests was designed to look at the effect of three upwind 60 foot tower-turbine structures on the power performance of a downwind 130 foot tower-turbine. Runs 23 and 25 provided reference data conditions for the consideration of all five turbines in the tunnel but with only one 130 foot tower-turbine operational. In runs 24 and 25 all five turbines were operating, but different upwind positions of the three 60 foot tower-turbines were stipulated. The position where the 60 foot tower-turbines were directly upwind of the 130 foot tower-turbines (runs 23 and 24) show a very slight improvement in power performance over those in which the 60 foot tower-turbine array was offset laterally by 40 feet (runs 25 and 26). This is in contrast to the 140 foot tower cases (runs 7 and 10) where no difference was observed. In all cases flow accelerations over 60 foot tower arrays improved the power performance of the downwind 130 foot tower-turbines by 14 percent.

Figure 62 compares the power performance data for runs 19, 27 and 28. This test sequence was designed to look at the effect of two downwind 140 foot tower-turbines on the power performance of an upwind 60 foot tower-turbine array. Run 19 provides a base case where the downwind 140

foot towers were not in the wind tunnel. Run 27 shows the case where the 140 foot towers are in the tunnel, but the turbines are not active. Run 28 provides data for the situation when all five turbines were operating. Observation of the data in this figure show that there is little influence on the 60 foot tower-turbine by the introduction of a 140 foot tower but when the 140 foot tower-turbines are active there appears to be a loss of performance by roughly from 2 to 4 percent.

5.4.3. *Third Test Series*

The purpose of this test series was to investigate more thoroughly the effect of downwind 140 foot and 130 foot tower-turbines on the power performance of an upwind 60 foot tower-turbine array. These tests employed a considerably improved data acquisition technique. For each position tested a reference run was obtained where the 140 or 130 foot tower-turbines were inactive. The reference runs for the 140 foot tower case were runs 29, 31, 33, 35 and 37. The data where all five turbines were operating for the 140 foot tower case were runs 30, 32, 34, 36 and 38. Each active run along with its reference run are presented in Figure 63 through Figure 67. The reference runs for the 130 foot tower case were runs 39, 42 and 44. The data where all five turbines were operating for the 130 foot tower case were runs 40, 43 and 45. Each active run along with its reference run are presented in Figure 68 through Figure 70. Observation of the data in these figures shows that there is no noticeable influence on the 60 foot tower-turbines power performance due to the operating condition of a downwind 130' or 140 foot tower-turbine at the positions tested.

Since these conclusions were in conflict with the 2 to 4 percent loss that was observed in the second test series an additional set of four runs were performed. Two of the tests repeated the second test series runs 27 and 28 (runs 46 and 47, see Figure 71) but with a entrance grid right-side-up. The other two of the tests repeated the second test series runs 27 and 28 (runs 48 and 49, see Figure 72) with a entrance grid up-side-down as was the case in the second test series. These figures show that for unknown reasons with the entrance grid up-side-down there is a 2 to 4 percent power loss whereas with the grid right-side-up there is no discernable difference.

REFERENCES

- Baker, R.W. and Walker, S.N., WAKE STUDIES AT THE GOODNOE HILLS MOD-2 SITE, Report to Bonneville Power Administration, Oregon State University, Report No. BPA 82-111, 89 pp. 1982.
- Baker, R.W., Walker, S.N. and Katen, P.C., WAKE STUDIES AT THE FLOWIND VERTICAL AXIS WIND TURBINE GENERATOR SITE, Oregon State University for Bonneville Power Administration, Portland, Oregon, Report No. 83-10, 77 pp., March, 1984.
- Bate, E.R., Jr, Lissaman, P.B.S. and Zalay, A.D., A STUDY TO ASSESS EFFECTS OF TURBINE WAKE INTERFERENCE ON ENERGY PRODUCTION FROM WIND TURBINE ARRAYS, Report to U.S. Dept. of Interior, Science Technology Associates Report STA FR 8101, 1981.
- Builtjes, P., WIND TURBINE WAKE EFFECTS, TNO Report 79-08375. Apeldoorn, The Netherlands, 1979.
- Builtjes, P.J.H., THE INTERACTION OF WINDMILL WAKES, Second Int. Symp. on Wind Energy Systems, pp. B5-49 to B5-58, October 3-6, 1978.
- Burley, R.R., Savino, J.M., Wagner, L.H. and Diedrich, J.H., SOME TECHNIQUES FOR REDUCING THE TOWER SHADOW OF THE DOE/NASA MOD-0 WIND TURBINE TOWER, U.S. Department of Energy, Nat'l Aeronautics and Space Administration, Lewis Research Center, September, 1979.
- Cao, H.V. and Wentz, W.H., Jr., PERFORMANCE AND AERODYNAMIC BRAKING OF A HORIZONTAL-AXIS WIND TURBINE FROM SMALL-SCALE WIND TUNNEL TESTS, U.S. Department of Energy, Lewis Research Center, Conservation and Renewable Energy, Wind/Ocean Technology Division, July, 1987.
- Connell, J., A NEW LOOK AT TURBULENCE EXPERIENCED BY A ROTATING BLADE, Proceedings of ASME Wind Energy Symposium, Houston, TX, February, 1984.
- Faxen, T., WAKE INTERACTION IN AN ARRAY OF WINDMILLS: Theory and Preliminary Results, Second Int'l. Symposium on Wind Energy Systems, pp. B6-59 to B6-72, October, 1978.
- Hadley, D. L. and Renne, D.S., WAKE RESEARCH IN THE FEERAL WIND ENERGY PROGRAM, Workshop on Wind Characteristics, Minneapolis, MN, June, 1983.
- Meroney, R.N., CHARACTERISTICS OF WIND AND TURBULENCE IN AND ABOVE MODEL FORESTS, Journal of Applied Meteorology, Vol. 4, No. 5, pp. 780-788, October, 1968.

- Meroney, R.N. WIND IN THE PERTURBED ENVIRONMENT: ITS INFLUENCE ON WECS, Proceedings of AWEA Spring Conference, Boulder, CO, 27 pp., May 11-14, 1977.
- Meroney, R.N., TURBULENT DIFFUSION NEAR BUILDINGS, Engineering Meteorology, Chapter 11, E.J. Plater, Ed., Elsevier Scientific Pub. Co., Amsterdam, pp. 481-525, 1982.
- Meroney, R.N., GUIDELINE FOR FLUID MODELING OF LIQUEFIED NATURAL GAS CLOUD DISPERSION, Vol. II: Technical Support Document, Final Document for Gas Research Institute, Contract No. 5083-252-0962, May, 1986.
- Milborrow, D.J., THE PERFORMANCE OF ARRAYS OF WIND TURBINES, Report for Central Electricity Research Laboratories, Journal of Industrial Aerodynamics, 5, pp. 403-30, 1980.
- Neff, D.E. and Meroney, R.N., MEASUREMENT IN A WIND TUNNEL OF THE MODIFICATION OF MEAN WIND AND TURBULENCE CHARACTERISTICS DUE TO INDUCTION EFFECTS NEAR WIND TURBINE ROTORS, Report for Pacific Northwest Laboratories, CER85-86DEN-RNM10, October, 1985.
- Rae, W.H., Jr. and Pope, A., LOW-SPEED WIND TUNNEL TESTING, Wiley-Interscience Publication, 1984.
- Riley, J.J., Geller, E.W., Coon, M.D. and Schedvin, J.C., A REVIEW OF WIND TURBINE WAKE EFFECTS, Dept. of Energy Report, DOE/ET/23160-80/1, Flow Research Company, 118 pp., 1980.
- Savineo, J.M. and Wagner, J.M., WIND TUNNEL MEASUREMENTS OF THE TOWER SHADOW ON MODELS OF THE ERDA/NASA 100 KW WIND TURBINE TOWER, NASA Technical Memorandum, Lewis Research Center, Cleveland, OH, November, 1976.
- Snyder, W.H., GUIDELINES FOR FLUID MODELING OF ATMOSPHERIC DIFFUSION, EPA Report EPA-600/8-81-009, 185 pp., 1981.
- Taylor, P.A., WAKE DECAY AND POWER REDUCTION IN WIND FARM ARRAYS--AN APPLICATION TO THE ARRAY PROPOSED FOR THE KAHUKU HILLS, Wind Engineering, Vol. 4, No. 2, pp. 760-79, 1980.
- Templin, J., AN ESTIMATE OF THE INTERACTION OF WINDMILLS IN WIDESPREAD ARRAYS, National Research Council of Canada, LTR-LA-171, 1974.
- Troller, T., MORGAN SMITH WIND-TURBINE SITE TESTS, Summary Report, June, 1940.
- Vermeulen, P.E.J., STUDIES OF THE WAKE STRUCTURE OF MODEL WIND TURBINE GENERATORS, Department of Fluid Flow Technology, Apeldoorn, The Netherlands, November, 1979.

Vermeulen, P. A WIND TUNNEL STUDY OF THE WAKE OF A HORIZONTAL AXIS WIND TURBINE, Organization for Industrial Research, Apeldoorn, The Netherlands, September, 1978.

Vermeulen, P.E.J. and Builtjes, P.J.H., MATHEMATICAL MODELLING OF WAKE INTERACTION IN WIND TURBINE ARRAYS, Part I, Description and Evaluation of the Mathematical Model, Organization for Industrial Research, Apeldoorn, The Netherlands, February, 1981.

TABLES

Table 1 TASK 1 Sixty Foot Tower Wake Data

		Normalized Velocity								
X/D =		1.00	1.50	2.00	4.00	6.00	7.00	8.00	9.00	10.00
Z/D										
0.33		0.92	0.90	0.90	0.94	0.98	0.99	1.01	1.01	1.03
0.67		0.91	0.94	0.96	1.01	1.05	1.05	1.06	1.06	1.06
1.08		0.97	0.98	0.99	1.00	1.02	1.02	1.03	1.04	1.04
1.50		1.00	1.00	1.00	1.01	1.02	1.02	1.02	1.03	1.04
2.00		1.01	1.01	1.01	1.02	1.02	1.02	1.03	1.03	1.04
2.50		0.99	1.00	1.00	1.01	1.02	1.01	1.02	1.02	1.03
REF (m/s)		9.46	9.37	9.40	9.43	9.30	9.47	9.39	9.43	9.33

Table 2 TASK 1 Rotor # 2 Loaded Wake Data

		X Velocity Deficits Normalized w.r.t. Tower Only Data								
X/D =		1.00	1.50	2.00	4.00	6.00	7.00	8.00	9.00	10.00
Z/D										
0.33		-2	-1	-2	1	-0	0	0	0	-1
0.67		10	11	12	13	14	13	12	12	9
1.08		51	45	41	35	27	24	21	19	15
1.50		23	21	19	14	11	10	9	8	7
2.00		-1	-1	-1	-1	-1	-2	-1	-1	-0
2.50		-2	-1	-2	-1	-1	-1	-2	-1	-1

notes: Tunnel Wind Speed = 9.3 m/s

Table 3 TASK 1 Rotor # 2 Unloaded Wake Data

		X Velocity Deficits Normalized w.r.t. Tower Only Data								
X/D =		1.00	1.50	2.00	4.00	6.00	7.00	8.00	9.00	10.00
Z/D										
0.33		-1	0	-1	1	0	0	0	-0	-2
0.67		11	10	9	10	10	9	9	8	5
1.08		52	43	38	30	24	22	20	18	13
1.50		15	14	13	10	9	9	8	8	6
2.00		-1	-0	-0	-0	-1	-1	-1	-1	-0
2.50		-1	-1	-1	-1	-1	-1	-1	-1	-1

notes: Tunnel Wind Speed = 9.3 m/s

Table 4 TASK 1 Passive Device Wake Data

% Velocity Deficits Normalized w.r.t. Tower Only Data

X/D =	1.00	1.50	2.00	4.00	6.00	7.00	8.00	9.00	10.00
Z/D									
0.33	-6	-3	-2	2	3	3	3	4	3
0.67	44	31	27	20	18	16	15	14	13
1.08	54	51	49	37	26	22	20	18	16
1.50	34	24	18	14	12	11	9	9	8
2.00	-2	-1	-2	-1	-2	-2	-2	-2	-2
2.50	-3	-2	-2	-2	-1	-2	-2	-1	-1

notes: Tunnel Wind Speed = 9.3 m/s

Table 5 TASK 2 Rotor # 6 Loaded Wake Data

% Velocity Deficits Normalized w.r.t. Tower Only Data

X/D =	1.00	1.50	2.00	4.00	6.00	7.00	8.00	9.00	10.00
Z/D									
0.33	1	-3	-4	4					
0.67	19	21	21	22					
1.08	53	46	40	32					
1.50	17	15	13	8					
2.00	-3	-3	-3	-2					
2.50	-4	-4	-4	-3					

notes: Tunnel Wind Speed = 9.3 m/s

Table 6 TASK 2 Graupner and USWP 10-20 Rotor Thrust Data

ROTOR		Graupner (#2)		Graupner (#2)		USWP 10-20 (#6)		USWP 10-20 (#6)	
Uref (m/s)	=	9.4		9.4		9.3		9.3	
LOAD (in-oz)	=	0.3		6.5		1.5		1.5	
Speed (rpm)	=	2700.0		1900.0		2750.0		2750.0	
Position X/D	=	1.0		1.0		1.0		2.0	
r/R		Pressure	Velocity	Pressure	Velocity	Pressure	Velocity	Pressure	Velocity
		(mmHg)	(% deficit)	(mmHg)	(% deficit)	(mmHg)	(% deficit)	(mmHg)	(% deficit)
0.000		-0.025	51.8	-0.045	54.2	-0.026	57.2	-0.014	41.4
0.330		-0.012	23.6	-0.019	28.6	-0.019	28.3	-0.011	27.7
0.660		-0.007	13.2	-0.010	22.1	-0.010	18.7	-0.007	18.9
1.000		-0.007	2.6	-0.018	6.4	-0.013	9.0	-0.008	6.6
1.330		-0.008	-0.5	-0.009	-1.0	-0.008	-1.3	-0.007	-0.3
2.000		0.002	-1.3	0.000	-1.0	0.000	-0.2	-0.001	0.0
3.000		0.005	0.5	0.004	0.1	0.005	-0.9	0.002	0.0

Table 7 TASK 2 TNO 10 and TNO 6 Rotor Thrust Data

ROTOR		TNO 10 (#8)		TNO 10 (#8)		TNO 8 (#10)		TNO 6 (#10)	
Uref (m/s)	=	9.4		9.4		9.2		9.2	
LOAD (in-oz)	=	0.3		6.5		0.3		5.5	
Speed (rpm)	=	2600.0		1700.0		3850.0		2750.0	
Position X/D	=	1.0		1.0		1.0		1.0	
r/R		Pressure	Velocity	Pressure	Velocity	Pressure	Velocity	Pressure	Velocity
		(mmHg)	(% deficit)						
0.000		-0.050	71.2	-0.037	55.5	-0.080	95.0	-0.058	90.7
0.330		-0.050	57.6	-0.032	31.5	-0.084	89.9	-0.061	75.1
0.660		-0.037	41.4	-0.020	26.6	-0.085	76.8	-0.052	52.3
1.000		-0.035	14.4	-0.039	13.9	-0.080	63.3	-0.051	57.1
1.330		-0.025	-2.7	-0.015	-2.1	-0.092	23.9	-0.056	-1.0
2.000		-0.014	-1.6	-0.006	-1.3	-0.045	-6.6	-0.023	-3.5
3.000		-0.002	-1.6	0.003	-1.2	-0.021	-3.8	-0.009	-2.9

Table 8 TASK 2 Rotors # 2, 6, 8, 10 Thrust Coefficient Data

ROTOR No.	=	# 2	# 2	# 6	# 6	# 8	# 8	# 10	# 10
Desc.	=	Graupner	Graupner	USWP 10-20	USWP 10-20	TNO 10	TNO 10	TNO 6	TNO 6
Uref (m/s)	=	9.4	9.4	9.3	9.3	9.4	9.4	9.2	9.2
LOAD (in-oz)	=	0.3	6.5	1.5	1.5	0.3	6.5	0.3	5.5
Speed (rpm)	=	2700.0	1900.0	2750.0	2750.0	2600.0	1700.0	3850.0	2750.0
Position X/D	=	1.0	1.0	1.0	2.0	1.0	1.0	1.0	1.0
Ct (r/R=1)	=		0.632	0.372	0.349			0.983	0.710
Ct (r/R=2)	=								
Ct (r/R=3)	=		0.362	0.370	0.370			1.350	0.860
Ct (direct)	=	0.280				0.690		1.120	0.930

note: Ct is the thrust coefficient

Table 9 TASK 1 Rotor # 2 Power Test with Pulley Drive

Speed RPM	Torque in-oz	Drive Eff.	Turbine Power (watts)	Power Coeff.	Tip speed ratio
2300	0.50	0.35	2.43	0.06	4.76
2200	1.00	0.47	3.46	0.09	4.56
2060	2.00	0.52	5.86	0.15	4.27
2000	3.00	0.57	7.78	0.20	4.14
1880	4.00	0.57	9.76	0.25	3.89
1800	5.00	0.58	11.48	0.30	3.73
1700	6.00	0.61	12.37	0.32	3.52
1550	7.00	0.65	12.34	0.32	3.21

notes: Tunnel Wind Speed = 9.10 m/s
Turbine Blade Radius = 0.18 m

Table 10 TASK 2 Rotor # 2 Power Test with Chain Drive

Speed RPM	Torque in-oz	Drive Eff.	Turbine Power (watts)	Power Coeff.	Tip speed ratio
2600	0.30	0.88	0.66	0.02	5.33
2540	1.00	0.88	2.13	0.06	5.20
2370	2.00	0.88	3.98	0.11	4.85
2250	3.00	0.88	5.67	0.15	4.61
2150	4.00	0.88	7.23	0.19	4.40
2010	5.00	0.88	8.45	0.23	4.12
1900	6.00	0.88	9.58	0.26	3.89
1800	7.00	0.88	10.59	0.28	3.69
1690	8.00	0.88	11.36	0.30	3.46
1630	9.00	0.88	12.33	0.33	3.34
1520	9.50	0.88	12.13	0.32	3.11

notes: Tunnel Wind Speed (m/s) = 9.10
Turbine Blade Radius (m) = 0.18

Table 11 TASK 2 Rotor # 6 Power Performance Data

Speed RPM	Torque in-oz	Drive Eff.	Turbine Power (watts)	Power Coeff.	Tip speed ratio
3160	0.35	0.88	0.93	0.02	6.47
3100	0.50	0.88	1.30	0.03	6.35
2910	1.00	0.88	2.45	0.07	5.96
2710	1.50	0.88	3.42	0.09	5.55
2620	1.60	0.88	3.52	0.09	5.37

notes: Tunnel Wind Speed = 9.10 m/s
Turbine Blade Radius = 0.18 m

Table 12 TASK 2 Rotor # 7 Power Performance Data

Speed RPM	Torque in-oz	Drive Eff.	Turbine Power (watts)	Power Coeff.	Tip speed ratio
3041	0.30	0.88	0.77	0.02	6.23
2650	2.50	0.88	5.57	0.15	5.43
2620	3.00	0.88	6.61	0.18	5.37
2425	3.50	0.88	7.13	0.19	4.97
2340	3.75	0.88	7.37	0.20	4.79

notes: Tunnel Wind Speed = 9.10 m/s
Turbine Blade Radius = 0.18 m

Table 13 TASK 2 Rotor # 8 Power Performance Data

Speed RPM	Torque in-oz	Drive Eff.	Turbine Power (watts)	Power Coeff.	Tip speed ratio
2540	0.30	0.88	0.64	0.02	5.20
2430	1.00	0.88	2.04	0.05	4.98
2390	1.50	0.88	3.01	0.08	4.90
2320	2.00	0.88	3.90	0.10	4.75
2300	2.50	0.88	4.83	0.13	4.71
2250	3.00	0.88	5.67	0.15	4.61
2200	3.50	0.88	6.47	0.17	4.51
2150	4.00	0.88	7.23	0.19	4.40
2020	4.50	0.88	7.64	0.20	4.14
1980	5.00	0.88	8.32	0.22	4.06
1840	5.50	0.88	8.50	0.23	3.77
1750	6.00	0.88	8.82	0.24	3.58
1700	6.50	0.88	9.29	0.25	3.48
1600	6.75	0.88	9.08	0.24	3.28
1530	6.90	0.88	8.87	0.24	3.13

notes: Tunnel Wind Speed = 9.10 m/s
Turbine Blade Radius = 0.18 m

Table 14 TASK 2 Rotor # 9 Power Performance Data

Speed RPM	Torque in-oz	Drive Eff.	Turbine Power (watts)	Power Coeff.	Tip speed ratio
3900	0.30	0.88	0.98	0.03	7.99
3300	3.00	0.88	8.32	0.22	6.76
3100	4.00	0.88	10.42	0.28	6.35
3030	4.50	0.88	11.46	0.31	6.21
2900	5.00	0.88	12.18	0.32	5.94
2700	5.75	0.88	13.05	0.35	5.53
2600	6.00	0.88	13.11	0.35	5.33
2450	6.20	0.88	12.76	0.34	5.02

notes: Tunnel Wind Speed (m/s) = 9.10
Turbine Blade Radius (m) = 0.18

Table 15 TASK 2 Rotor # 10 Power Performance Data

Speed RPM	Torque in-oz	Drive Eff.	Turbine Power (watts)	Power Coeff.	Tip speed ratio
3650	0.30	0.88	0.92	0.03	8.2
3500	1.00	0.88	2.94	0.10	7.9
3300	2.00	0.88	5.55	0.18	7.4
3120	3.00	0.88	7.87	0.26	7.0
2890	4.00	0.88	9.71	0.32	6.5
2550	5.00	0.88	10.71	0.36	5.7

notes: Tunnel Wind Speed (m/s) = 8.40
Turbine Blade Radius (m) = 0.18

Table 16 TASK 3 Rotor # 11 Power Performance Data

Speed RPM	Torque in-oz	Drive Eff.	Turbine Power (watts)	Power Coeff.	Tip speed ratio
3640	0.30	0.88	0.92	0.03	8.2
3500	1.00	0.88	2.94	0.10	7.9
3200	2.00	0.88	5.38	0.18	7.2
2910	3.00	0.88	7.34	0.24	6.5
2860	3.50	0.88	8.41	0.28	6.4
2500	3.90	0.88	8.19	0.27	5.6

notes: Tunnel Wind Speed (m/s) = 8.40
Turbine Blade Radius (m) = 0.18

Table 17 TASK 3 Rotor # 12 Power Performance Data

Speed RPM	Torque in-oz	Drive Eff.	Turbine Power (watts)	Power Coeff.	Tip speed ratio
3550	0.30	0.88	0.89	0.03	8.0
3400	1.00	0.88	2.86	0.09	7.6
3120	2.00	0.88	5.24	0.17	7.0
2800	3.00	0.88	7.06	0.23	6.3
2650	3.50	0.88	7.79	0.26	5.9
2500	3.75	0.88	7.88	0.26	5.6

notes: Tunnel Wind Speed (m/s) = 8.40
Turbine Blade Radius (m) = 0.18

Table 18 TASK 3 Rotor # 13 Power Performance Data

Speed RPM	Torque in-oz	Drive Eff.	Turbine Power (watts)	Power Coeff.	Tip speed ratio
3500	0.30	0.88	0.88	0.03	7.9
3330	1.00	0.88	2.80	0.09	7.5
3160	2.00	0.88	5.31	0.18	7.1
2930	3.00	0.88	7.39	0.24	6.6
2550	4.00	0.88	8.57	0.28	5.7

notes: Tunnel Wind Speed (m/s) = 8.40
Turbine Blade Radius (m) = 0.18

Table 19 TASK 3 Rotor # 14 Power Performance Data

Speed RPM	Torque in-oz	Drive Eff.	Turbine Power (watts)	Power Coeff.	Tip speed ratio
3600	0.30	0.88	0.91	0.03	8.1
3530	1.00	0.88	2.97	0.10	7.9
3250	2.00	0.88	5.46	0.18	7.3
2920	3.00	0.88	7.38	0.24	6.6
2550	4.00	0.88	8.57	0.28	5.7

notes: Tunnel Wind Speed (m/s) = 8.40
Turbine Blade Radius (m) = 0.18

Table 20 TASK 3 Rotor # 15 Power Performance Data

Speed RPM	Torque in-oz	Drive Eff.	Turbine Power (watts)	Power Coeff.	Tip speed ratio
3620	0.30	0.88	0.91	0.03	8.1
3530	1.00	0.88	2.97	0.10	7.9
3200	2.00	0.88	5.38	0.18	7.2
2800	3.00	0.88	7.06	0.23	6.3
2700	3.50	0.88	7.94	0.26	6.1
2500	3.75	0.88	7.88	0.26	5.6

notes: Tunnel Wind Speed (m/s) = 8.40
Turbine Blade Radius (m) = 0.18

Table 21 TASK 3 Rotor # 16 Power Performance Data

Speed RPM	Torque in-oz	Drive Eff.	Turbine Power (watts)	Power Coeff.	Tip speed ratio
3600	0.30	0.88	0.91	0.03	8.1
3550	1.00	0.88	2.98	0.10	8.0
3350	2.00	0.88	5.63	0.19	7.5
3160	3.00	0.88	7.97	0.26	7.1
3050	3.50	0.88	8.97	0.30	6.8
2900	4.00	0.88	9.75	0.32	6.5
2780	4.50	0.88	10.51	0.35	6.2
2560	5.00	0.88	10.76	0.36	5.7

notes: Tunnel Wind Speed (m/s) = 8.40
Turbine Blade Radius (m) = 0.18

Table 22 TASK 4 Disturbed Flow Test Locations

X	Y (ft)	Z (ft)	X/D (ft)	Y/D	Z/D
-60	0	45	-1.00	0.00	0.75
-60	0	60	-1.00	0.00	1.00
-60	0	75	-1.00	0.00	1.25
-60	0	90	-1.00	0.00	1.50
-60	0	135	-1.00	0.00	2.25
-60	0	150	-1.00	0.00	2.50
-60	0	200	-1.00	0.00	3.33
-60	60	45	-1.00	1.00	0.75
-60	60	60	-1.00	1.00	1.00
-60	60	75	-1.00	1.00	1.25
-60	60	90	-1.00	1.00	1.50
-60	60	135	-1.00	1.00	2.25
-60	60	150	-1.00	1.00	2.50
-60	60	200	-1.00	1.00	3.33
0	60	45	0.00	1.00	0.75
0	60	60	0.00	1.00	1.00
0	60	75	0.00	1.00	1.25
0	60	90	0.00	1.00	1.50
0	60	135	0.00	1.00	2.25
0	60	150	0.00	1.00	2.50
0	60	200	0.00	1.00	3.33
0	120	45	0.00	2.00	0.75
0	120	60	0.00	2.00	1.00
0	120	75	0.00	2.00	1.25
0	120	90	0.00	2.00	1.50
0	120	135	0.00	2.00	2.25
0	120	150	0.00	2.00	2.50
0	120	200	0.00	2.00	3.33

note: D = 60 feet

Table 23 TASK 4 Disturb Flow Normalized Data

Z/D	X/D = -1.00	-1.00	0.00	0.00	Z ft
0.75	0.98	0.98	0.99	1.00	45
1.00	0.99	0.99	1.00	0.99	60
1.25	0.99	0.99	1.00	1.00	75
1.50	0.99	0.99	1.01	1.00	90
2.25	1.00	0.98	1.00	1.00	135
2.50	1.01	1.00	1.01	1.00	150
3.33	1.01	1.01	1.01	1.00	200

X ft = -60 -60 0 0
Y ft = 0 60 60 120

notes: D = 60 feet
Tunnel Wind Speed = 10 m/s

Table 26 TASK 5 Tunnel Only Velocity Data

	X/D = 6.67	10.00	15.00	20.00	20.00	20.00	25.00	30.00
Z/D	0.00	0.00	0.00	-1.67	0.00	1.67	0.00	0.00
0.50	0.87	0.88	0.89	0.86	0.90	0.90	0.92	0.94
0.75	0.90	0.90	0.91	0.88	0.92	0.92	0.94	0.96
1.00	0.91	0.91	0.92	0.89	0.93	0.93	0.95	0.97
1.25	0.92	0.92	0.93	0.90	0.94	0.94	0.96	0.97
1.50	0.93	0.93	0.94	0.92	0.95	0.94	0.97	0.98
1.75	0.94	0.94	0.94	0.92	0.95	0.94	0.97	0.98
2.00	0.95	0.95	0.95	0.93	0.96	0.95	0.98	1.00
2.25	0.95	0.95	0.95	0.93	0.96	0.95	0.98	1.00
2.50	0.94	0.94	0.95	0.93	0.96	0.95	0.98	1.00
3.00	0.93	0.94	0.94	0.92	0.95	0.95	0.97	1.00
3.33	0.96	0.95	0.96	0.94	0.97	0.97	0.99	1.02
Ref (m/s) =	9.92	9.85	9.88	9.88	9.89	9.84	9.82	9.80
D =	60 feet							

Table 27 TASK 5 Tower Wake Deficits, Test 2a

	X/D = 6.67	10.00	15.00	20.00	25.00	30.00	20.00	20.00
Z/D	0.00	0.00	0.00	0.00	0.00	0.00	-1.67	1.67
0.50	5	5	3	3	4	4	4	2
0.75	7	5	3	3	3	3	4	2
1.00	6	5	3	2	3	3	3	2
1.25	4	3	2	2	2	2	3	1
1.50	1	2	1	1	2	2	2	0
1.75	-1	1	0	1	1	1	1	0
2.00	-1	1	0	0	1	2	1	0
2.25	0	2	-1	0	1	1	1	-1
2.50	-1	1	-1	-1	0	0	0	-2
3.00	-2	0	-2	-2	-1	0	-1	-2
3.33	1	1	-1	-1	0	0	0	0

note: D = 60 feet

Table 28 TASK 5 Wake Deficits for Test 2

	X/D = 6.67	10.00	15.00	20.00	25.00	30.00	20.00	20.00
Z/D	0.00	0.00	0.00	0.00	0.00	0.00	-1.67	1.67
0.50	13	14	12	11	10	9	4	4
0.75	18	16	13	11	9	9	5	3
1.00	20	16	13	11	9	8	7	4
1.25	17	14	12	9	8	7	7	3
1.50	11	11	9	8	6	6	6	3
1.75	3	6	6	5	4	5	4	2
2.00	0	3	3	3	3	3	4	1
2.25	-3	0	0	0	0	1	1	-1
2.50	-4	-2	-1	-1	-1	1	0	-1
3.00	-3	-2	-2	-3	-3	-2	-1	-2
3.33	-3	-2	-2	-3	-3	-2	-2	-2

note: D = 60 feet

Table 29 TASK 5 Wake Deficits for Test 3

	X/D = 6.67	10.00	15.00	20.00	25.00	30.00	20.00	20.00
Y/D =	0.00	0.00	0.00	0.00	0.00	0.00	-1.67	1.67
Z/D								
0.50	-1	-2	-2	0	0	1	-4	-3
0.75	-1	-2	-2	0	0	1	-4	-4
1.00	-1	-2	-1	1	2	3	-4	-3
1.25	0	0	2	4	4	5	-3	-2
1.50	2	4	6	6	6	7	-2	-1
1.75	8	9	11	9	7	8	0	0
2.00	16	13	13	11	8	8	1	1
2.25	20	15	15	11	9	9	1	2
2.50	18	14	14	12	9	9	2	3
3.00	3	6	8	7	5	6	1	2
3.33	-1	1	2	4	3	4	0	1

note: D = 60 feet

Table 30 TASK 5 Wake Deficits for Test 4

	X/D = 6.67	10.00	15.00	20.00	25.00	30.00	20.00	20.00
Y/D =	0.00	0.00	0.00	0.00	0.00	0.00	-1.67	1.67
Z/D								
0.50	14	15	15	14	12	13	2	-4
0.75	20	17	16	16	14	14	5	-2
1.00	19	16	17	16	14	15	7	-1
1.25	14	15	17	17	14	15	7	0
1.50	9	14	17	16	14	15	6	0
1.75	9	14	17	15	13	13	4	-1
2.00	15	16	16	14	11	12	2	-2
2.25	19	16	15	13	9	10	1	-3
2.50	17	13	12	10	7	8	-1	-2
3.00	-1	1	5	5	3	4	-2	-3
3.33	-7	-5	-1	0	-1	1	-4	-5

note: D = 60 feet

Table 31 TASK 5 Wake Deficits for Test 5

	X/D = 6.67	10.00	15.00	20.00	25.00	30.00	20.00	20.00
Y/D =	0.00	0.00	0.00	0.00	0.00	0.00	-1.67	1.67
Z/D								
0.50	10	10	10	10	8	7	6	2
0.75	15	12	12	11	10	8	8	3
1.00	14	12	12	12	11	9	9	4
1.25	12	11	12	12	12	9	8	5
1.50	7	10	13	12	11	9	7	5
1.75	4	9	13	12	11	9	6	4
2.00	6	10	12	11	9	7	3	2
2.25	8	10	11	9	8	6	2	1
2.50	5	7	9	8	6	4	1	1
3.00	-5	-1	4	2	2	1	-2	-2
3.33	-7	-5	-1	-1	-1	-1	-3	-3

note: D = 60 feet

Table 32 TASK 5 Wake Deficits for Test 6

Z/D	X/D = 6.67	10.00	15.00	20.00	25.00	30.00	20.00	20.00
	Y/D = 0.00	0.00	0.00	0.00	0.00	0.00	-1.67	1.67
0.50	11	7	7	5	5	6	4	5
0.75	15	10	9	7	7	7	5	7
1.00	15	10	9	8	8	8	6	8
1.25	12	9	10	8	8	8	6	9
1.50	7	8	9	8	8	8	6	8
1.75	3	7	9	8	8	8	6	7
2.00	3	6	9	7	7	7	5	6
2.25	3	6	7	6	6	6	3	4
2.50	1	4	6	5	4	5	2	3
3.00	-4	-2	1	1	1	2	0	0
3.33	-5	-4	-2	-2	-1	0	-2	-1

note: D = 60 feet

Table 33 TASK 5 Wake Deficits for Test 7

Z/D	X/D = 6.67	10.00	15.00	20.00	25.00	30.00	20.00	20.00
	Y/D = 0.00	0.00	0.00	0.00	0.00	0.00	-1.67	1.67
0.50	13	9	7	4	4	4	3	3
0.75	15	10	8	5	5	4	3	3
1.00	16	10	8	6	6	5	4	5
1.25	14	8	8	6	6	5	5	5
1.50	9	6	7	6	5	5	5	5
1.75	2	2	5	5	4	5	5	5
2.00	-2	-1	3	3	3	4	4	3
2.25	-2	-2	2	2	2	3	4	2
2.50	-2	-2	1	1	1	2	3	1
3.00	-3	-4	-1	-2	-1	0	2	-1
3.33	-3	-4	-2	-3	-2	-1	0	-2

note: D = 60 feet

Table 34 TASK 6 Series 1 Test Program

Run No.	Rotor 11			Rotor 14			Rotor 12			Rotor 16			Rotor 15			
	State	X	Y	Z	State	X	Y	Z	State	X	Y	Z	State	X	Y	Z
1	off	0	-80	60	data	0	0	60	off	0	80	60	out			
2	on	0	-80	60	data	0	0	60	on	0	80	60	out			
3	on	0	-80	60	data	0	0	60	on	0	80	60	off	-50	-80	140
4	on	0	-80	60	data	0	0	60	on	0	80	60	on	-50	-80	140
5	on	0	-80	60	data	0	0	60	on	0	80	60	off	-50	-60	140
6	on	0	-80	60	data	0	0	60	on	0	80	60	on	-50	-60	140
7	out				out				out				off	0	-80	140
8	on	-50	-80	60	on	-50	0	60	on	-50	80	60	on	0	-80	140
9	on	-30	-120	60	on	-30	-40	60	on	-30	40	60	on	0	-80	140
10	on	-50	-120	60	on	-50	-40	60	on	-50	40	60	on	0	-80	140
11	off	0	-80	60	data	0	0	60	off	0	80	60	out			
12	on	0	-80	60	data	0	0	60	on	0	80	60	out			
13	off	0	-100	60	data	0	0	60	off	0	100	60	out			
14	on	0	-100	60	data	0	0	60	on	0	100	60	out			
15	off	0	-120	60	data	0	0	60	off	0	120	60	out			
16	on	0	-120	60	data	0	0	60	on	0	120	60	out			
17	off	0	-160	60	data	0	0	60	off	0	160	60	out			
18	on	0	-160	60	data	0	0	60	on	0	160	60	out			

Table 35 TASK 6 Series 2 Test Program

Test No.	Rotor 11			Rotor 14			Rotor 12			Rotor 16			Rotor 15			
	State	X	Y	Z	State	X	Y	Z	State	X	Y	Z	State	X	Y	Z
19	off	0	-80	60	data	0	0	60	off	0	80	60	out			
20	off	0	-80	60	data	0	0	60	off	0	80	60	off	-50	-80	130
21	on	0	-80	60	data	0	0	60	on	0	80	60	off	-50	-80	130
22	on	0	-80	60	data	0	0	60	on	0	80	60	on	-50	-80	130
23	off	-50	-80	60	off	-50	0	60	off	-50	80	60	off	0	-80	130
24	on	-50	-80	60	on	-50	0	60	on	-50	80	60	on	0	-80	130
25	off	-50	-120	60	off	-50	-40	60	off	-50	40	60	off	0	-80	130
26	on	-50	-120	60	on	-50	-40	60	on	-50	40	60	on	0	-80	130
27	on	0	-80	60	data	0	0	60	on	0	80	60	off	50	-40	140
28	on	0	-80	60	data	0	0	60	on	0	80	60	on	50	-40	140

Table 36 TASK 6 Series 3 Test Program

Test No.	Rotor 11			Rotor 14			Rotor 12			Rotor 16			Rotor 15			
	State	X	Y	Z	State	X	Y	Z	State	X	Y	Z	State	X	Y	Z
29	on	0	-80	60	data	0	0	60	on	0	80	60	off	30	-80	140
30	on	0	-80	60	data	0	0	60	on	0	80	60	on	30	-80	140
31	on	0	-80	60	data	0	0	60	on	0	80	60	off	50	-80	140
32	on	0	-80	60	data	0	0	60	on	0	80	60	on	50	-80	140
33	on	0	-80	60	data	0	0	60	on	0	80	60	off	100	-80	140
34	on	0	-80	60	data	0	0	60	on	0	80	60	on	100	-80	140
35	on	0	-80	60	data	0	0	60	on	0	80	60	off	30	-40	140
36	on	0	-80	60	data	0	0	60	on	0	80	60	on	30	-40	140
37	on	0	-80	60	data	0	0	60	on	0	80	60	off	100	-40	140
38	on	0	-80	60	data	0	0	60	on	0	80	60	on	100	-40	140
39	on	0	-80	60	data	0	0	60	on	0	80	60	off	50	-80	130
40	on	0	-80	60	data	0	0	60	on	0	80	60	on	50	-80	130
41	off	0	-80	60	data	0	0	60	off	0	80	60	off	30	-40	130
42	on	0	-80	60	data	0	0	60	on	0	80	60	off	30	-40	130
43	on	0	-80	60	data	0	0	60	on	0	80	60	on	30	-40	130
44	on	0	-80	60	data	0	0	60	on	0	80	60	off	50	-40	130
45	on	0	-80	60	data	0	0	60	on	0	80	60	on	50	-40	130

Table 37 TASK 6 Series 1 Data Summary

Run No.	Data Set	Torque (in-oz)	Speed (RPM)	Velocity (m/s)	Tip Speed Ratio	Power Coeff.	Tower (feet)	Grid Data No.	Tech.
1	1	3.5	2695	8.64	5.88	0.241	60	2A	1
2	1	3.5	2757	8.64	6.01	0.247	60	2A	1
3	1	3.5	2364	8.64	5.16	0.212	60	2A	1
	2	3.5	2328	8.64	5.08	0.209	60	2A	1
4	1	4.0	2345	8.64	5.12	0.240	60	2A	1
	2	3.8	2415	8.64	5.27	0.235	60	2A	1
	3	3.5	2595	8.64	5.66	0.232	60	2A	1
	4	3.5	2599	8.64	5.67	0.233	60	2A	1
	5	3.0	2855	8.64	6.23	0.219	60	2A	1
	6	2.5	3011	8.64	6.57	0.193	60	2A	1
5	1	3.5	2404	8.64	5.24	0.215	60	2A	1
	2	3.5	2424	8.64	5.29	0.217	60	2A	1
6	1	4.0	2368	8.55	5.22	0.250	60	2A	1
	2	3.5	2660	8.55	5.88	0.246	60	2A	1
	3	3.5	2644	8.55	5.83	0.244	60	2A	1
	4	3.0	2874	8.55	6.34	0.228	60	2A	1
	5	2.5	3074	8.55	6.78	0.203	60	2A	1
7	1	3.5	2835	8.64	6.19	0.254	140	2A	1
8	1	4.0	2804	8.64	6.12	0.287	140	2A	1
	2	3.5	3054	8.64	6.66	0.274	140	2A	1
	3	3.0	3239	8.64	7.07	0.249	140	2A	1
	4	2.5	3410	8.64	7.44	0.218	140	2A	1
9	1	4.0	2758	8.50	6.12	0.297	140	2A	1
	2	3.5	3020	8.57	6.64	0.277	140	2A	1
	3	3.0	3236	8.63	7.07	0.249	140	2A	1
	4	2.5	3396	8.54	7.50	0.225	140	2A	1
10	1	4.1	2550	8.67	5.54	0.265	140	2A	1
	2	3.5	3056	8.62	6.68	0.276	140	2A	1
	3	3.0	3256	8.67	7.08	0.247	140	2A	1
	4	2.5	3426	8.67	7.45	0.217	140	2A	1
11	1	3.5	2587	8.64	5.64	0.232	60	2A	1
12	1	3.5	2698	8.64	5.89	0.242	60	2A	1
13	1	3.5	2564	8.64	5.59	0.230	60	2A	1
14	1	3.5	2642	8.64	5.76	0.237	60	2A	1
15	1	3.5	2543	8.64	5.55	0.228	60	2A	1
16	1	3.5	2635	8.64	5.75	0.236	60	2A	1
17	1	3.5	2508	8.64	5.47	0.225	60	2A	1
	2	3.5	2439	8.55	5.38	0.225	60	2A	1
	3	3.5	2442	8.55	5.38	0.226	60	2A	1
18	1	3.5	2606	8.64	5.69	0.233	60	2A	1
	2	3.5	2507	8.55	5.53	0.232	60	2A	1

Table 38 TASK 6 Series 2 Data Summary

Run Data No.	Data Set	Torque (in-oz)	Speed (RPM)	Velocity (m/s)	Tip Speed Ratio	Power Coeff.	Tower (feet)	Grid Data No.	Tech.
19	1	3.5	3107	9.35	6.26	0.220	60	2B	1
	2	3.0	3258	9.35	6.57	0.197	60	2B	1
	3	2.5	3372	9.35	6.80	0.170	60	2B	1
20	1	3.5	2856	9.35	5.76	0.202	60	2B	1
21	1	3.5	2985	9.35	6.02	0.211	60	2B	1
22	1	3.5	3074	9.35	6.20	0.217	60	2B	1
	2	3.0	3205	9.35	6.46	0.194	60	2B	1
	3	2.5	3331	9.35	6.72	0.168	60	2B	1
23	1	3.5	2681	8.55	5.91	0.248	140	2B	1
24	1	3.5	3030	8.55	6.68	0.280	140	2B	1
	2	3.0	3193	8.55	7.04	0.253	140	2B	1
	3	2.5	3363	8.55	7.41	0.222	140	2B	1
25	1	3.5	2561	8.55	5.65	0.237	140	2B	1
26	1	3.5	3010	8.55	6.64	0.278	140	2B	1
	2	3.0	3108	8.55	6.85	0.246	140	2B	1
	3	2.5	3290	8.55	7.25	0.217	140	2B	1
27	1	3.5	2964	9.12	6.13	0.226	60	2B	1
	2	3.0	3100	9.12	6.41	0.202	60	2B	1
	3	2.5	3296	9.12	6.81	0.179	60	2B	1
28	1	3.5	2840	9.12	5.87	0.216	60	2B	1
	2	3.5	2894	9.12	5.98	0.220	60	2B	1
	3	3.0	3069	9.12	6.34	0.200	60	2B	1
	4	3.0	3054	9.12	6.31	0.199	60	2B	1
	5	2.5	3183	9.12	6.58	0.173	60	2B	1

Table 39 TASK 6 Series 3 Data Summary

Run No.	Data Set	Torque (in-oz)	Speed (RPM)	Velocity (m/s)	Tip Speed Ratio	Power Coeff.	Tower (feet)	Grid No.	Data Tech.
29	1	3.5	2587	8.68	5.62	0.229	60	2A	2
	2	3.0	2861	8.68	6.21	0.217	60	2A	2
	3	2.5	3056	8.71	6.61	0.191	60	2A	2
	4	2.0	3197	8.74	6.90	0.158	60	2A	2
30	1	3.5	2596	8.70	5.62	0.228	60	2A	2
	2	3.0	2805	8.64	6.12	0.215	60	2A	2
	3	2.5	3033	8.66	6.60	0.193	60	2A	2
	4	2.0	3140	8.65	6.84	0.160	60	2A	2
31	1	3.5	2523	8.80	5.40	0.214	60	2A	2
	2	3.0	2817	8.75	6.07	0.208	60	2A	2
	3	2.5	3032	8.73	6.55	0.188	60	2A	2
	4	2.0	3171	8.72	6.85	0.158	60	2A	2
32	1	3.5	2494	8.70	5.40	0.219	60	2A	2
	2	3.0	2865	8.74	6.18	0.213	60	2A	2
	3	2.5	3013	8.74	6.50	0.186	60	2A	2
	4	2.0	3212	8.78	6.90	0.157	60	2A	2
33	1	3.5	2575	8.72	5.57	0.224	60	2A	2
	2	3.0	2837	8.74	6.12	0.210	60	2A	2
	3	2.5	3067	8.78	6.58	0.187	60	2A	2
	4	2.0	3172	8.72	6.86	0.158	60	2A	2
34	1	3.5	2532	8.68	5.50	0.224	60	2A	2
	2	3.0	2857	8.78	6.13	0.209	60	2A	2
	3	2.5	3051	8.78	6.55	0.186	60	2A	2
	4	2.0	3143	8.67	6.83	0.159	60	2A	2
35	1	3.5	2606	8.68	5.66	0.230	60	2A	2
	2	3.0	2846	8.73	6.15	0.212	60	2A	2
	3	2.5	3030	8.66	6.60	0.193	60	2A	2
	4	2.0	3190	8.71	6.90	0.159	60	2A	2
36	1	3.5	2607	8.72	5.64	0.227	60	2A	2
	2	3.0	2848	8.69	6.18	0.215	60	2A	2
	3	2.5	3052	8.69	6.62	0.192	60	2A	2
	4	2.0	3222	8.70	6.98	0.162	60	2A	2
37	1	3.5	2502	8.72	5.41	0.218	60	2A	2
	2	3.0	2845	8.73	6.14	0.212	60	2A	2
38	1	3.5	2419	8.65	5.27	0.216	60	2A	2
	2	3.0	2783	8.67	6.05	0.212	60	2A	2
	3	2.5	2976	8.61	6.52	0.192	60	2A	2
	4	2.0	3119	8.63	6.81	0.160	60	2A	2
39	1	3.5	2678	8.65	5.84	0.239	60	2A	2
	2	3.0	2920	8.58	6.42	0.229	60	2A	2
	3	2.5	3110	8.62	6.80	0.200	60	2A	2
	4	2.0	3239	8.63	7.07	0.166	60	2A	2
40	1	3.5	2641	8.59	5.80	0.241	60	2A	2
	2	3.0	2852	8.61	6.24	0.221	60	2A	2
	3	2.5	3076	8.60	6.74	0.200	60	2A	2
	4	2.0	3213	8.55	7.08	0.170	60	2A	2
41	1	3.5	2428	8.55	5.35	0.224	60	2A	2
	2	3.0	2760	8.57	6.07	0.217	60	2A	2
	3	2.5	2969	8.58	6.52	0.194	60	2A	2
	4	2.0	3153	8.59	6.92	0.164	60	2A	2
	5	2.0	3136	8.55	6.91	0.166	60	2A	2
42	1	3.5	2552	8.46	5.69	0.244	60	2A	2
	2	3.0	2835	8.45	6.32	0.233	60	2A	2
	3	2.5	3003	8.48	6.68	0.203	60	2A	2
	4	2.0	3192	8.50	7.08	0.172	60	2A	2
43	1	3.5	2611	8.41	5.85	0.254	60	2A	2
	2	3.0	2812	8.47	6.26	0.229	60	2A	2
	3	2.5	3051	8.52	6.75	0.204	60	2A	2
	4	2.0	3159	8.46	7.04	0.172	60	2A	2
44	1	3.5	2625	8.58	5.77	0.240	60	2A	2
	2	3.0	2864	8.55	6.31	0.227	60	2A	2
	3	2.5	3053	8.53	6.75	0.203	60	2A	2
	4	2.0	3220	8.51	7.13	0.173	60	2A	2
45	1	3.5	2614	8.58	5.74	0.239	60	2A	2
	2	3.0	2860	8.55	6.31	0.227	60	2A	2
	3	2.5	3026	8.54	6.68	0.201	60	2A	2
	4	2.0	3196	8.55	7.05	0.169	60	2A	2

Table 40 TASK 6 Series 3 Test Program (cont.)

Test No.	Rotor 11			Rotor 14			Rotor 12			Rotor 16			Rotor 15							
	State	X ft	Y ft	Z ft	State	X ft	Y ft	Z ft	State	X ft	Y ft	Z ft	State	X ft	Y ft	Z ft				
46	on	0	-80	60	data	0	0	60	on	0	80	60	off	50	-40	140	off	50	40	140
47	on	0	-80	60	data	0	0	60	on	0	80	60	on	50	-40	140	on	50	40	140
48	on	0	-80	60	data	0	0	60	on	0	80	60	off	50	-40	140	off	50	40	140
49	on	0	-80	60	data	0	0	60	on	0	80	60	on	50	-40	140	on	50	40	140

Table 41 TASK 6 Series 3 Data Summary (cont.)

Run No.	Data Set	Torque (in-oz)	Speed (RPM)	Velocity (m/s)	Tip Speed Ratio	Power Coeff.	Tower (feet)	Grid No.	Data Tech.
46	1	3.5	2561	8.72	5.54	0.223	60	2A	2
	2	3.0	2851	8.74	6.15	0.212	60	2A	2
	3	2.5	3066	8.81	6.56	0.185	60	2A	2
	4	2.0	3246	8.80	6.95	0.157	60	2A	2
47	1	3.5	2523	8.66	5.49	0.224	60	2A	2
	2	3.0	2829	8.74	6.10	0.210	60	2A	2
	3	2.5	3028	8.76	6.52	0.186	60	2A	2
48	4	2.0	3184	8.72	6.88	0.159	60	2A	2
	1	3.5	2656	8.91	5.62	0.217	60	2B	2
	2	3.0	2966	8.94	6.25	0.206	60	2B	2
	3	2.5	3057	8.91	6.47	0.178	60	2B	2
49	4	2.0	3204	8.80	6.86	0.155	60	2B	2
	1	3.5	2579	8.87	5.48	0.214	60	2B	2
	2	3.0	2853	8.68	6.20	0.216	60	2B	2
	3	2.5	3053	8.81	6.53	0.184	60	2B	2
	4	2.0	3194	8.69	6.93	0.161	60	2B	2

FIGURES

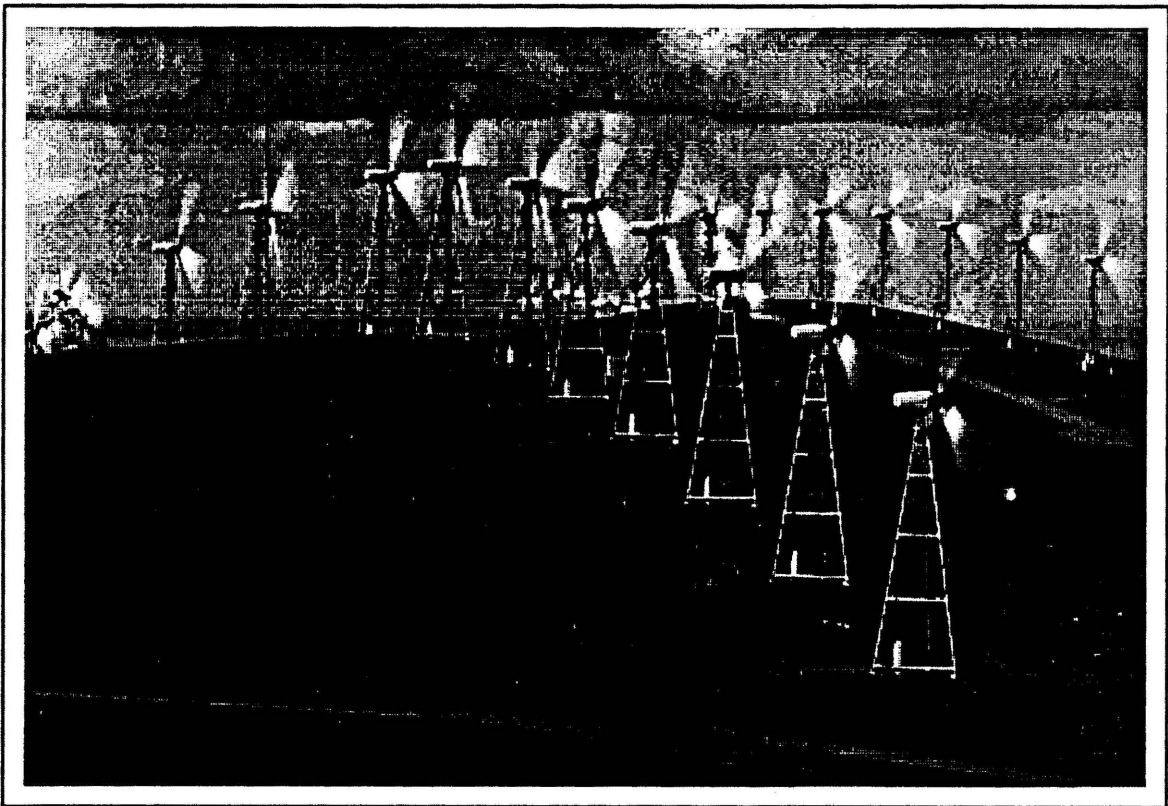


Figure 1 U.S. Windpower 60 ft Field Wind Turbine Array

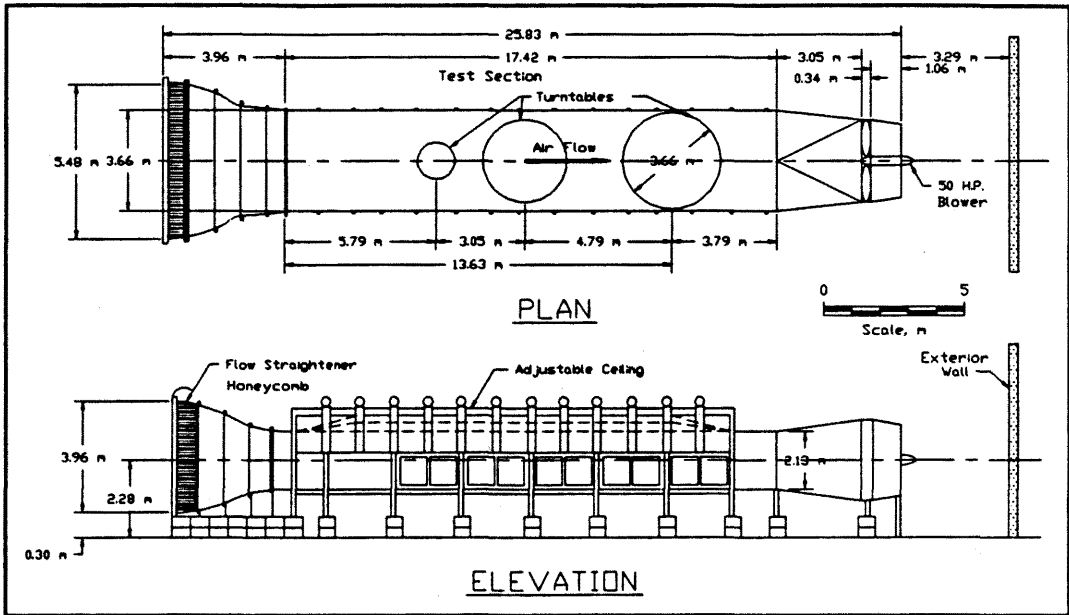


Figure 2 Environmental Wind Tunnel (EWT)

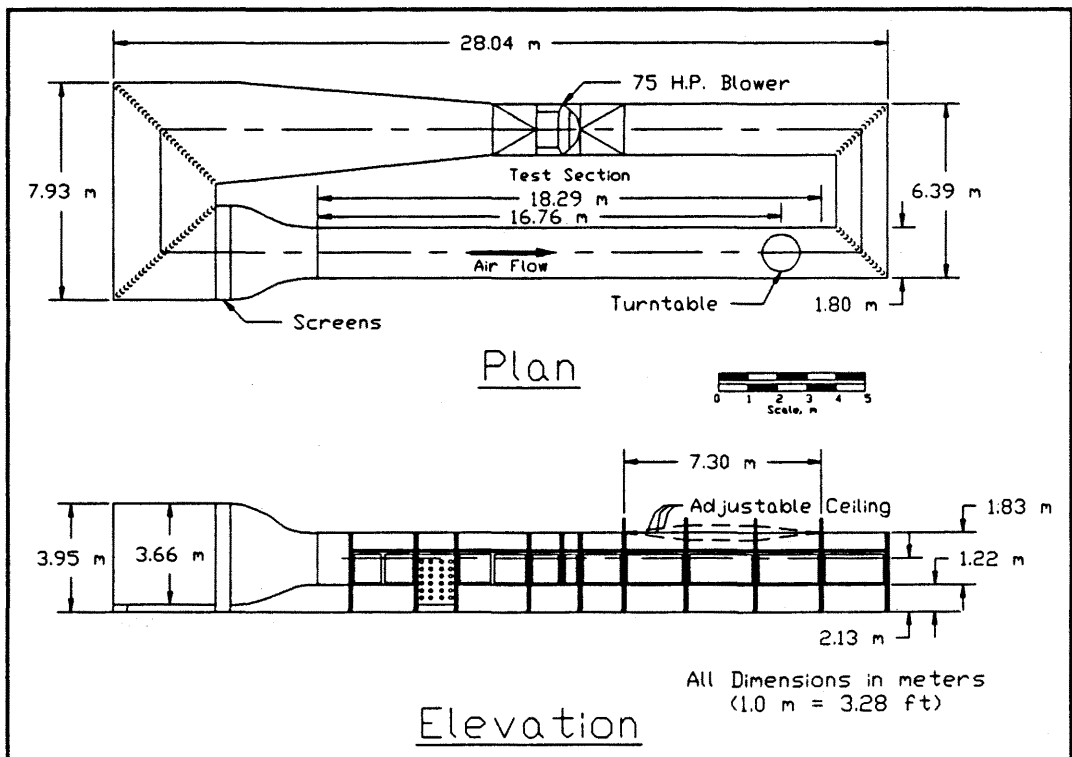


Figure 3 Industrial Wind Tunnel (IWT)

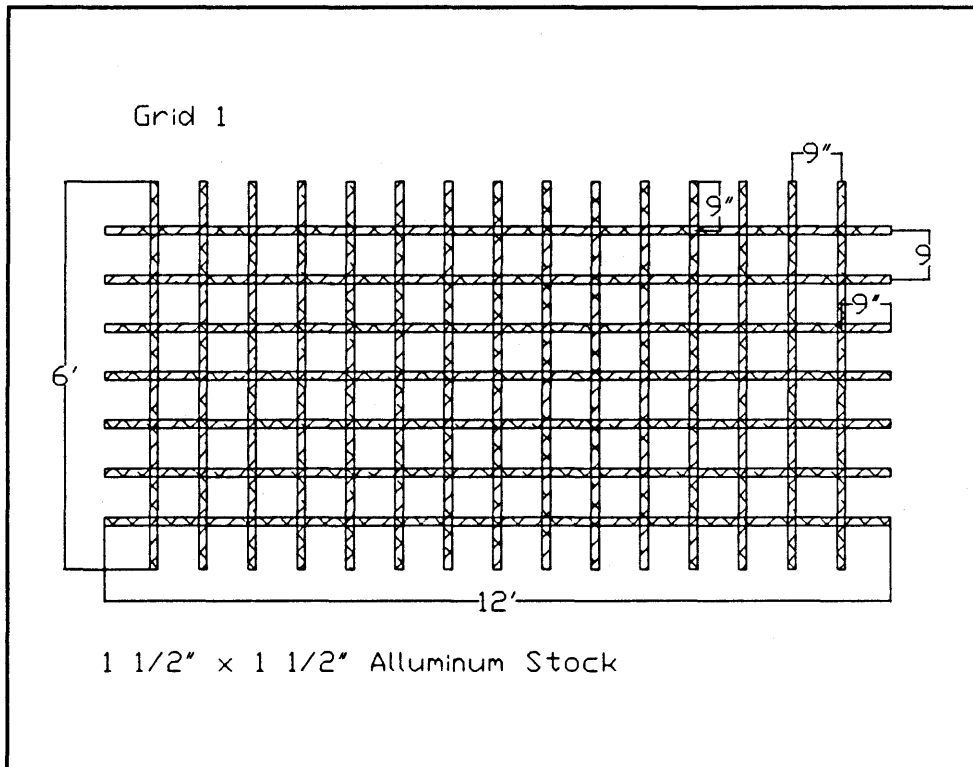


Figure 4 EWT Entrance Grid No. 1

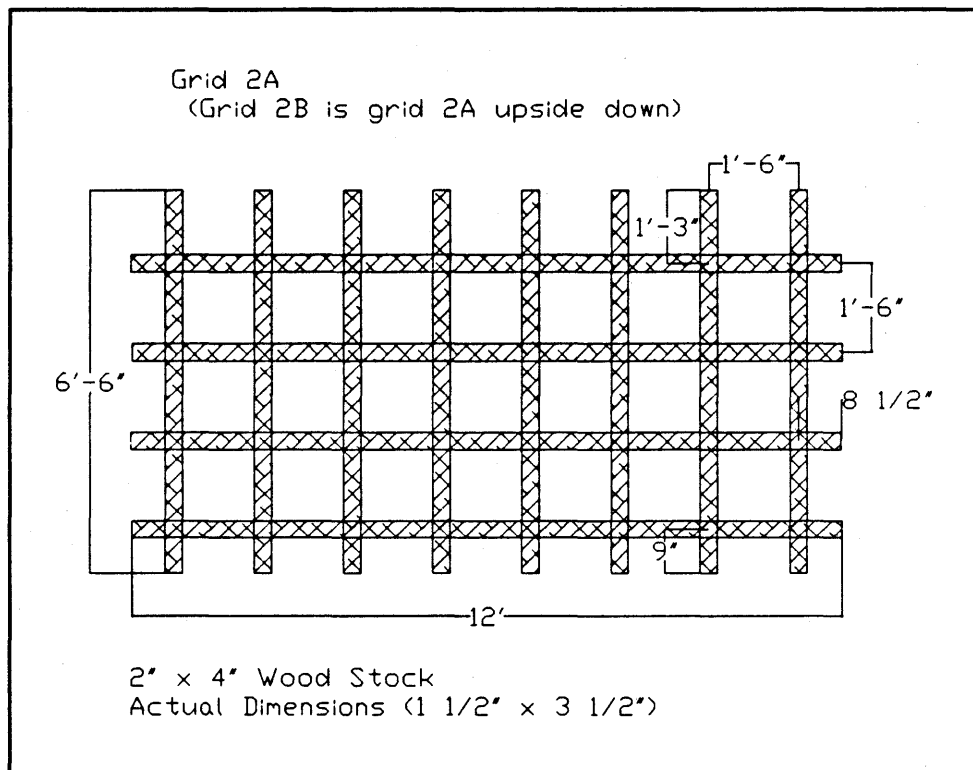


Figure 5 EWT Entrance Grids No. 2A and 2B

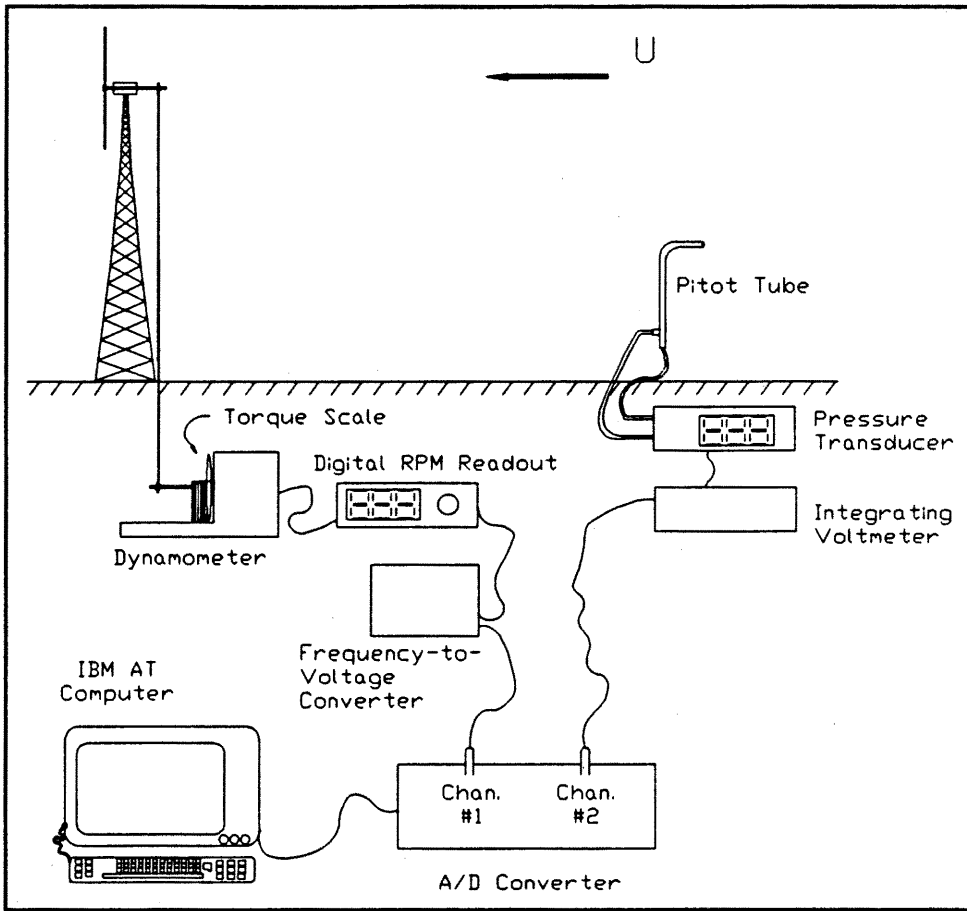


Figure 6 Power Measurement Schematic

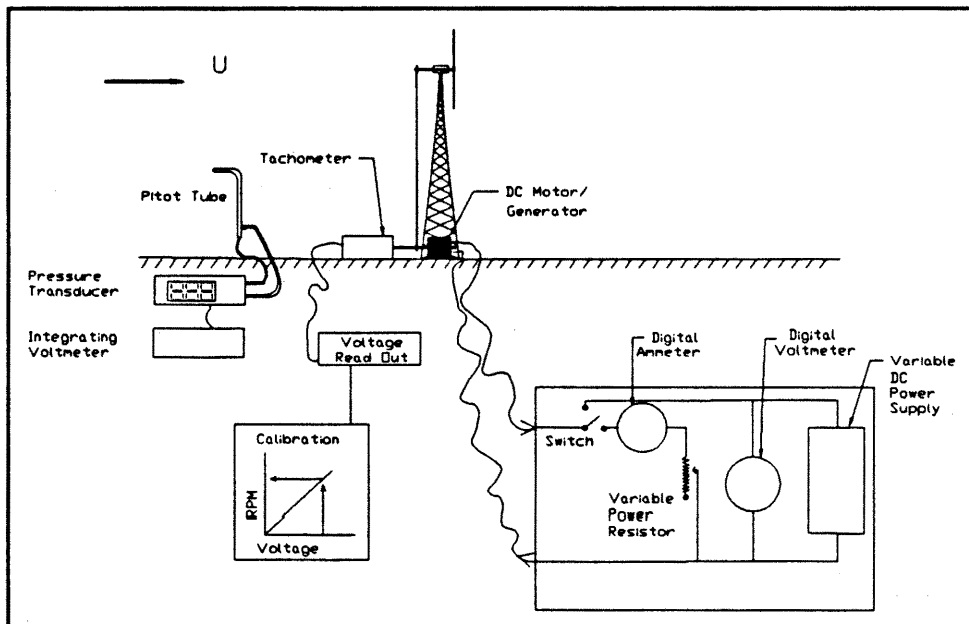


Figure 7 Turbine Loading Schematic

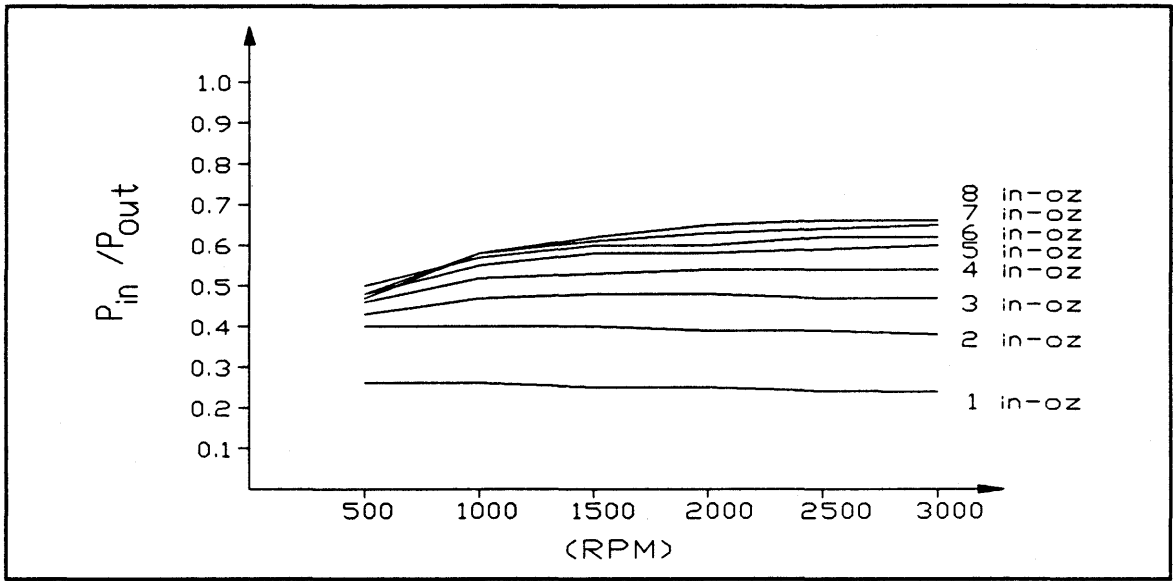


Figure 8 Clifton Motor Efficiency

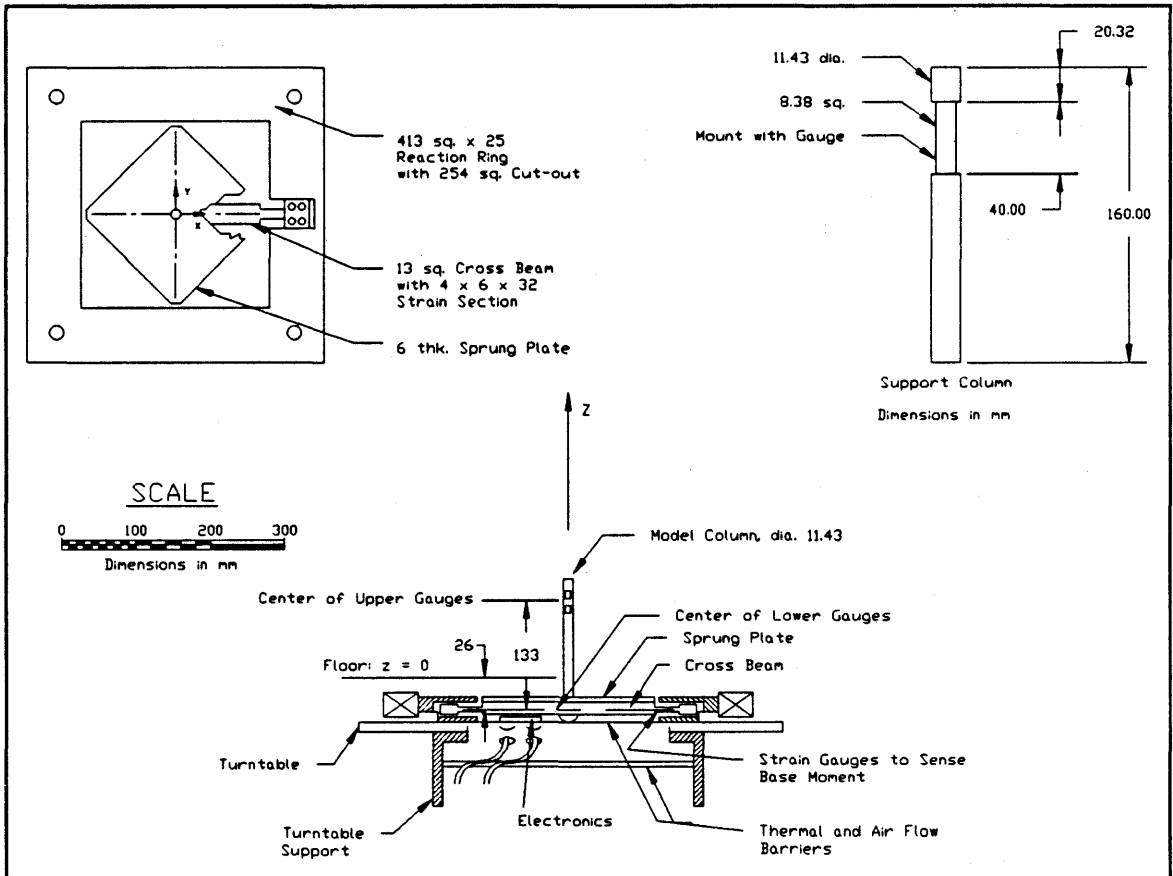


Figure 9 CSU Force Balance

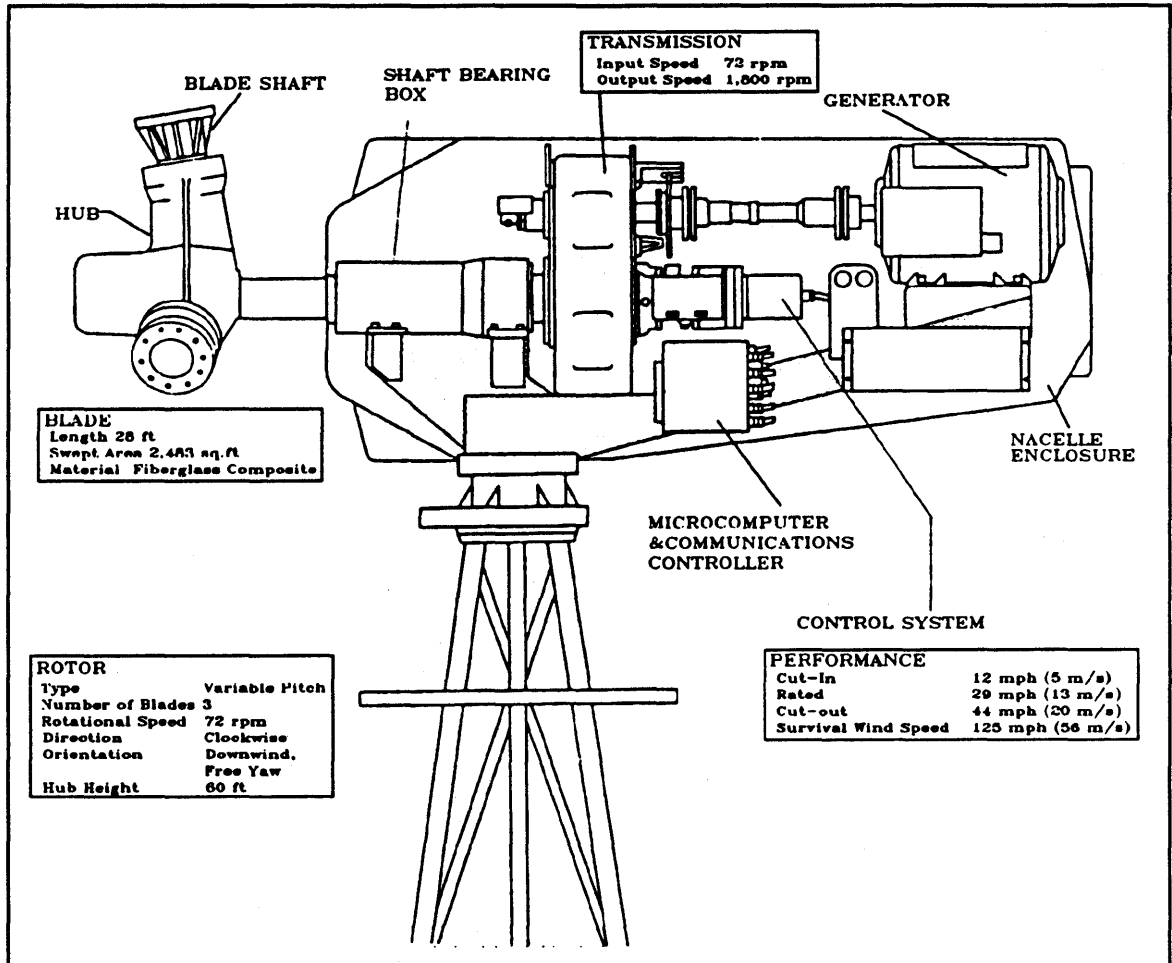


Figure 10 USW Model 56-100 Wind Turbine Generator

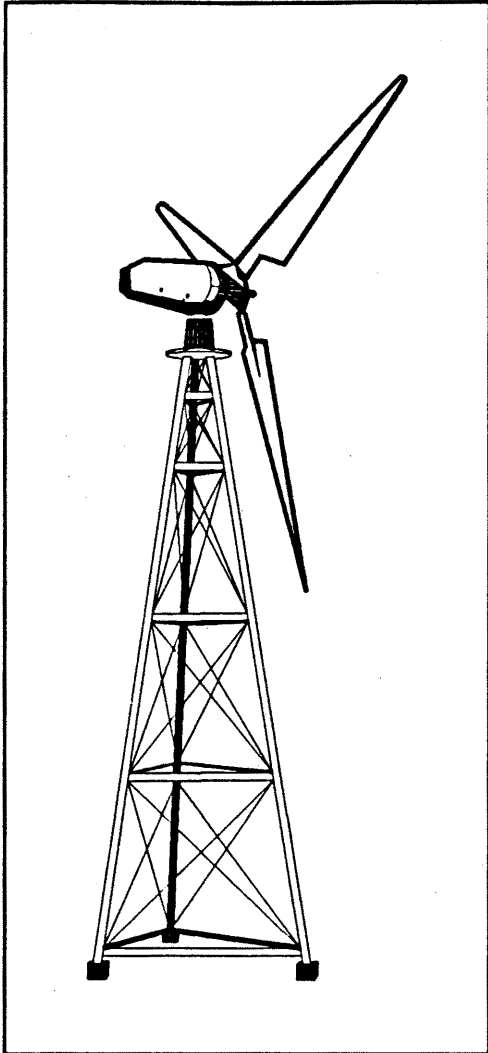


Figure 11 USW 56-100 Turbine on 60 foot Tower

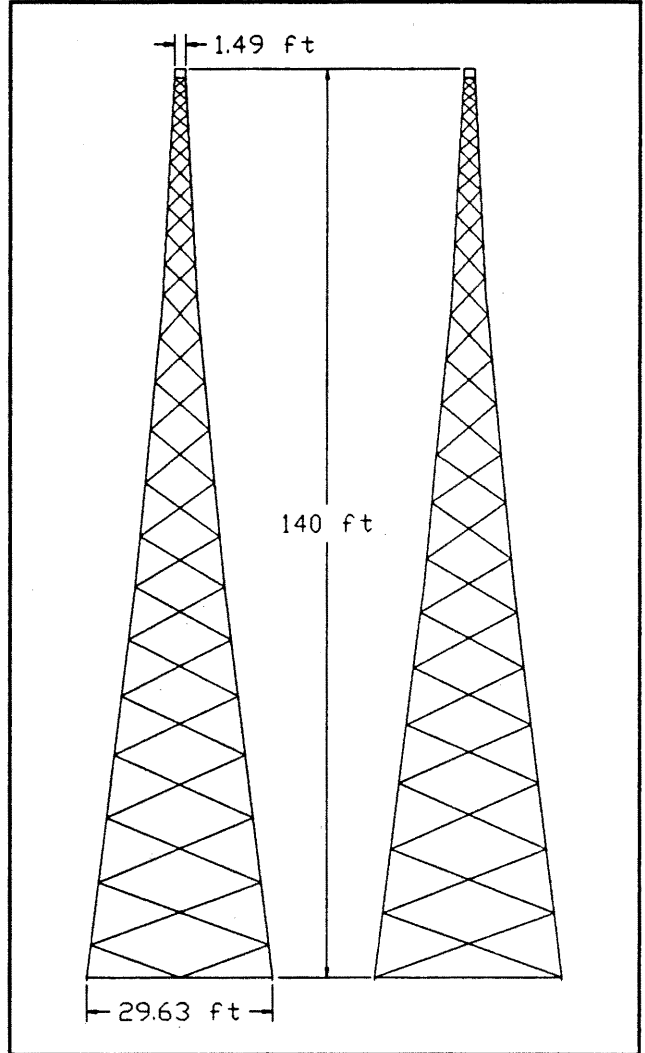


Figure 12 140 Foot Tower Design

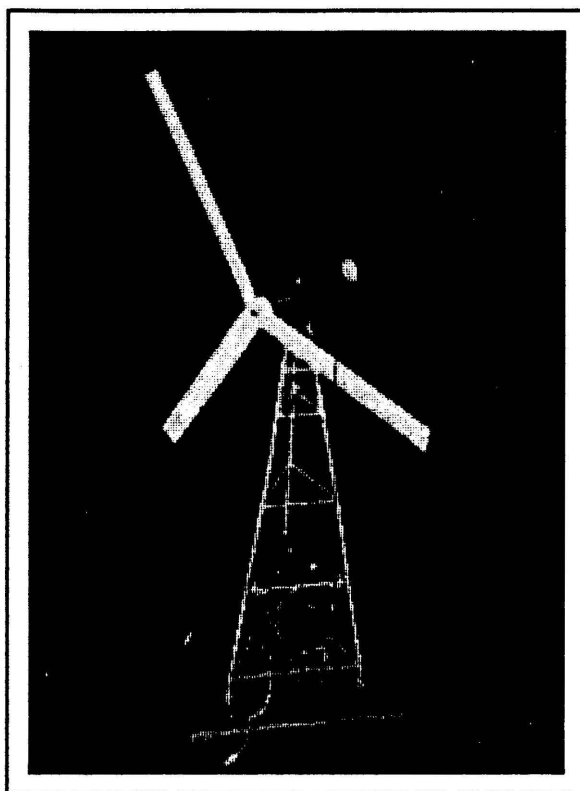


Figure 13 Model 60 foot Wind Turbine
Picture

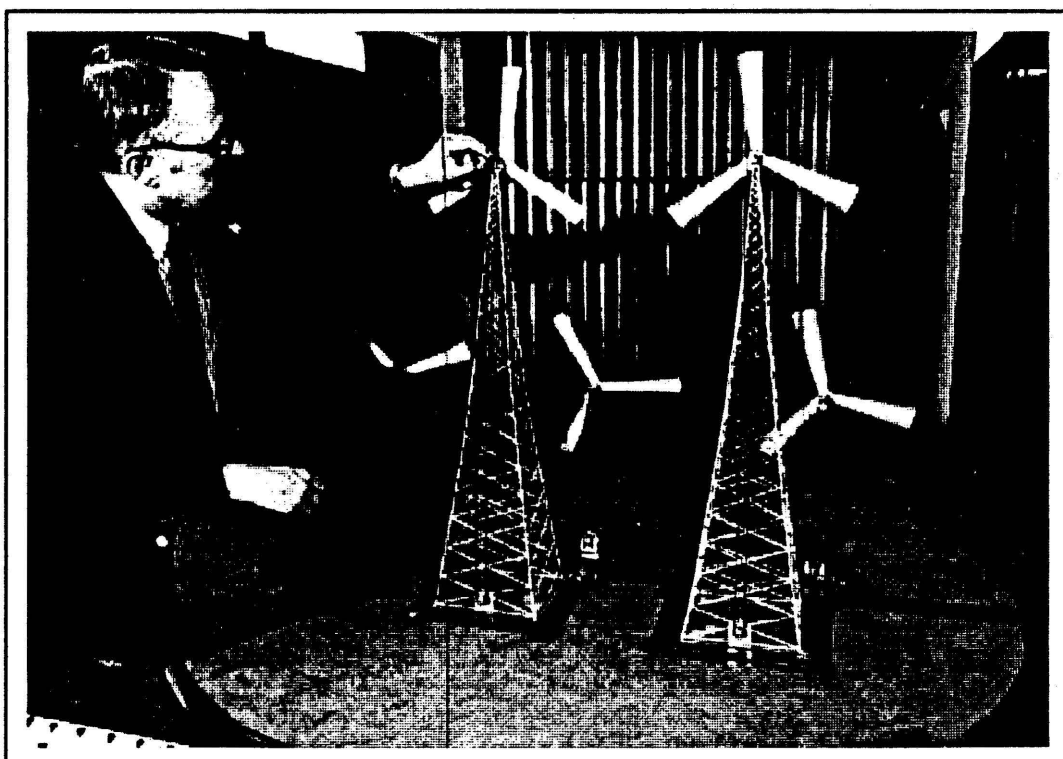


Figure 14 Model Wind Turbine Array Picture

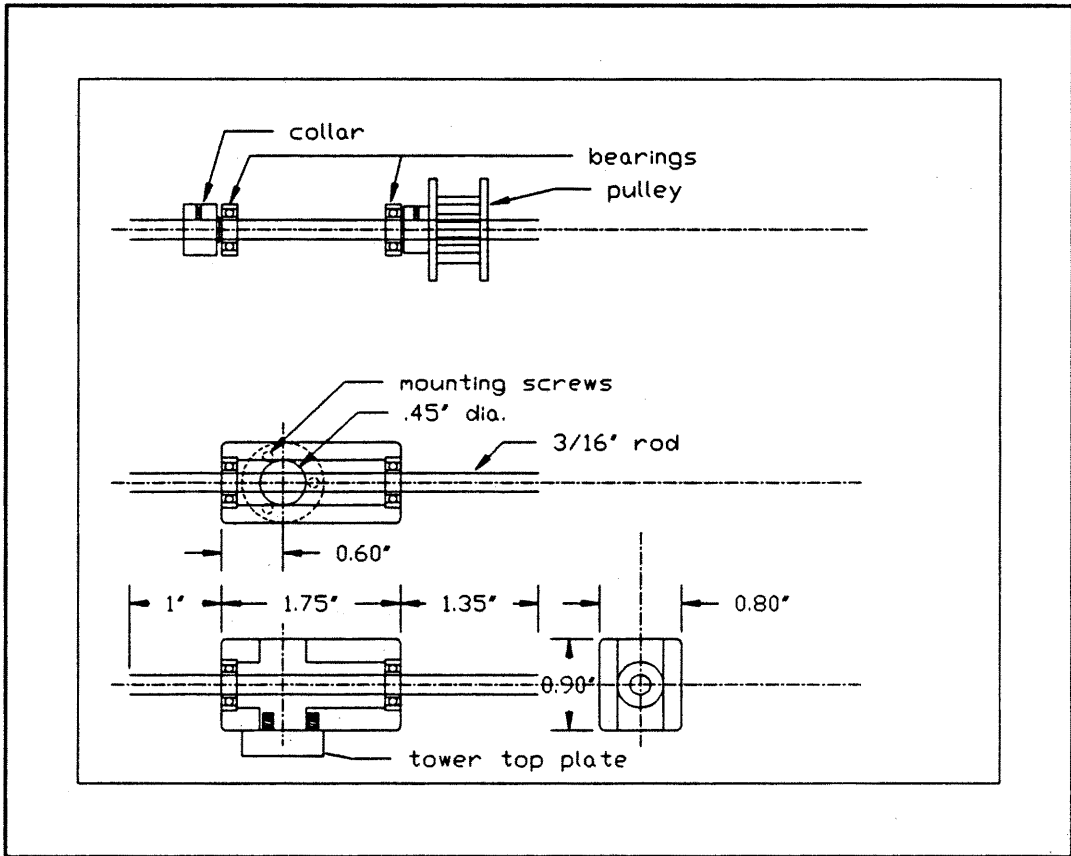


Figure 15 Model Shaft Bearing Housing

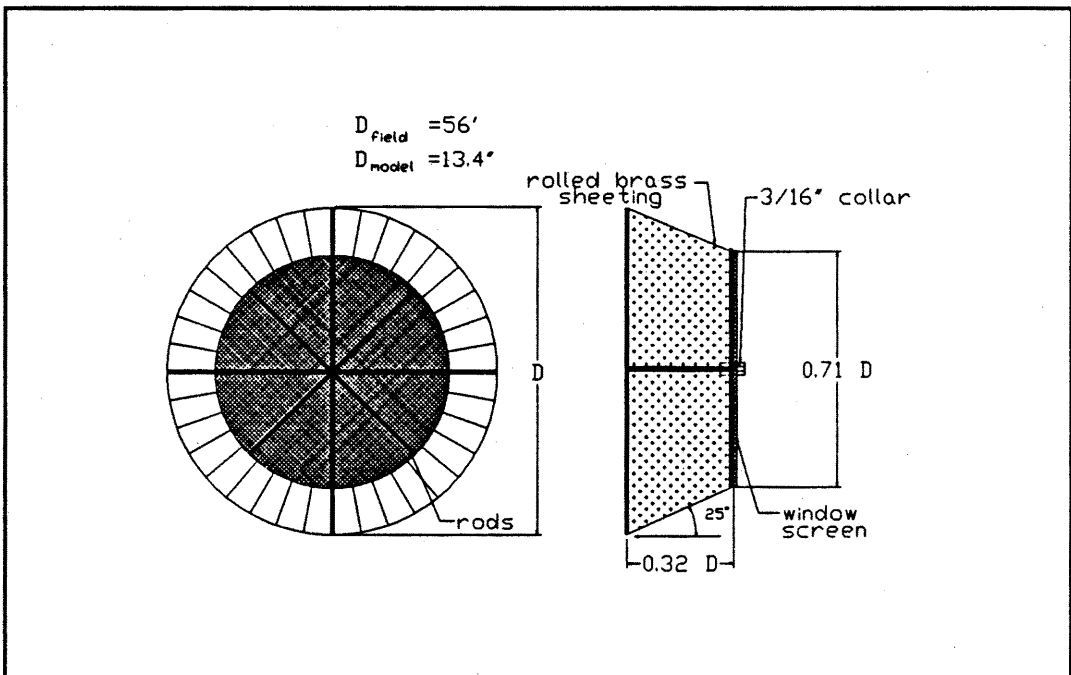


Figure 16 Passive Wake Device

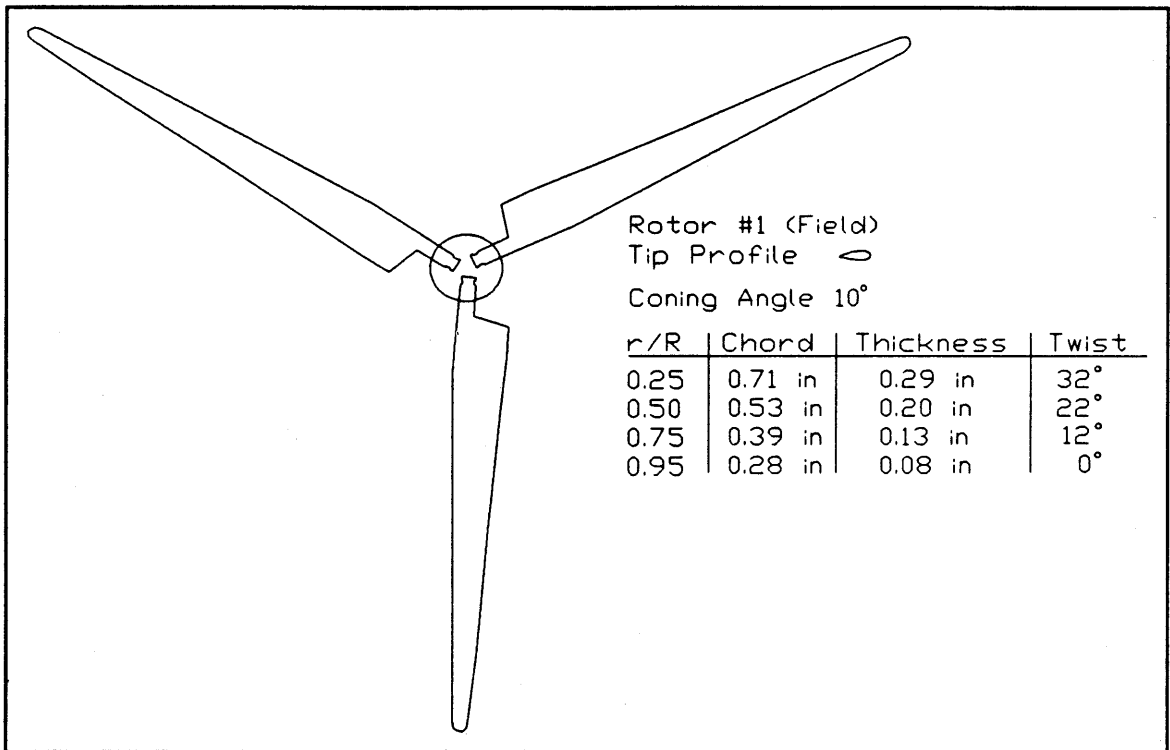


Figure 17 Geometrically Scaled USW Turbine Rotor Design

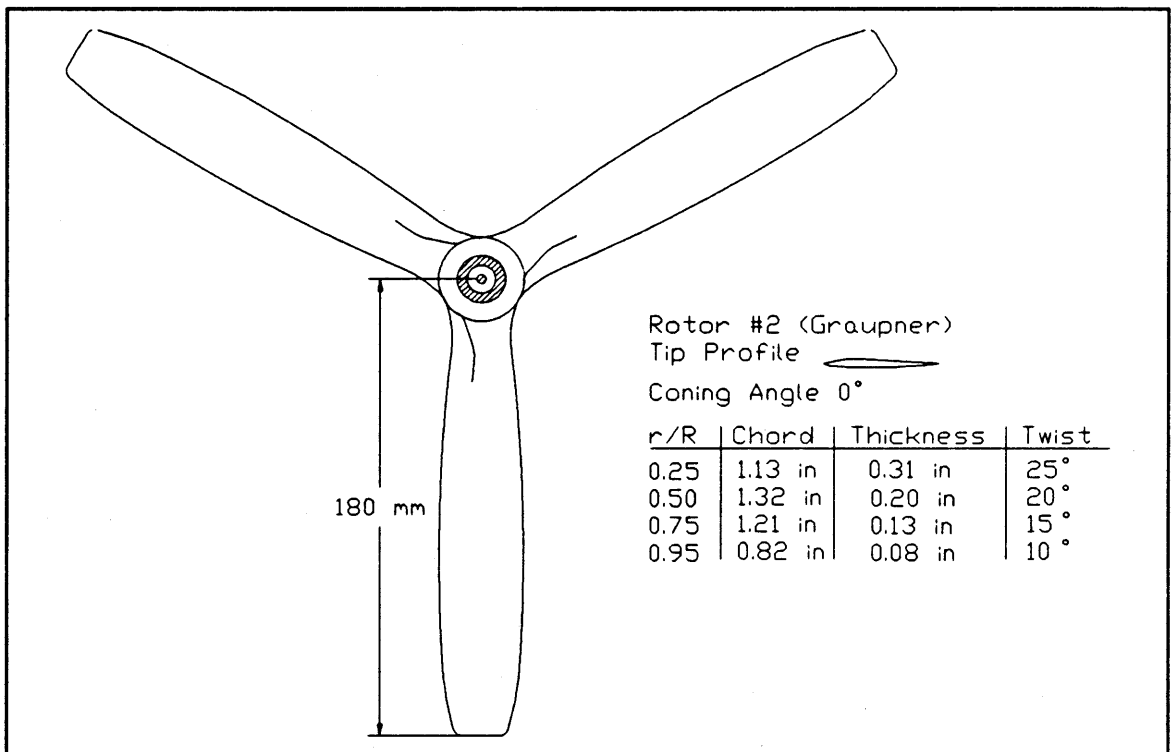


Figure 18 Graupner Rotor Design

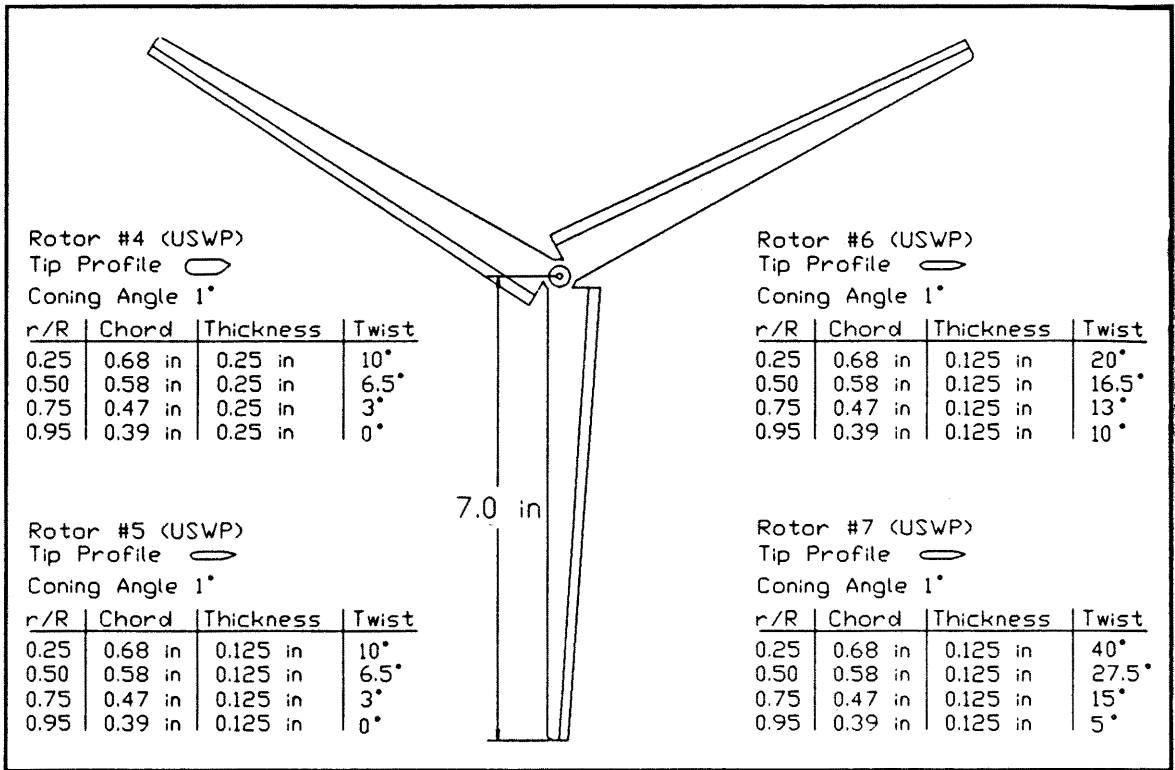


Figure 19 USWP Blade Design

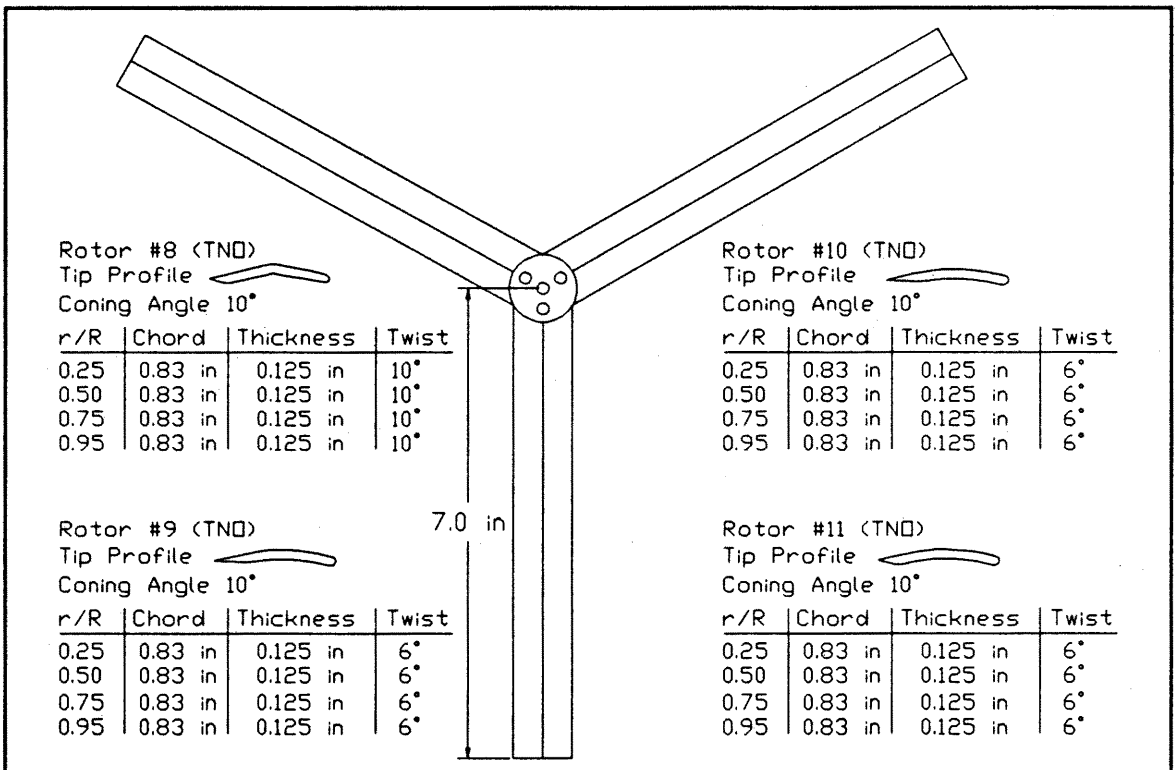


Figure 20 TNO Type Blade Design

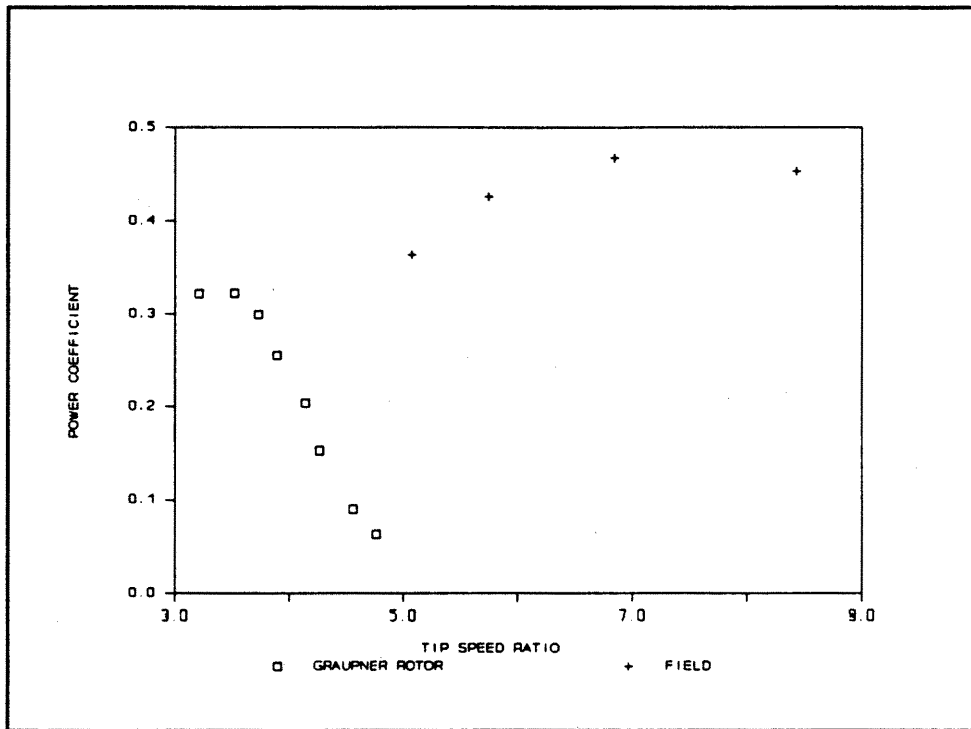


Figure 21 Graupner Power Performance Curve

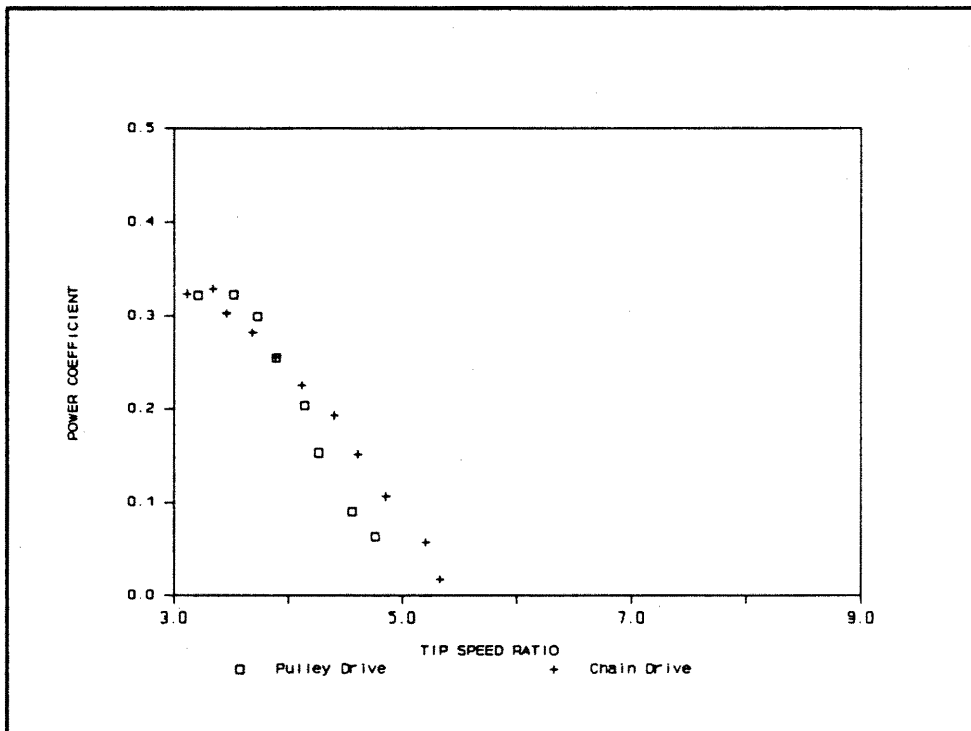


Figure 22 TASK 2 Pulley and Chain Drive Comparison

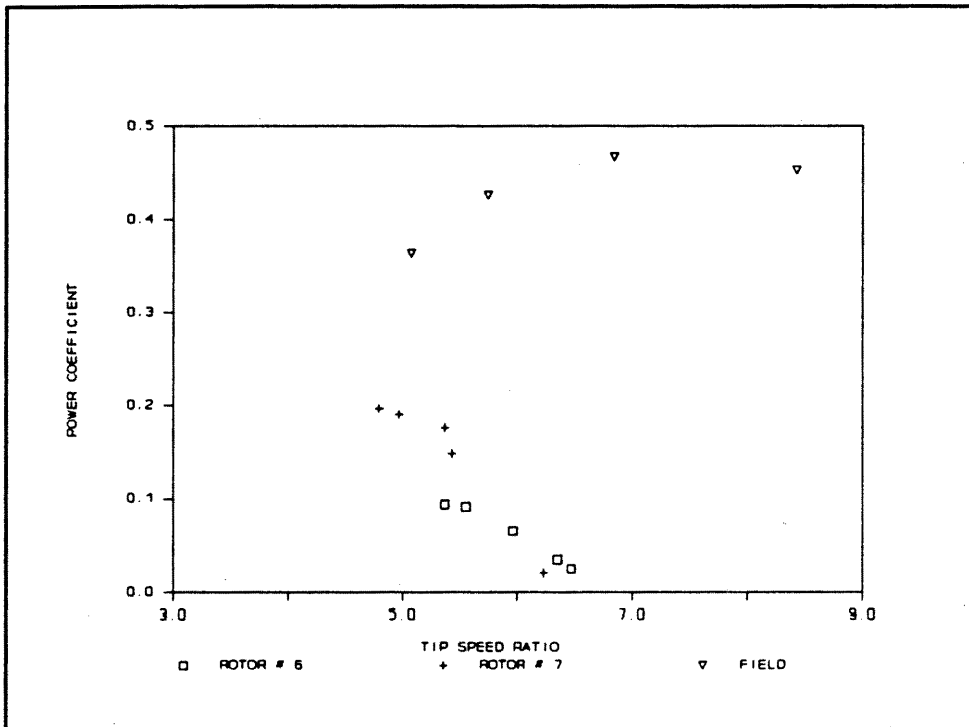


Figure 23 USWP Type Rotor Power Performance Comparisons

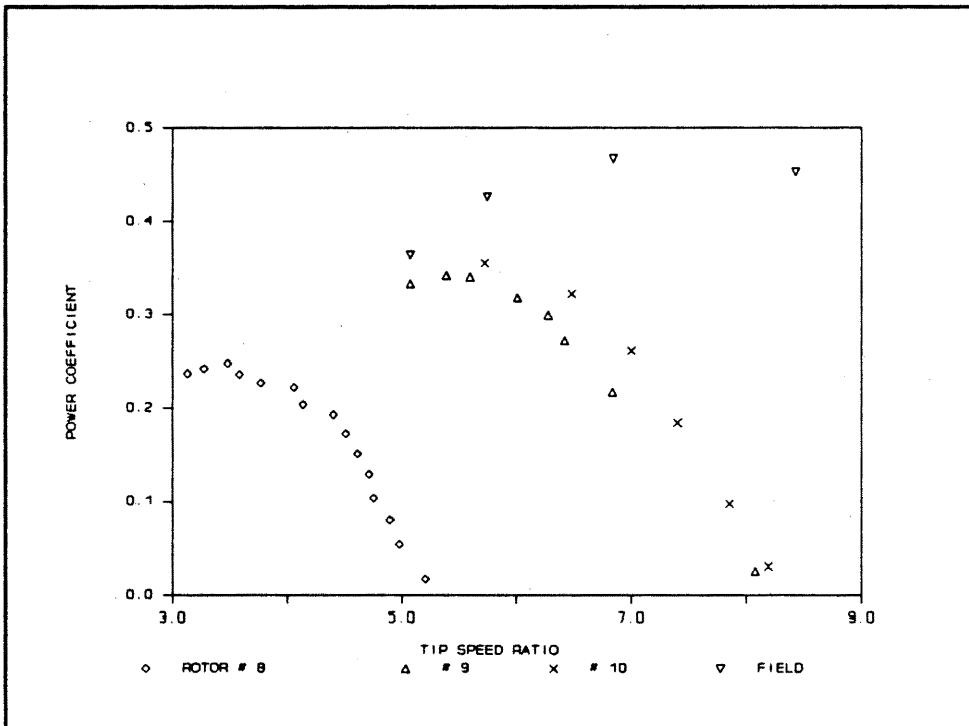


Figure 24 TNO Type Rotor Power Performance Comparisons

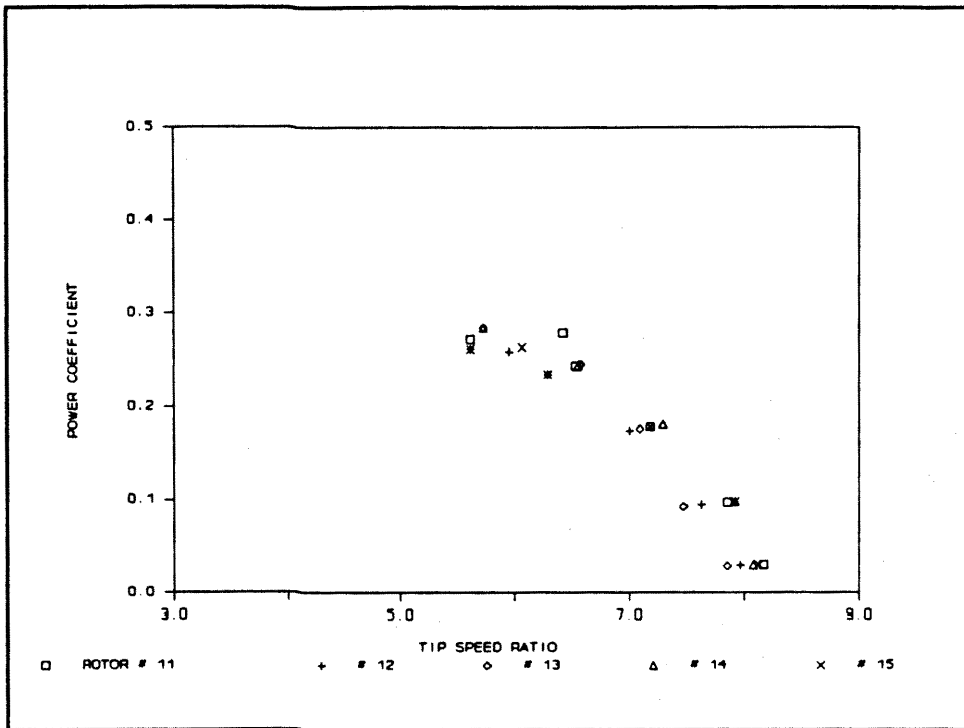


Figure 25 Power Performance Curves for Rotors 11 to 15

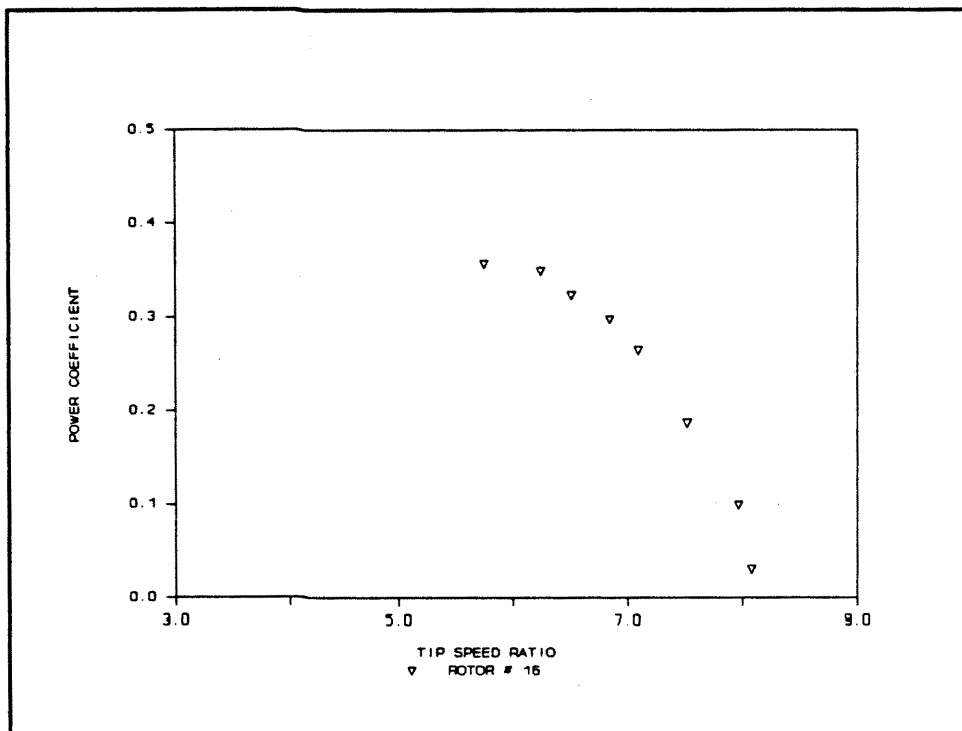


Figure 26 Power Performance Curve for Rotor 16

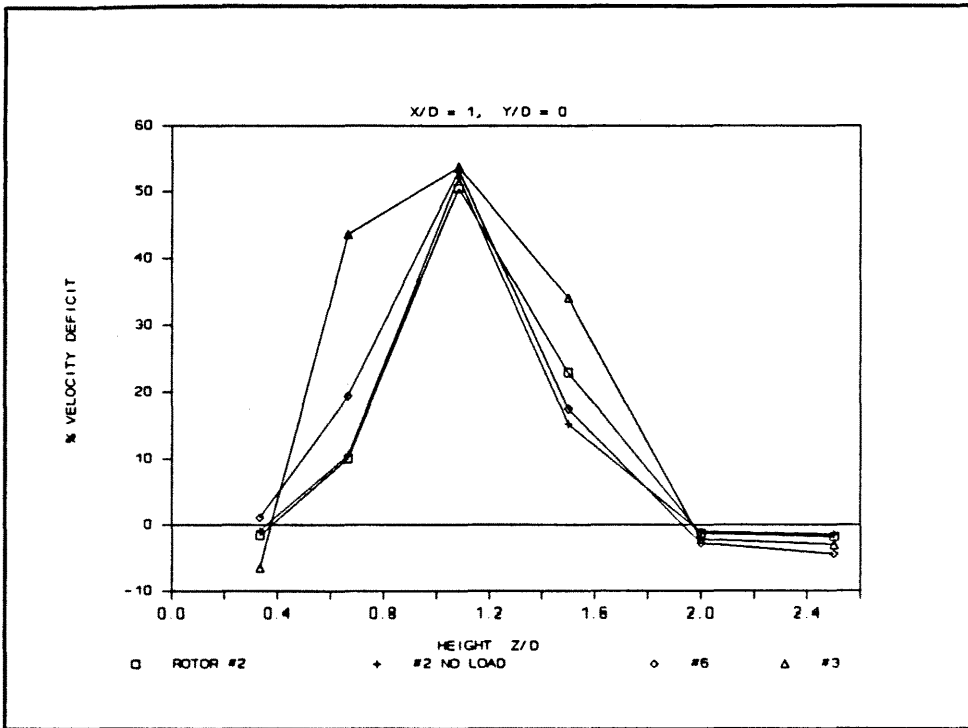


Figure 27 Single Turbine Wakes : Velocity Deficit vs. Height at $X/D=1$ for Rotors #2, #3, #6

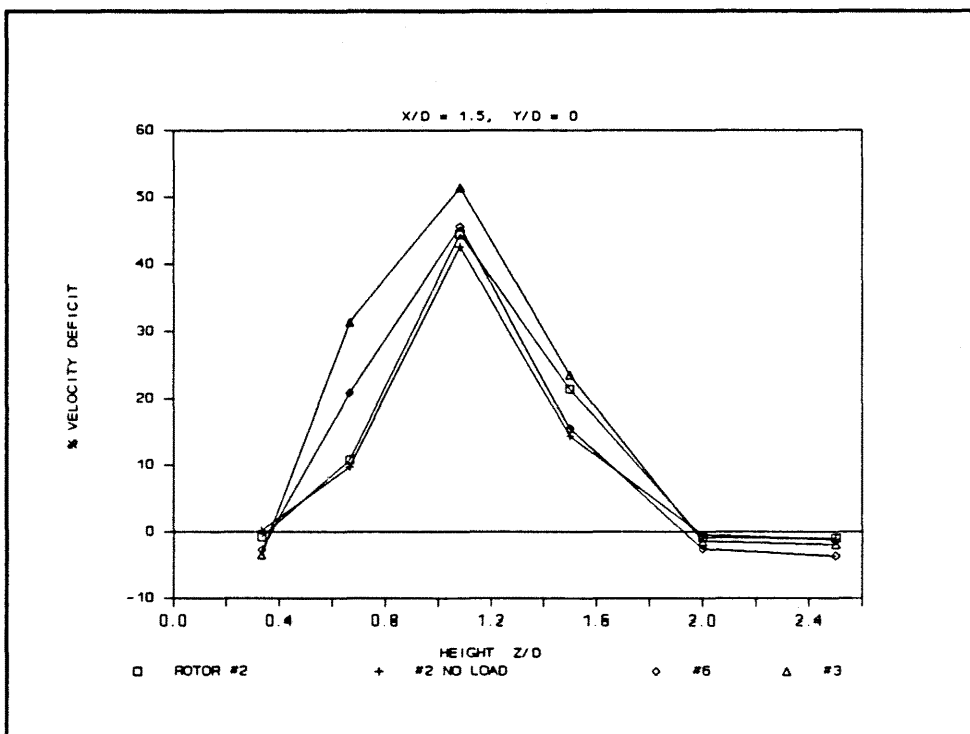


Figure 28 Single Turbine Wakes : Velocity Deficit vs. Height at $X/D=1.5$ for Rotors #2, #3, #6

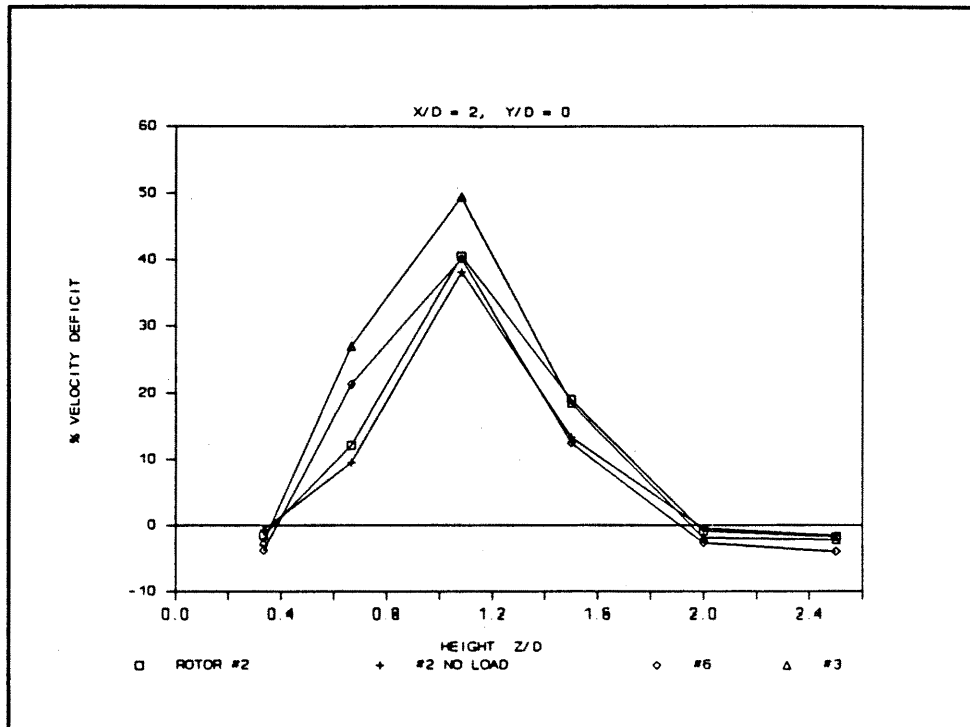


Figure 29 Single Turbine Wakes : Velocity Deficit vs. Height at X/D=2 for Rotors #2, #3, #6

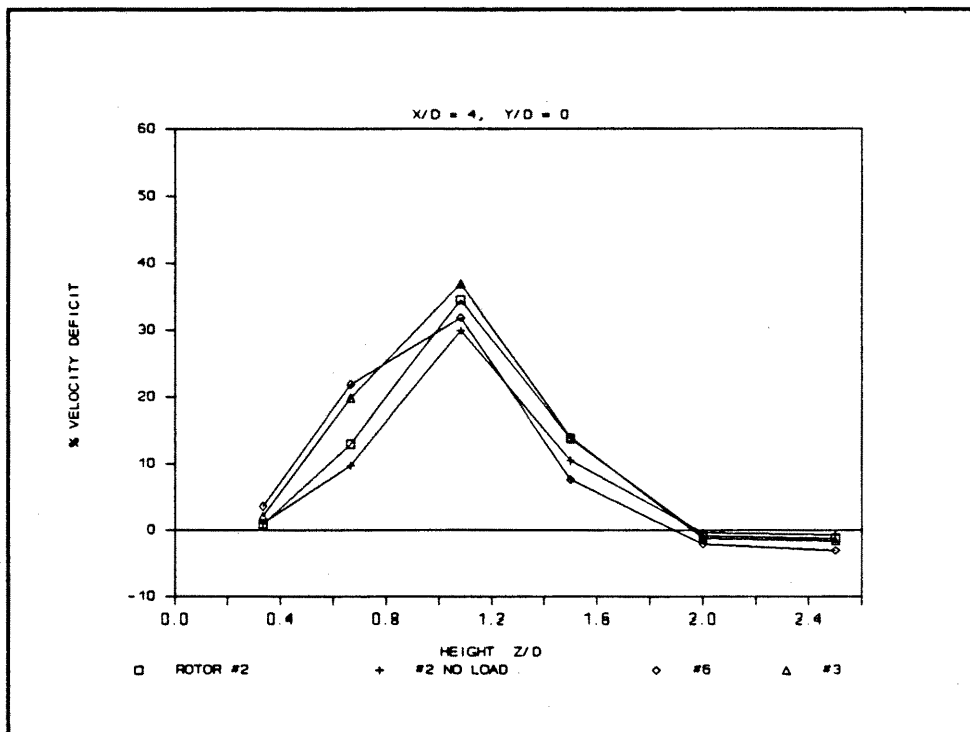


Figure 30 Single Turbine Wakes : Velocity Deficit vs. Height at X/D=4 for Rotors #2, #3, #6

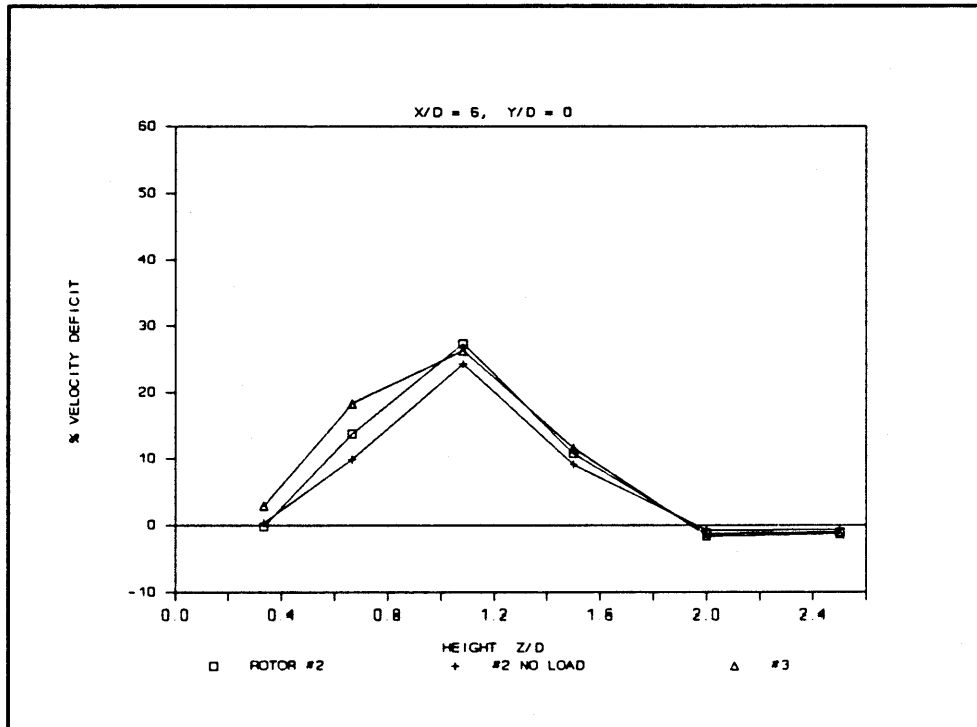


Figure 31 Single Turbine Wakes : Velocity Deficit vs. Height at X/D=6 for Rotors #2, #3

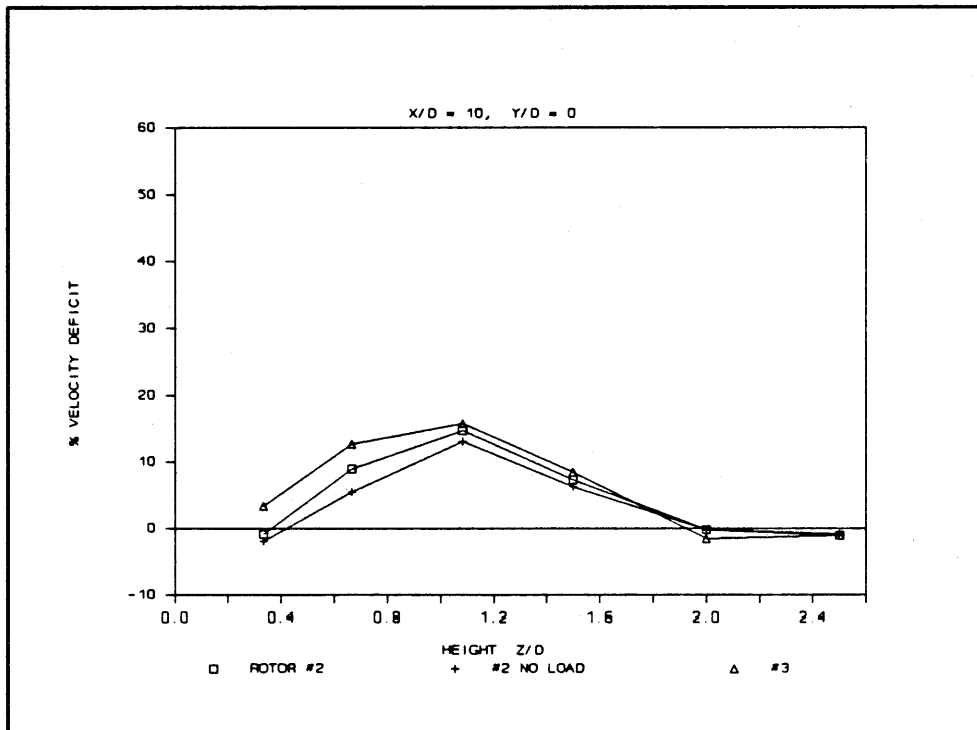


Figure 32 Single Turbine Wakes : Velocity Deficit vs. Height at X/D=10 for Rotors #2, #3

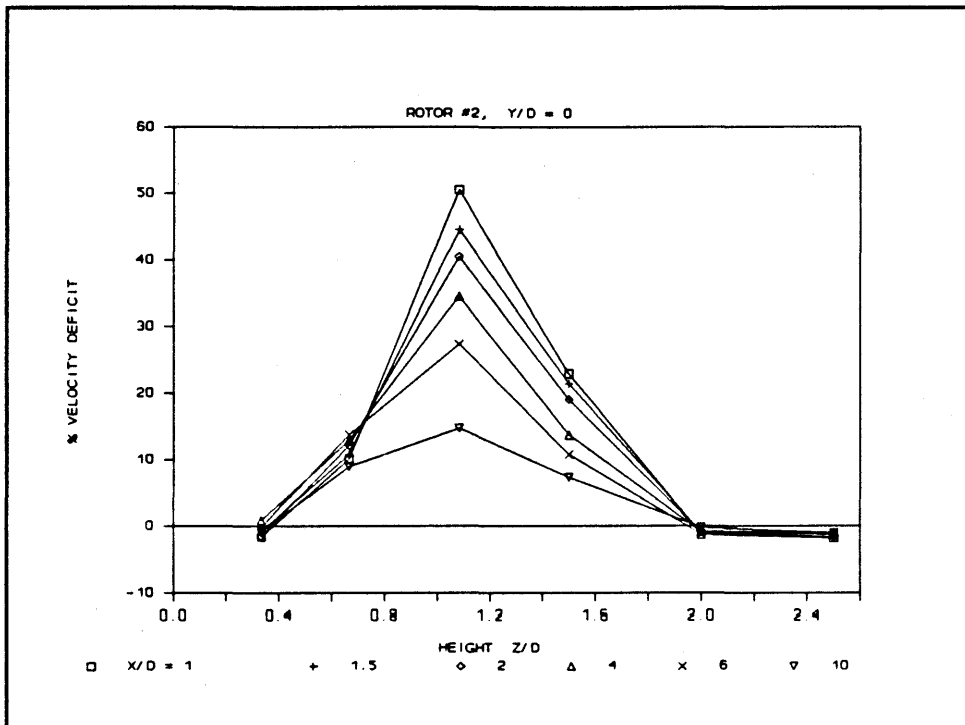


Figure 33 Single Turbine Wakes : Velocity Deficit vs. Height for Rotor # 2

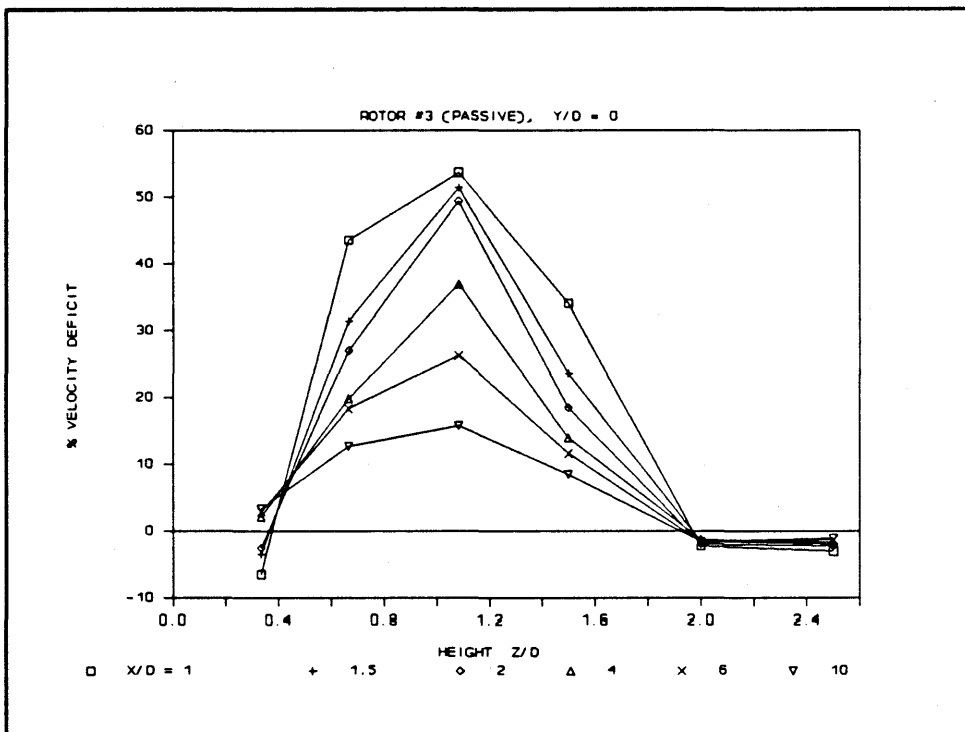


Figure 34 Single Turbine Wakes : Velocity Deficit vs. Height for Rotor # 3 (Passive)

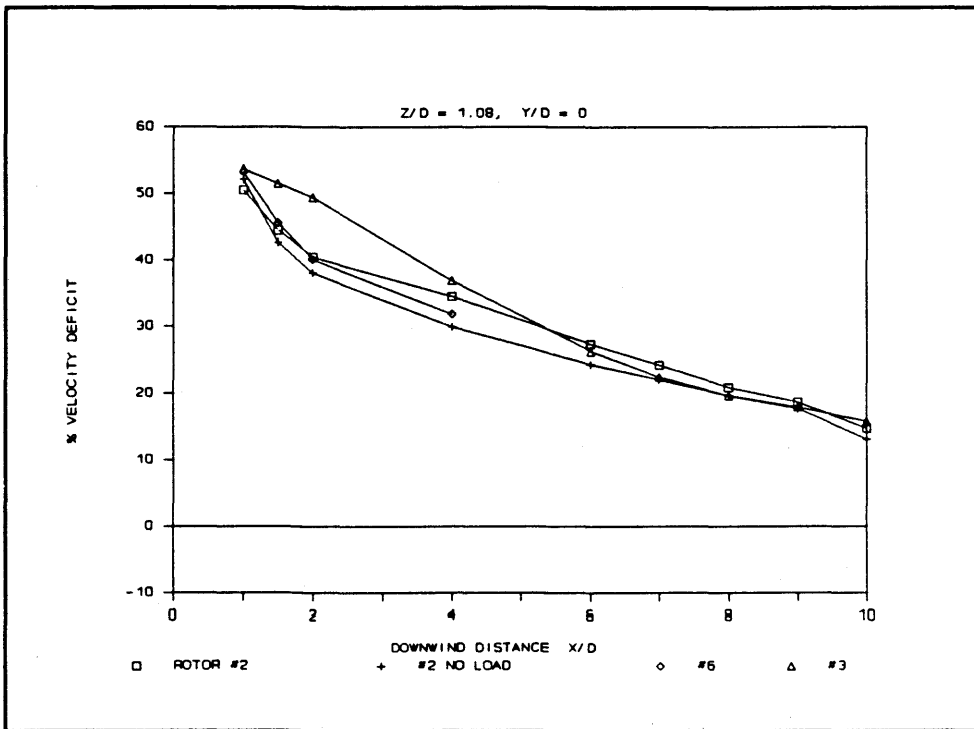


Figure 35 Single Turbine Wakes : Velocity Deficit vs. Downwind Distance for Rotors #2, #3, #6

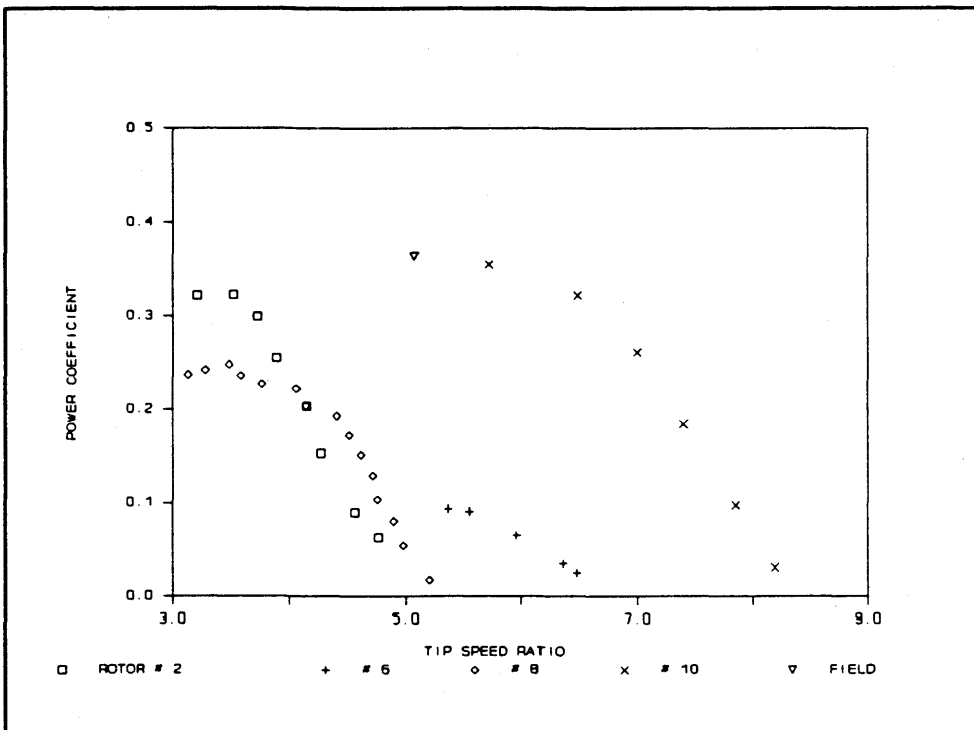


Figure 36 Power Performance Curves for Rotors 2, 6, 8 and 10

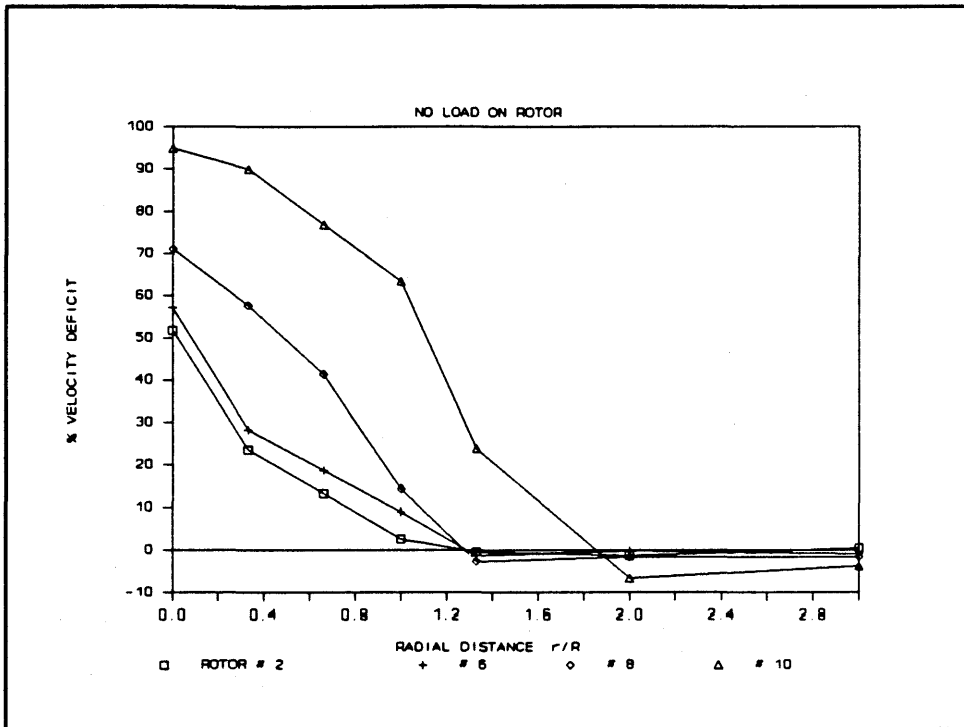


Figure 37 Single Turbine Wakes : Velocity Deficit vs. Radial Distance at $X/D=1$ for Rotors #2, #6, #8, #10 Unloaded

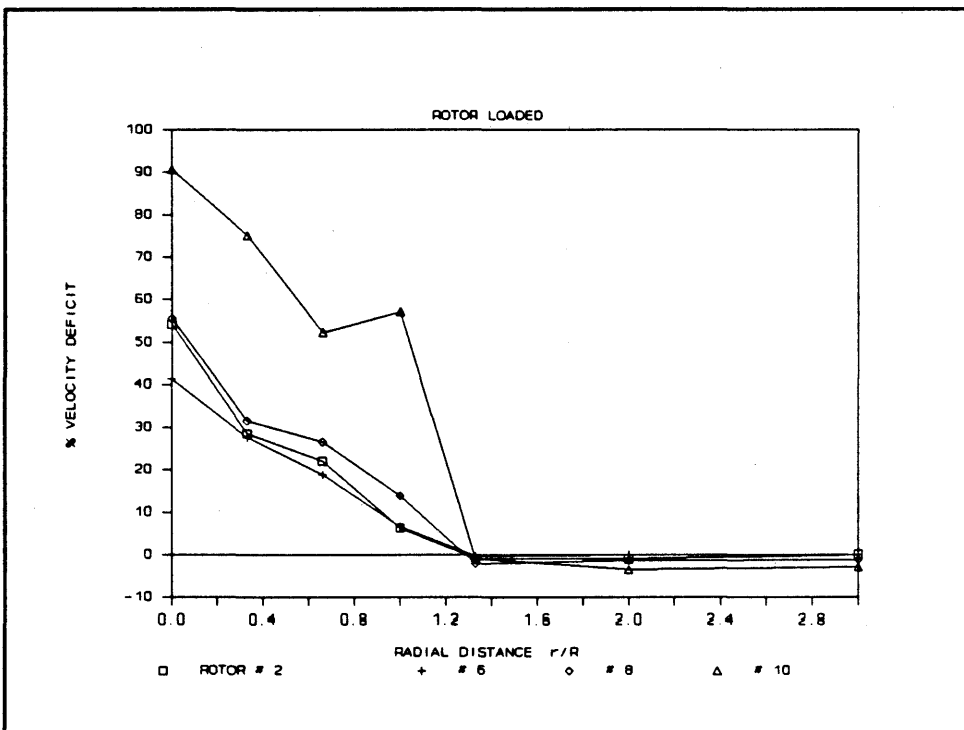


Figure 38 Single Turbine Wakes : Velocity Deficit vs. Radial Distance at $X/D=1$ for Rotors #2, #6, #8, #10 Loaded

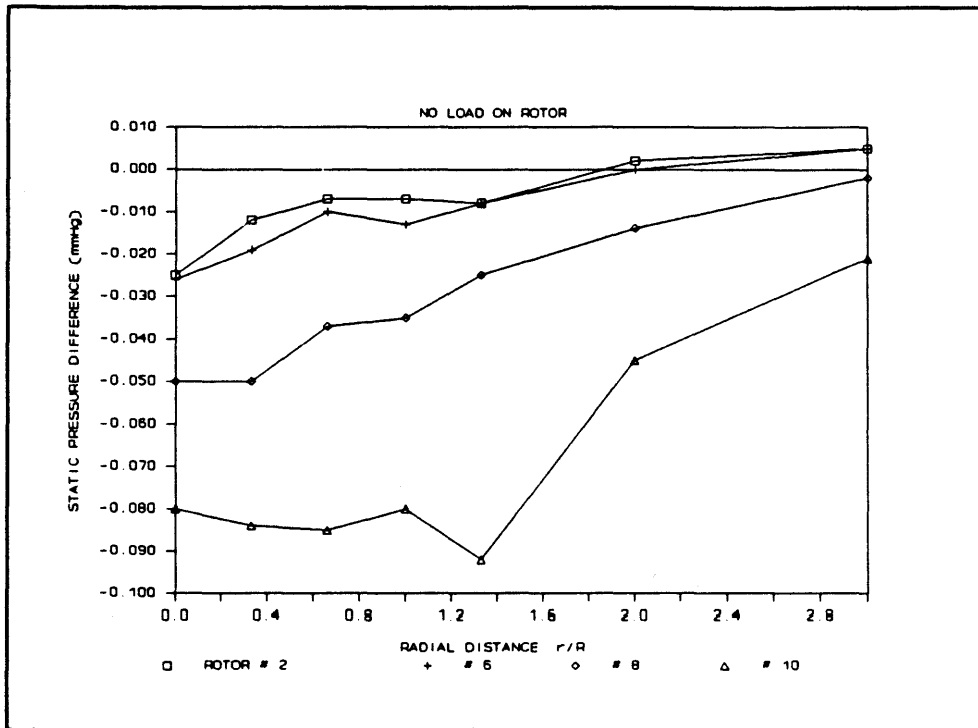


Figure 39 Single Turbine Wakes : Static Pressure vs. Radial Distance at $X/D=1$ for Rotors #2, #6, #8, #10 Unloaded

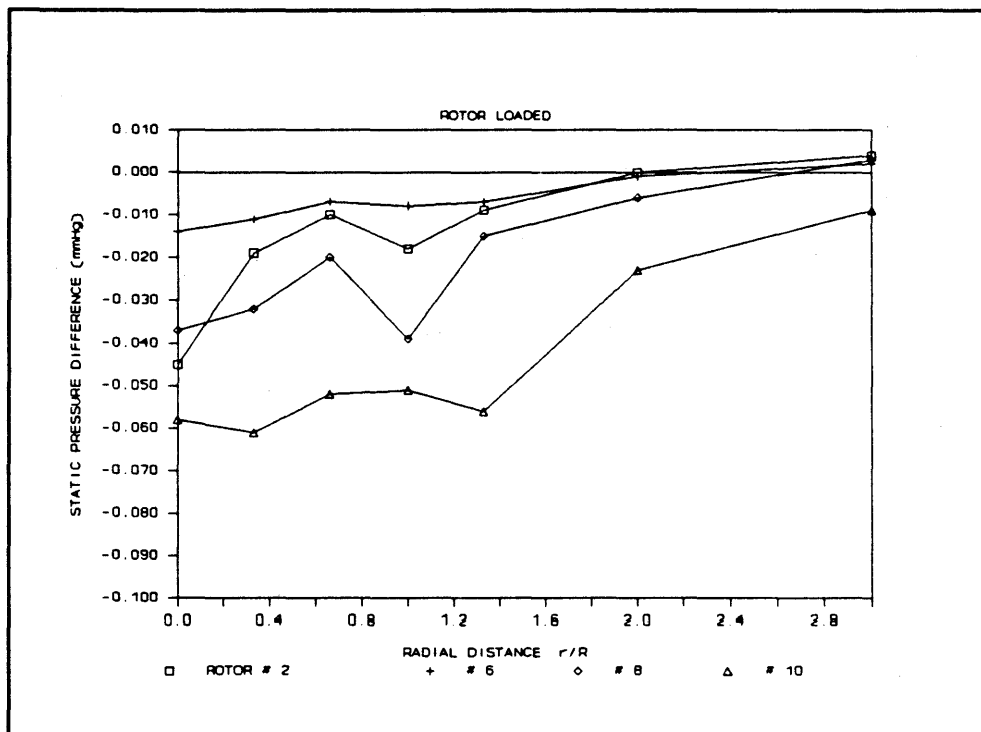


Figure 40 Single Turbine Wakes : Static Pressure vs. Radial Distance at $X/D=1$ for Rotors #2, #6, #8, #10 Loaded

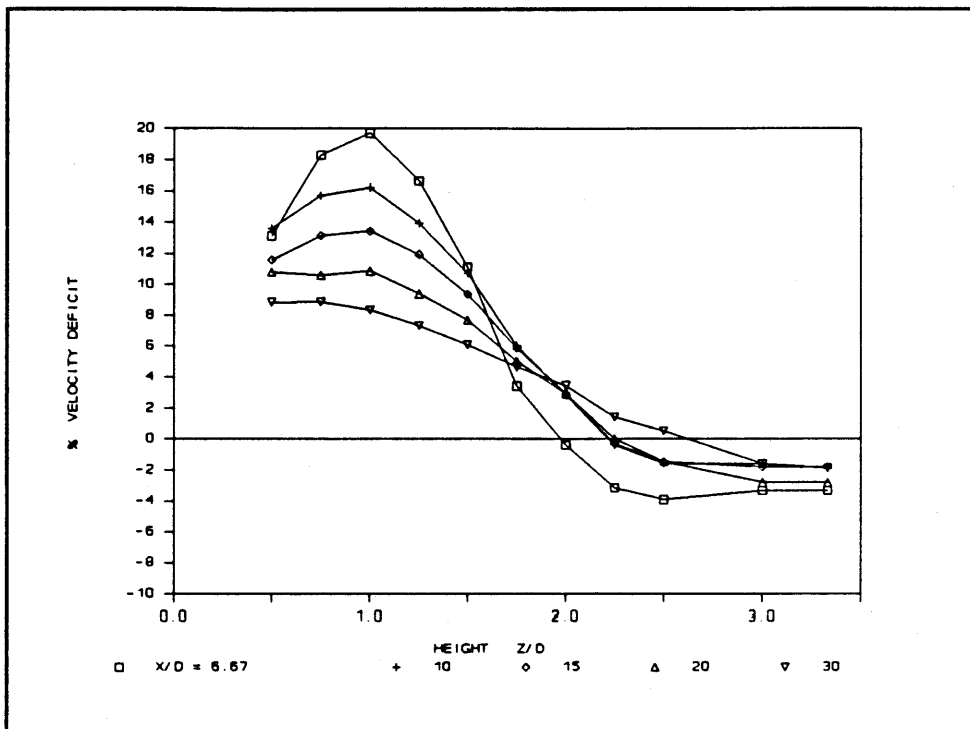


Figure 41 Multiple Turbine Wakes: Velocity Deficit vs. Height at Different Downwind Distances for Run 2 (Y/D=0)

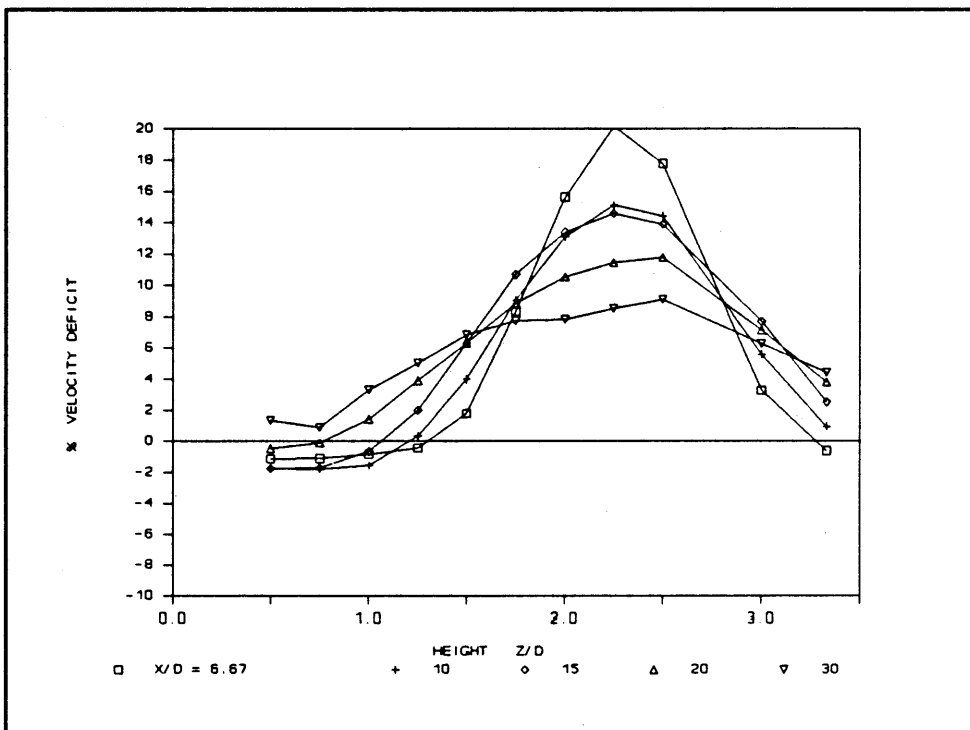


Figure 42 Multiple Turbine Wakes: Velocity Deficit vs. Height at Different Downwind Distances for Run 3 (Y/D=0)

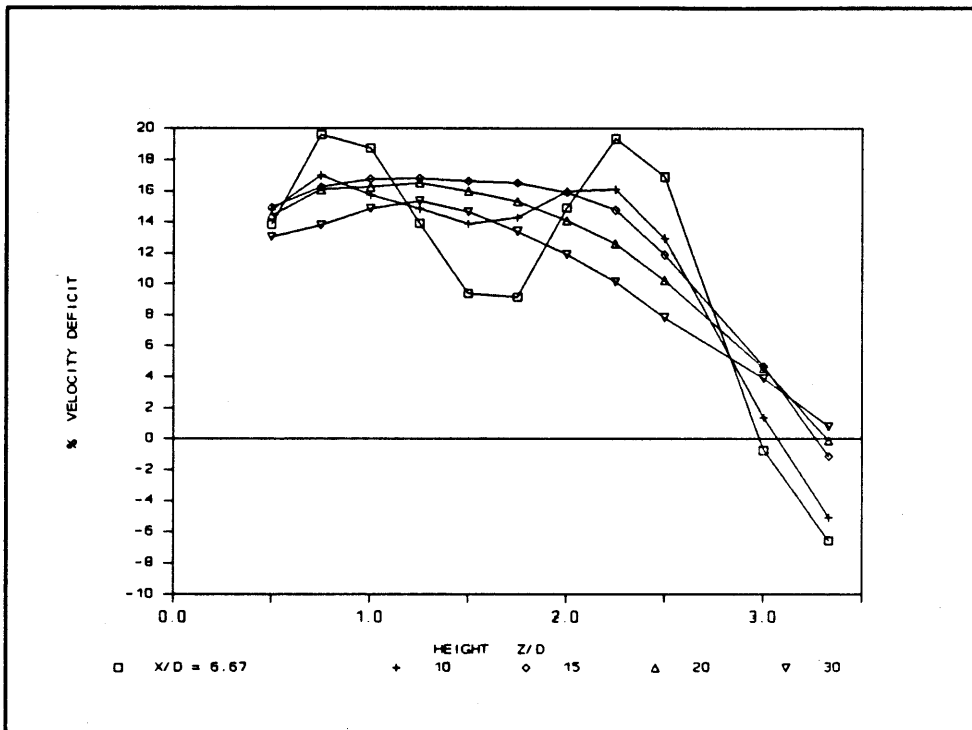


Figure 43 Multiple Turbine Wakes: Velocity Deficit vs. Height at Different Downwind Distances for Run 4 ($Y/D=0$)

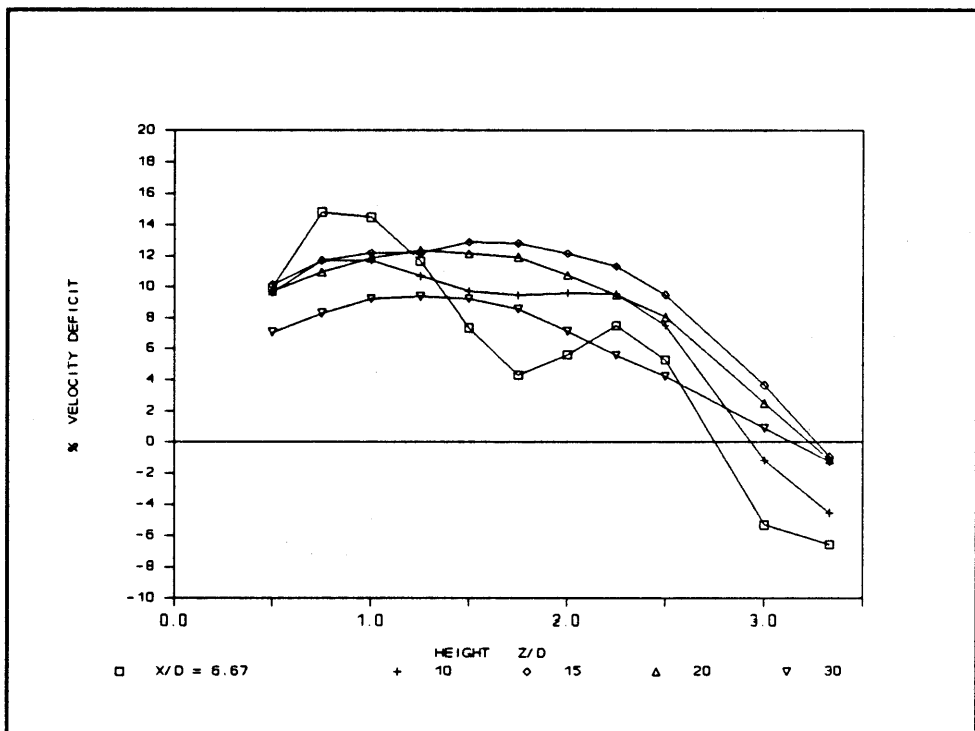


Figure 44 Multiple Turbine Wakes: Velocity Deficit vs. Height at Different Downwind Distances for Run 5 ($Y/D=0$)

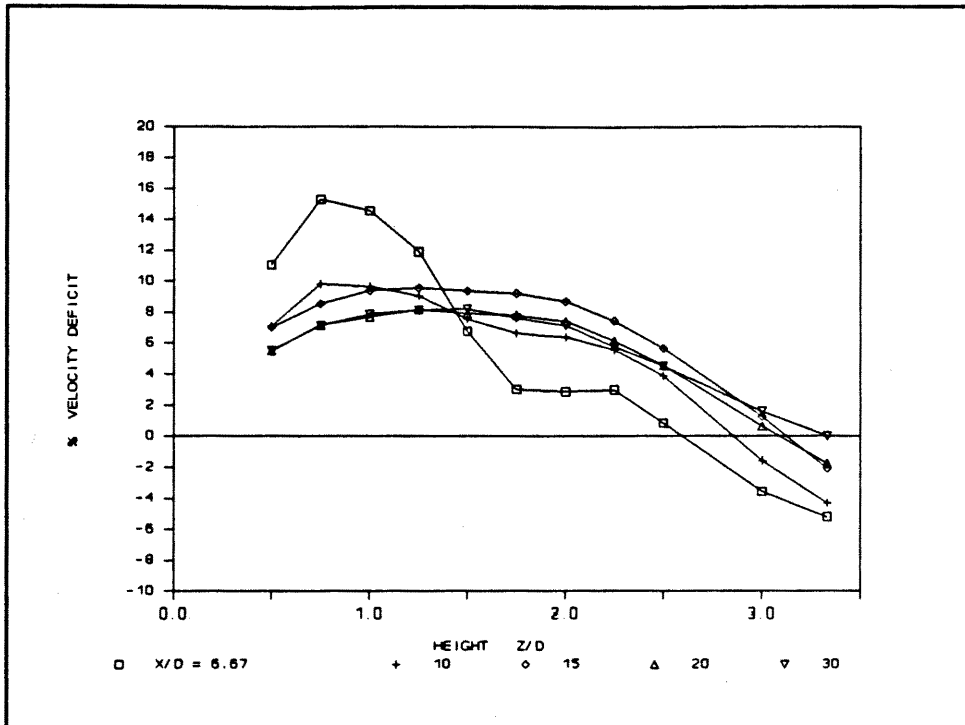


Figure 45 Multiple Turbine Wakes: Velocity Deficit vs. Height at Different Downwind Distances for Run 6 (Y/D=0)

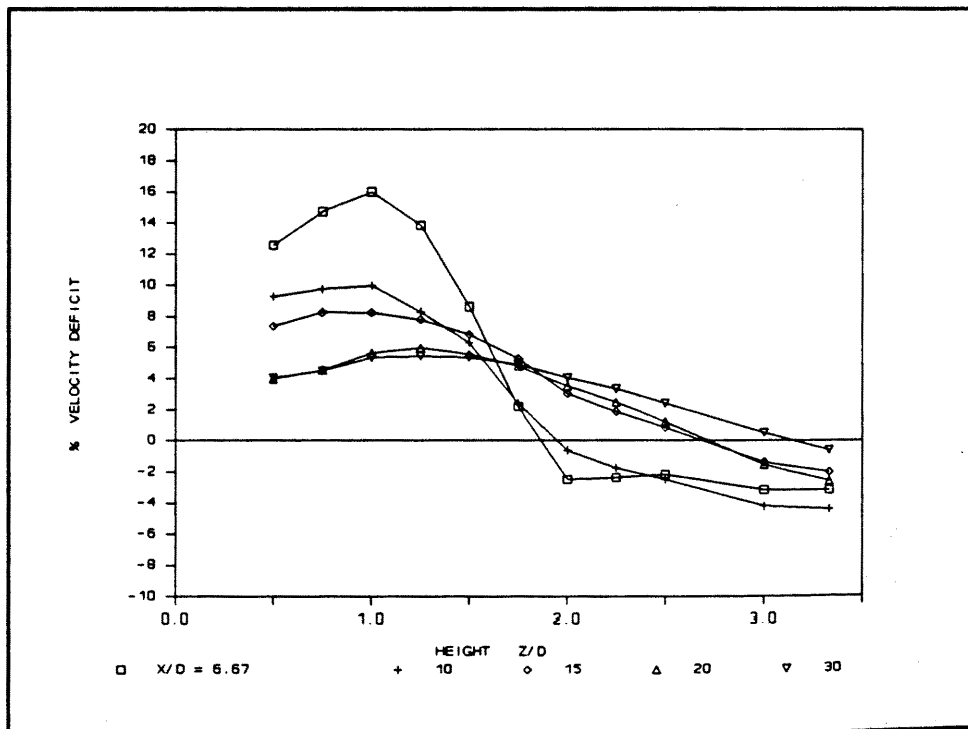


Figure 46 Multiple Turbine Wakes: Velocity Deficit vs. Height at Different Downwind Distances for Run 7 (Y/D=0)

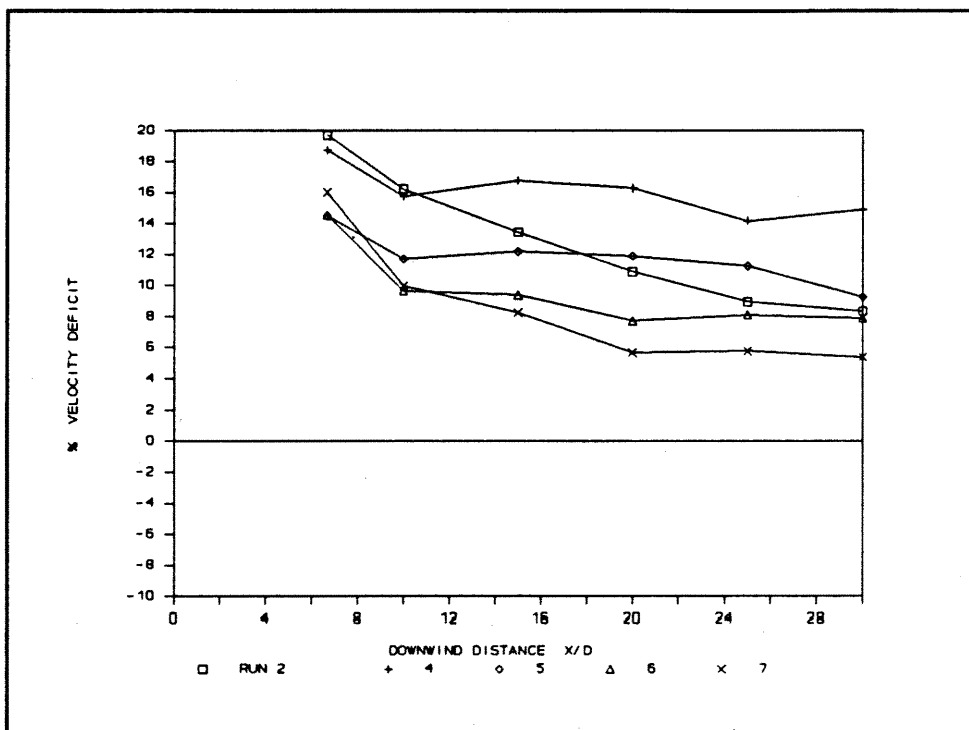


Figure 47 Multiple Turbine Wakes: Velocity Deficit vs. Downwind Distance for Runs 2,4,5,6,7 at Height Z/D = 1 (Y/D=0)

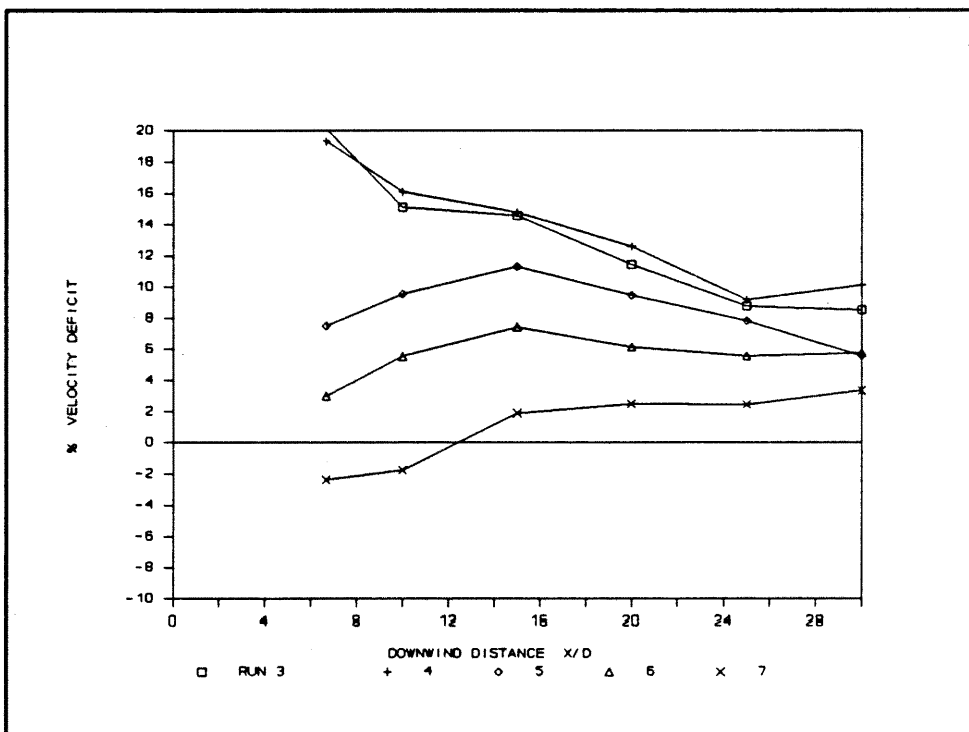


Figure 48 Multiple Turbine Wakes: Velocity Deficit vs. Downwind Distance for Runs 3,4,5,6,7 at Height Z/D = 2.25 (Y/D=0)

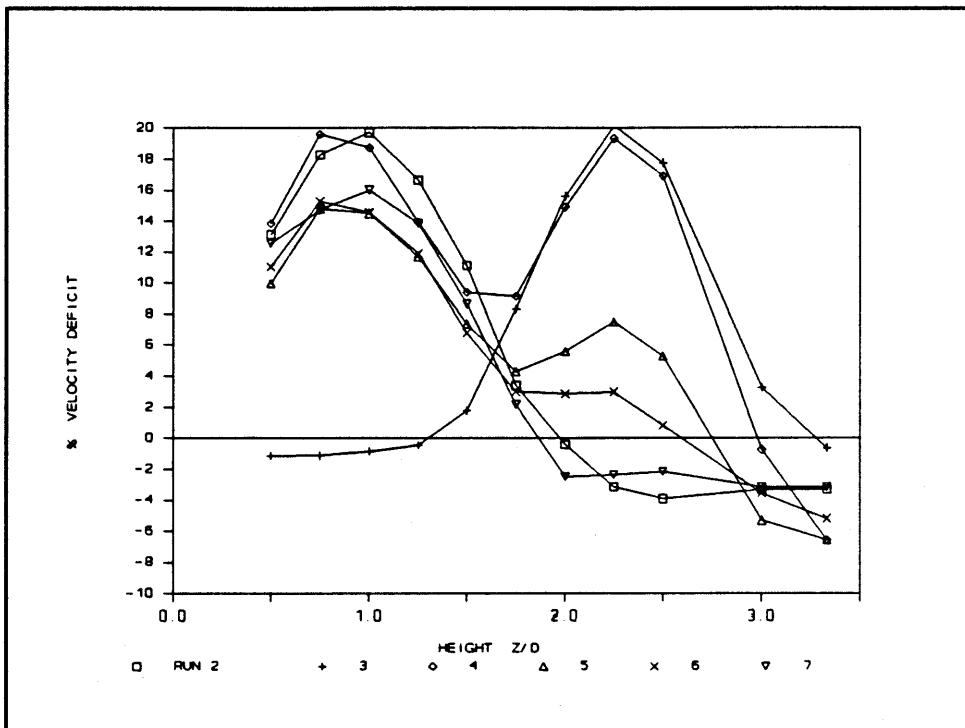


Figure 49 Multiple Turbine Wakes: Velocity Deficit vs. Height for all Runs at Downwind Distance $X/D = 6.67$ ($Y/D=0$)

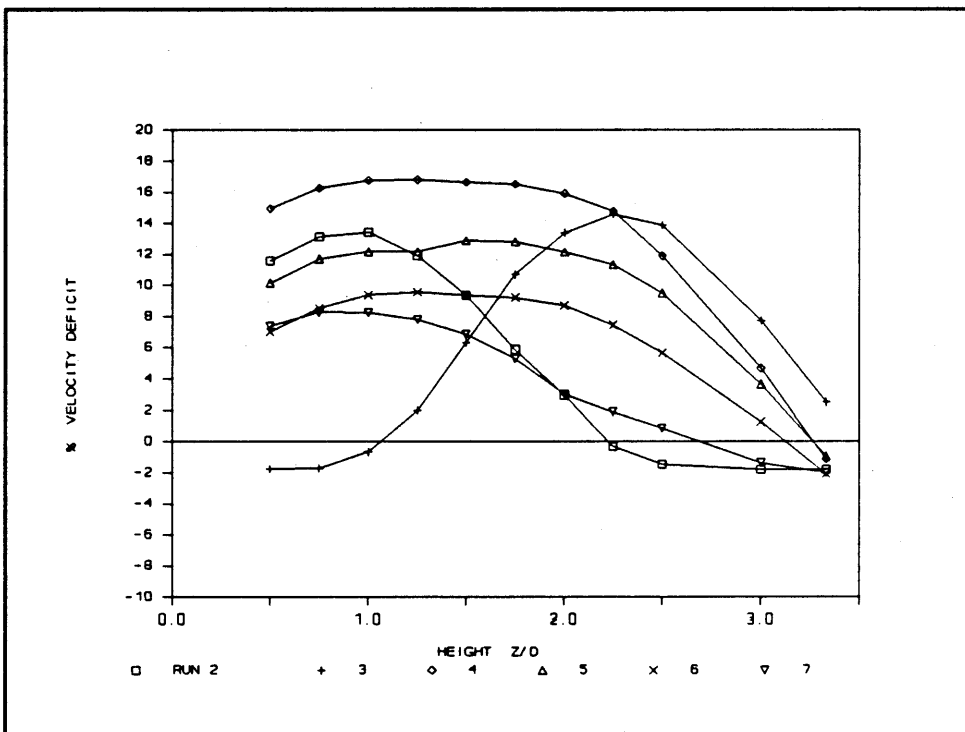


Figure 50 Multiple Turbine Wakes: Velocity Deficit vs. Height for all Runs at Downwind Distance $X/D = 15$ ($Y/D=0$)

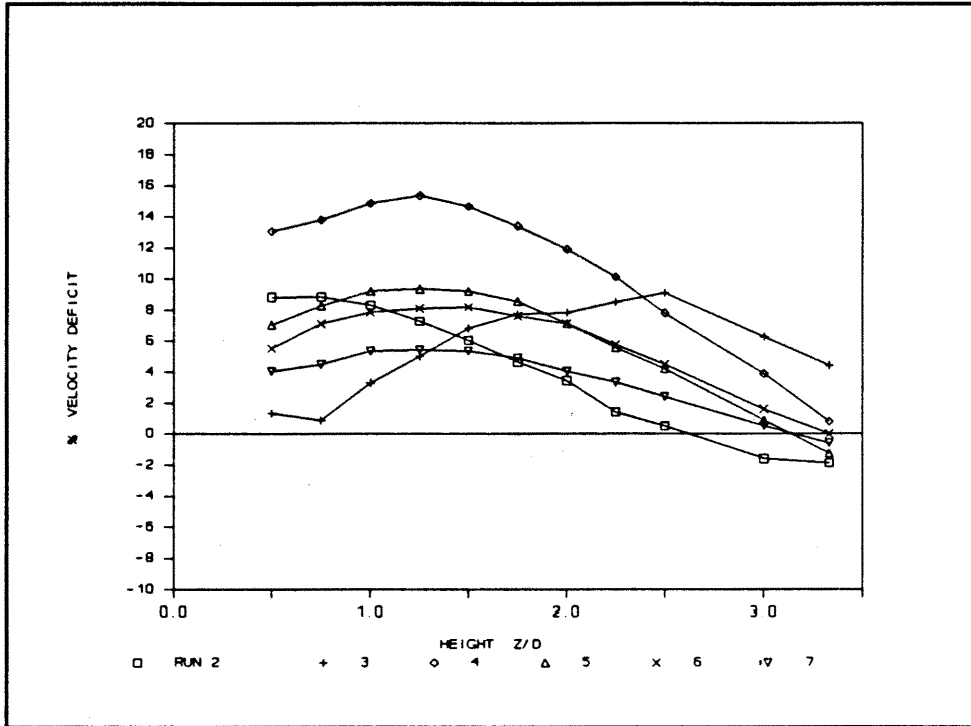


Figure 51 Multiple Turbine Wakes: Velocity Deficit vs. Height for all Runs at Downwind Distance $X/D = 30$ ($Y/D=0$)

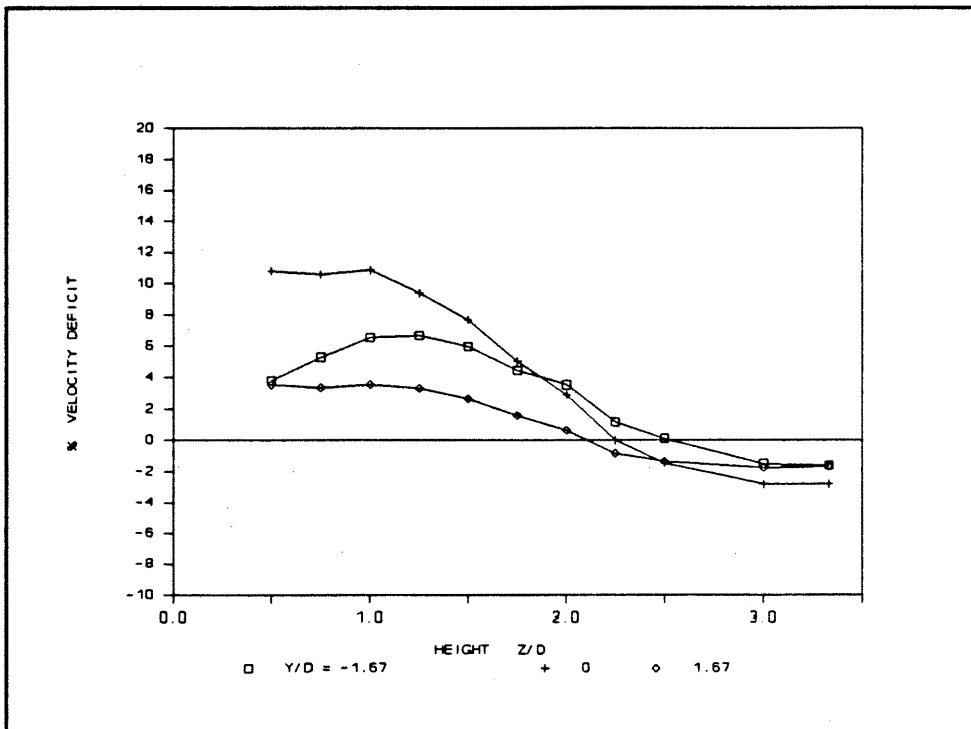


Figure 52 Multiple Turbine Wakes: Velocity Deficit vs. Height at Different Lateral Positions for Run 2 ($X/D=20$)

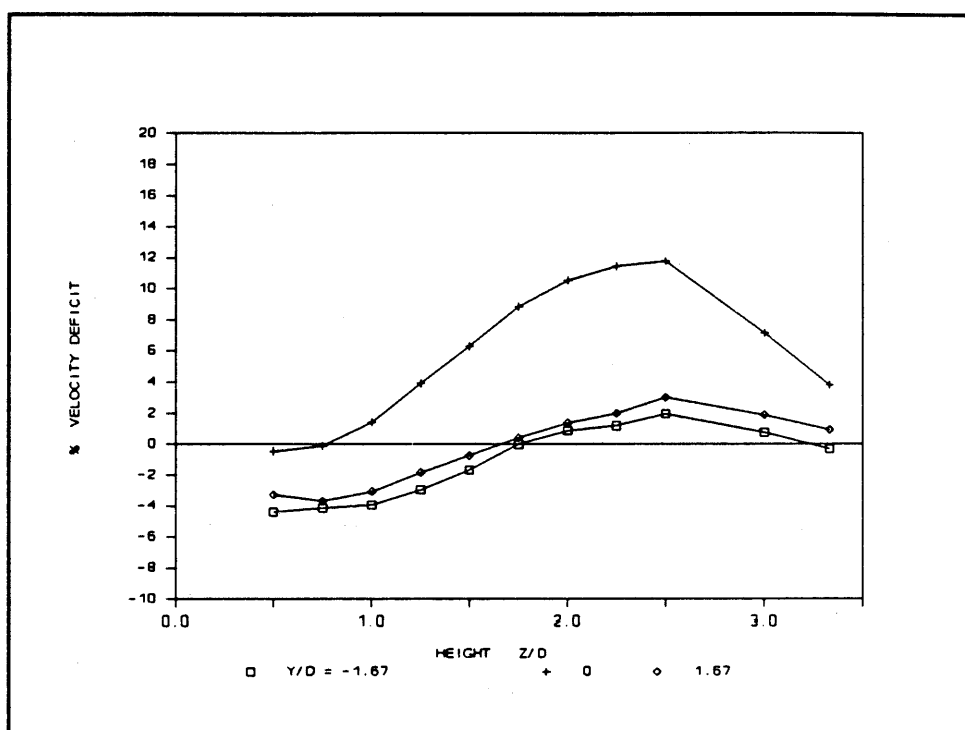


Figure 53 Multiple Turbine Wakes: Velocity Deficit vs. Height at Different Lateral Positions for Run 3 (X/D=20)

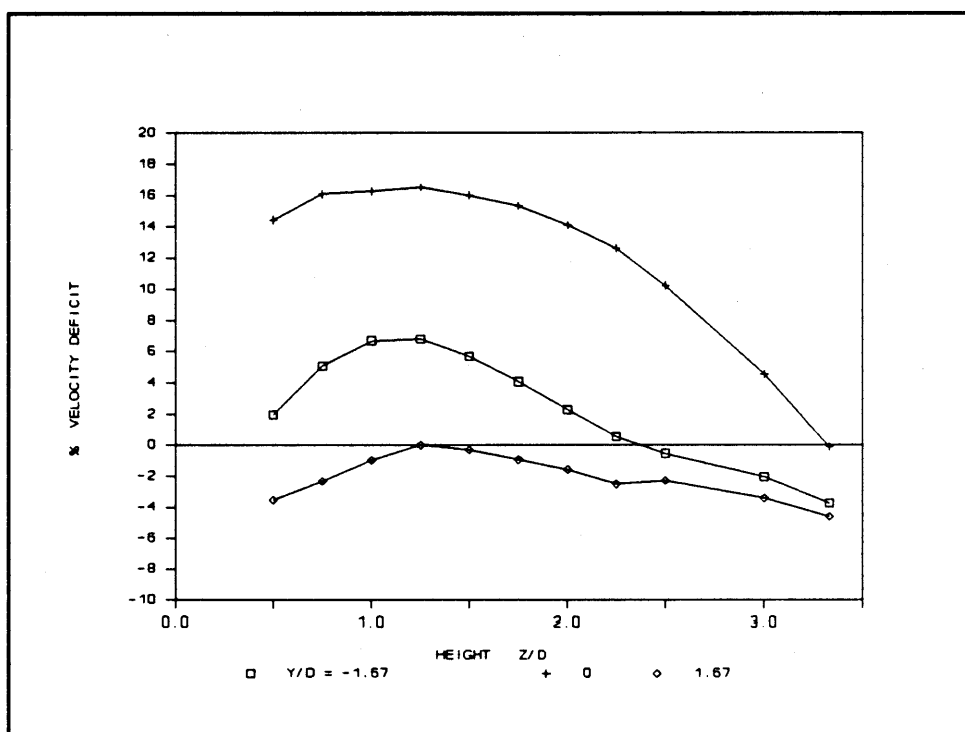


Figure 54 Multiple Turbine Wakes: Velocity Deficit vs. Height at Different Lateral Positions for Run 4 (X/D=20)

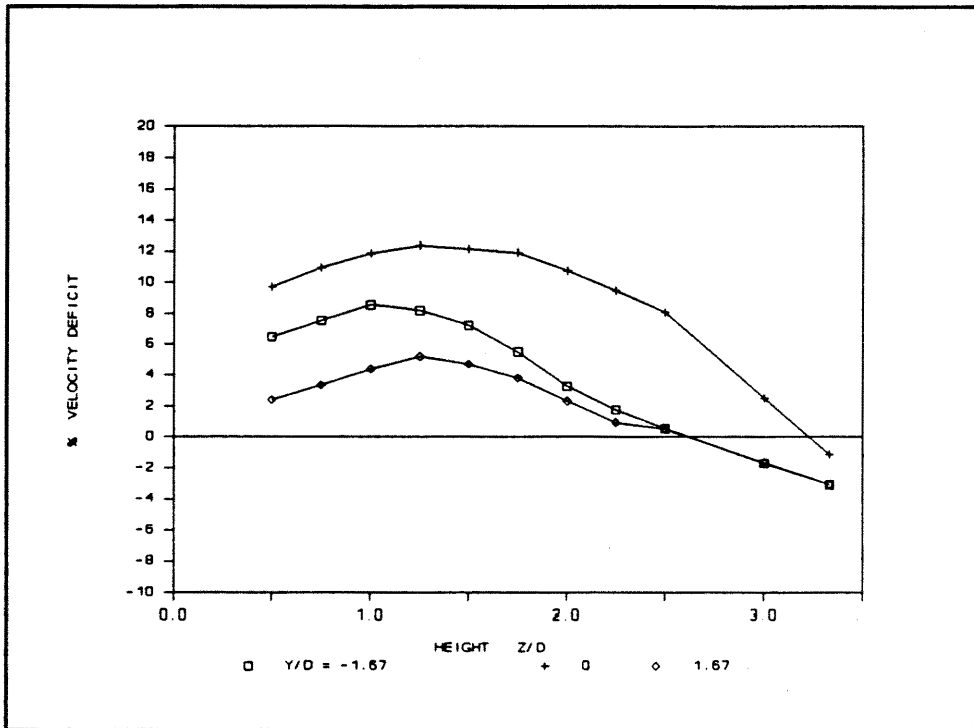


Figure 55 Multiple Turbine Wakes: Velocity Deficit vs. Height at Different Lateral Positions for Run 5 ($X/D=20$)

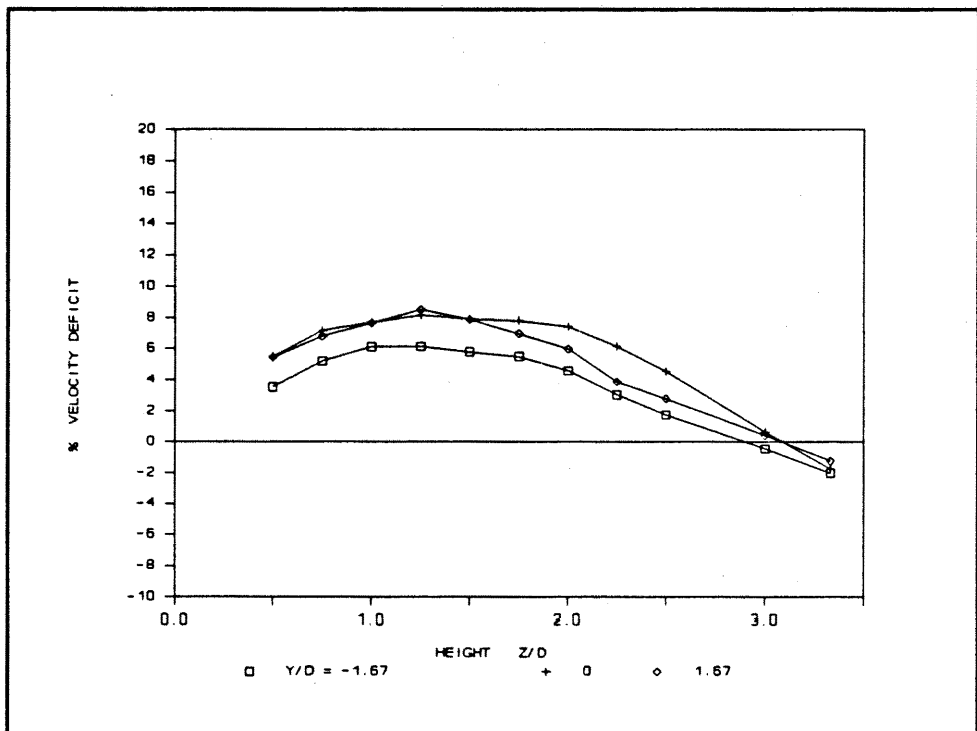


Figure 56 Multiple Turbine Wakes: Velocity Deficit vs. Height at Different Lateral Positions for Run 6 ($X/D=20$)

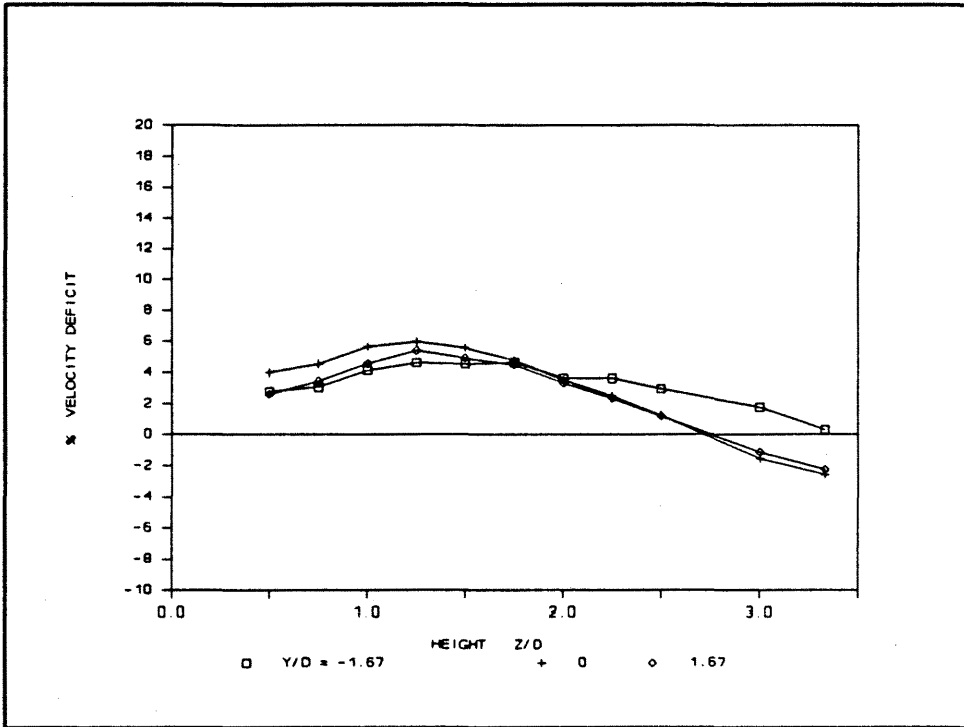


Figure 57 Multiple Turbine Wakes: Velocity Deficit vs. Height at Different Lateral Positions for Run 7 ($X/D=20$)

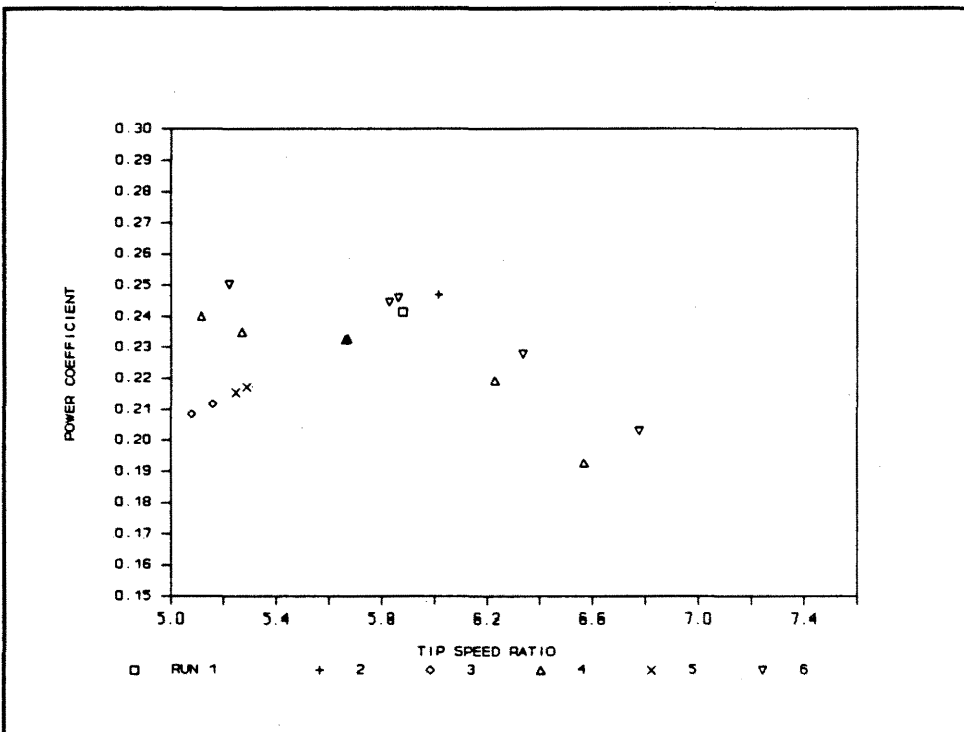


Figure 58 Multiple Turbine Power Interaction : Power Coefficient vs. Tip Speed Ratio for Run Numbers 1, 2, 3, 4, 5, 6

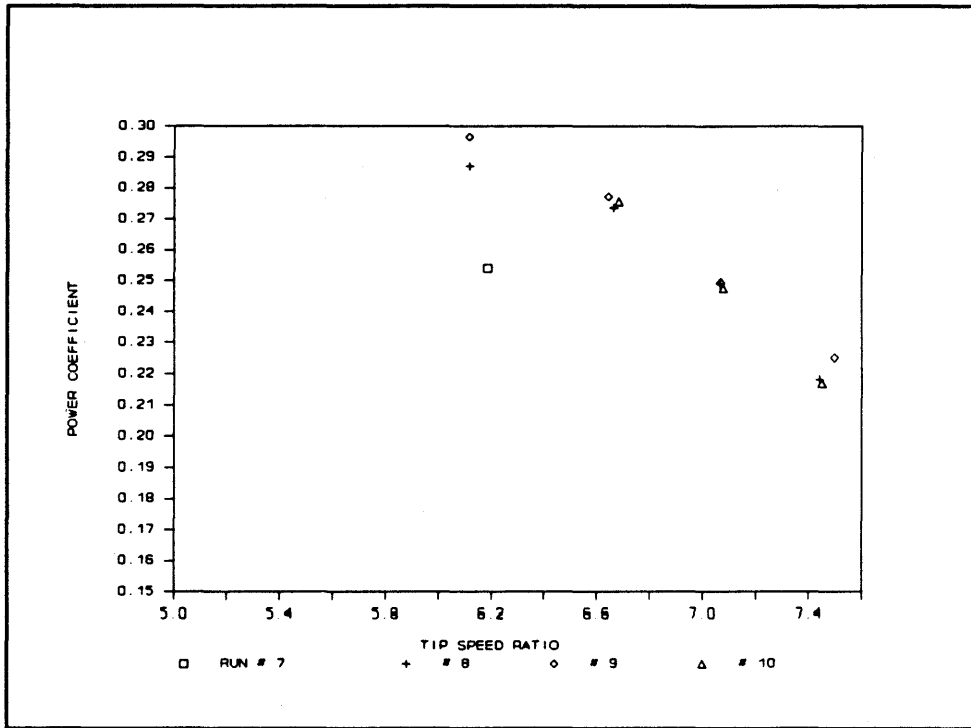


Figure 59 Multiple Turbine Power Interaction : Power Coefficient vs. Tip Speed Ratio for Run Numbers 7, 8, 9, 10

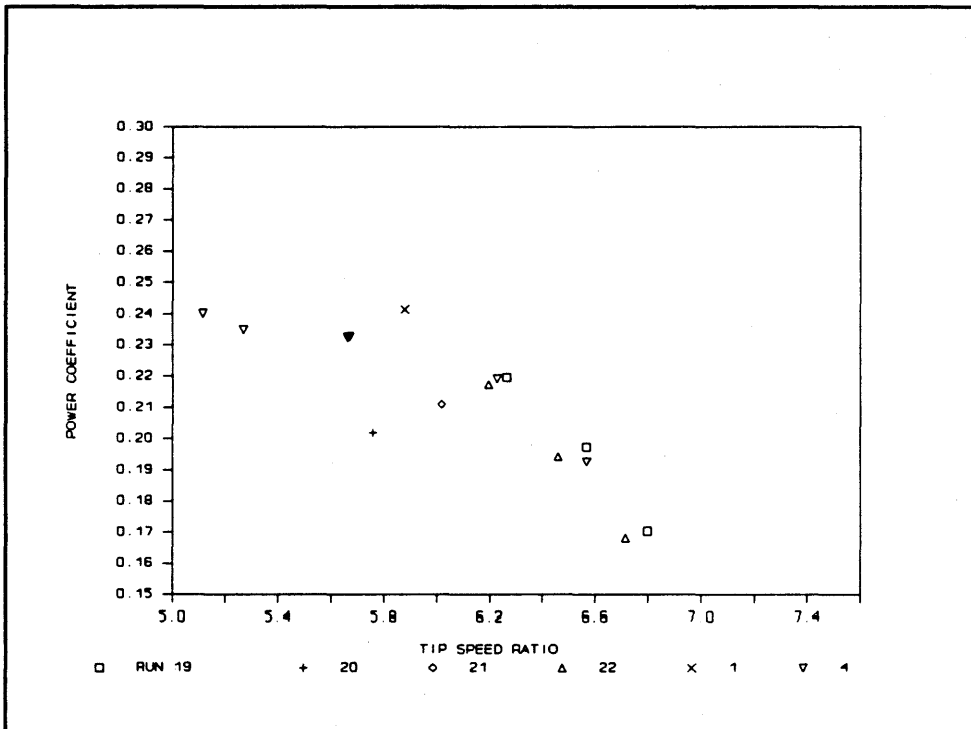


Figure 60 Multiple Turbine Power Interaction : Power Coefficient vs. Tip Speed Ratio for Run Numbers 19, 20, 21, 22, 1, 4

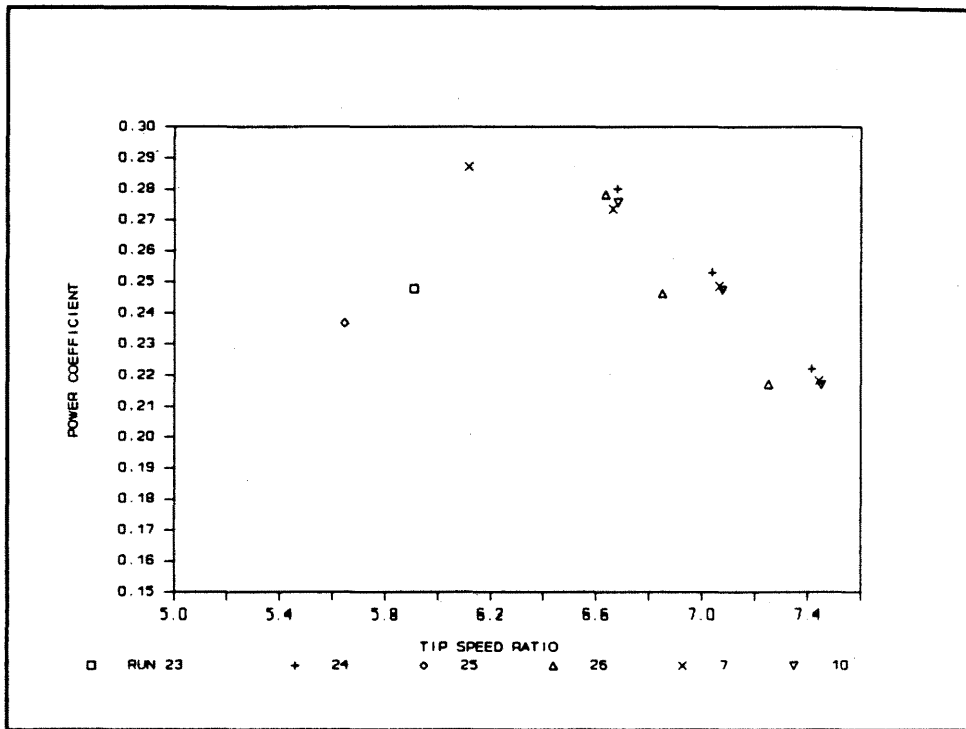


Figure 61 Multiple Turbine Power Interaction : Power Coefficient vs. Tip Speed Ratio for Run Numbers 23, 24, 25, 26, 7, 10

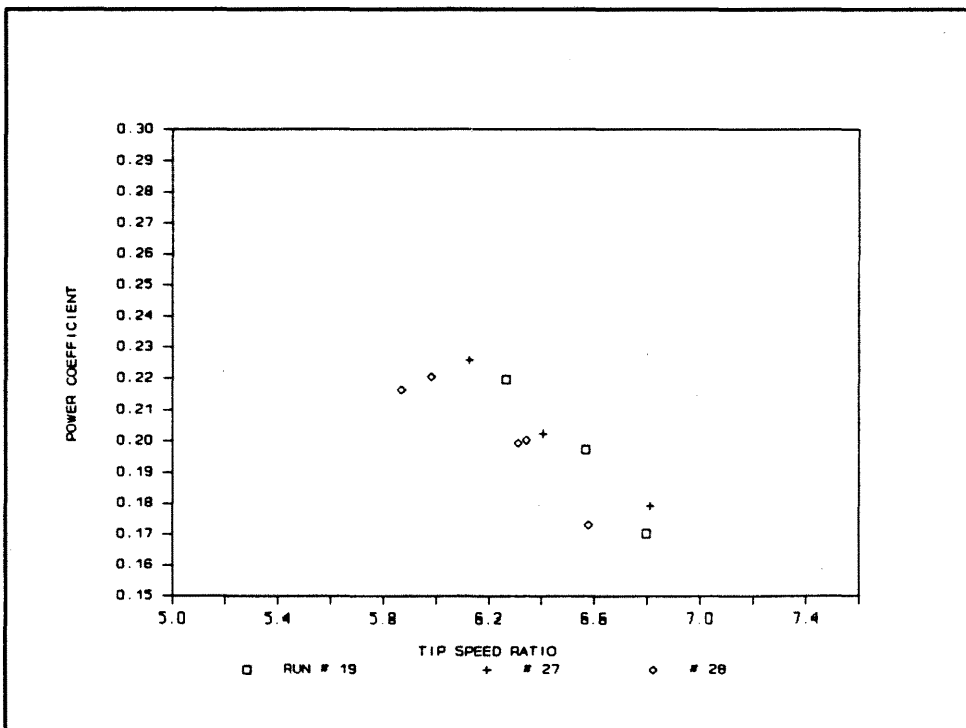


Figure 62 Multiple Turbine Power Interaction : Power Coefficient vs. Tip Speed Ratio for Run Numbers 19, 27, 28

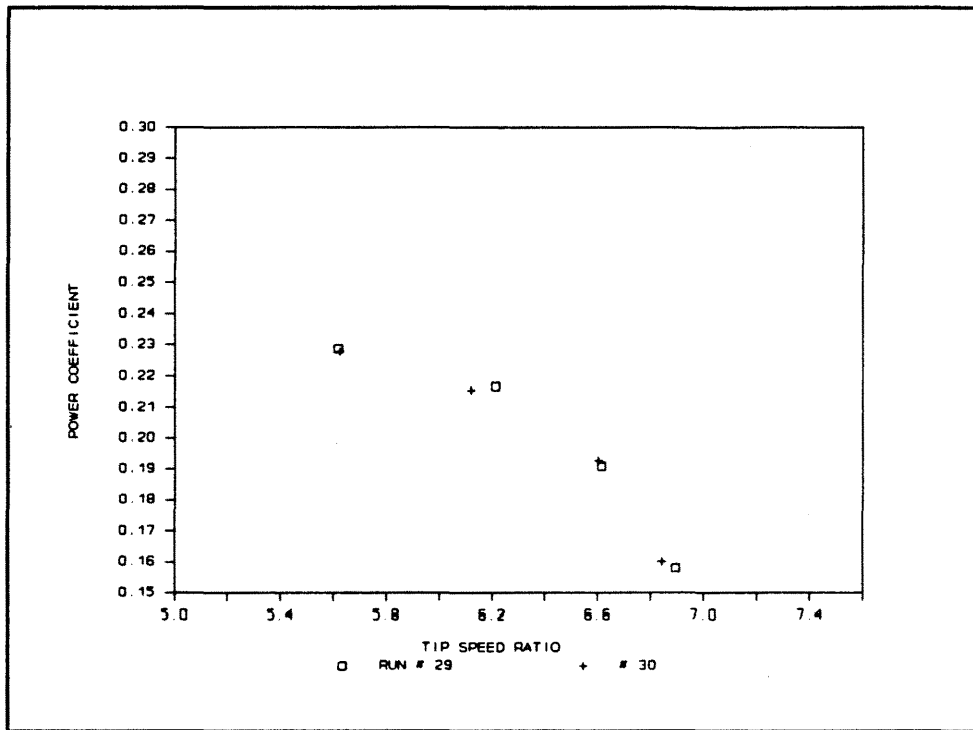


Figure 63 Multiple Turbine Power Interaction : Power Coefficient vs. Tip Speed Ratio for Run Numbers 29, 30

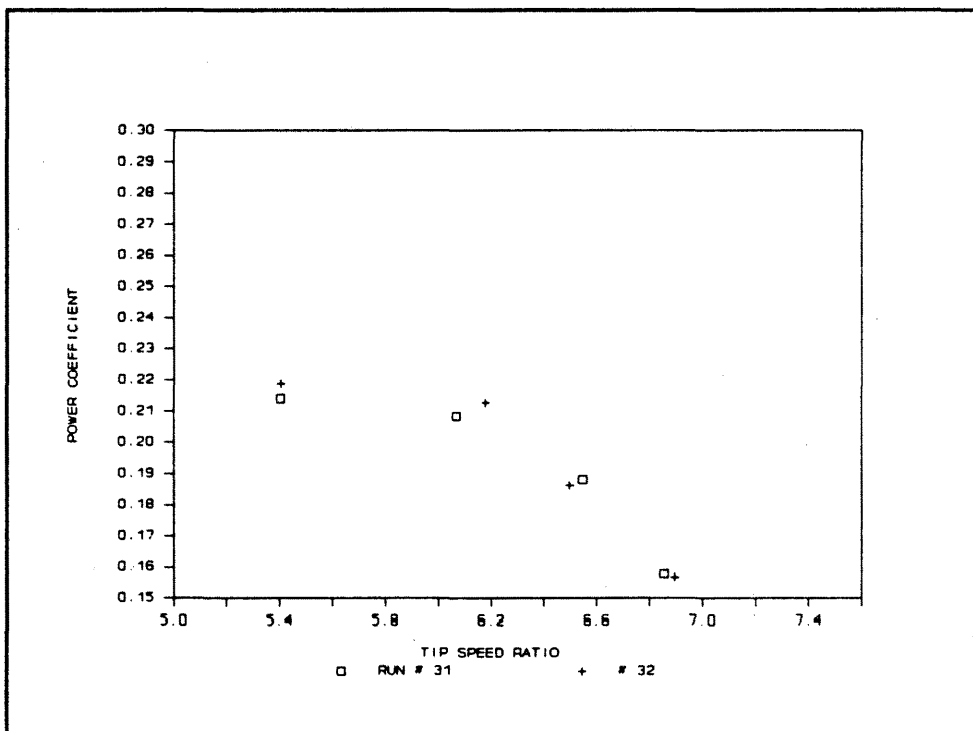


Figure 64 Multiple Turbine Power Interaction: Power Coefficient vs. Tip Speed Ratio for Run Numbers 31, 32

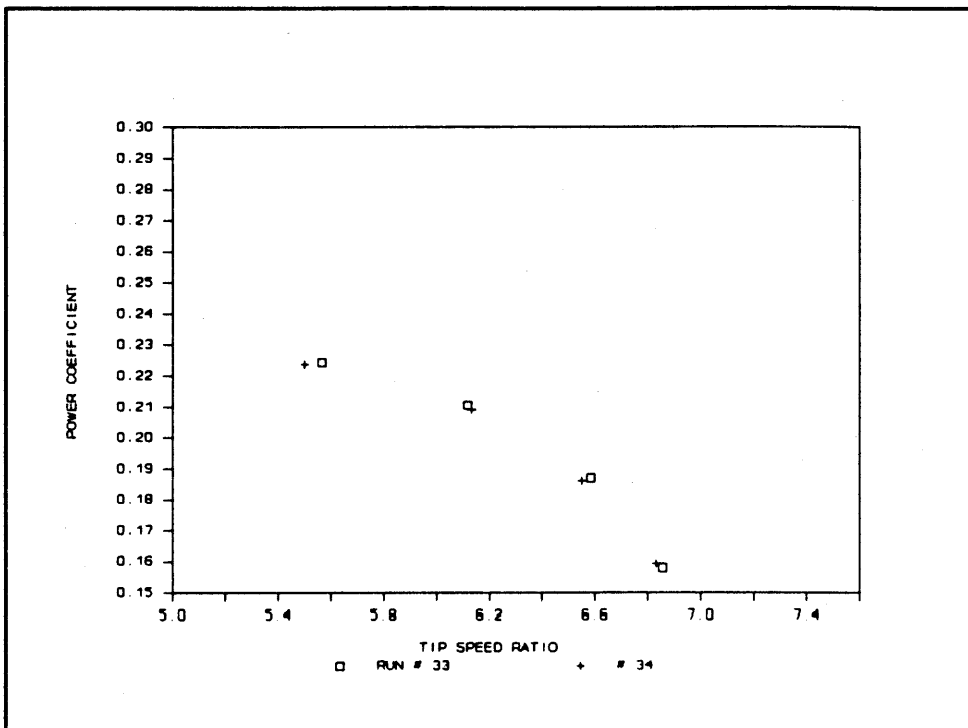


Figure 65 Multiple Turbine Power Interaction: Power Coefficient vs. Tip Speed Ratio for Run Numbers 33, 34

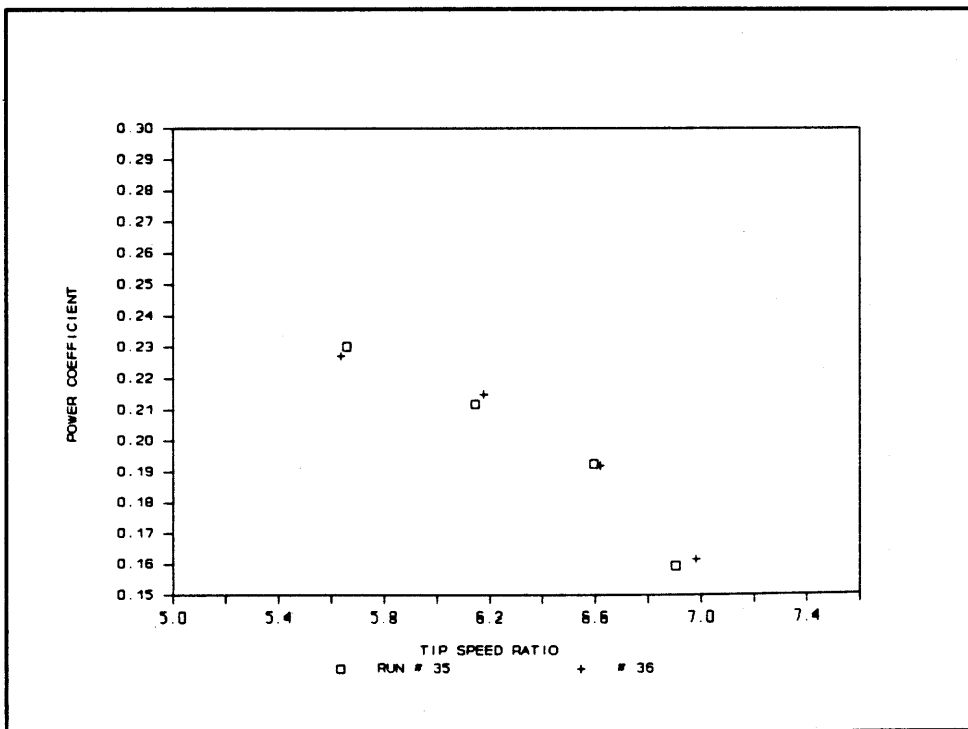


Figure 66 Multiple Turbine Power Interaction: Power Coefficient vs. Tip Speed Ratio for Run Numbers 35, 36

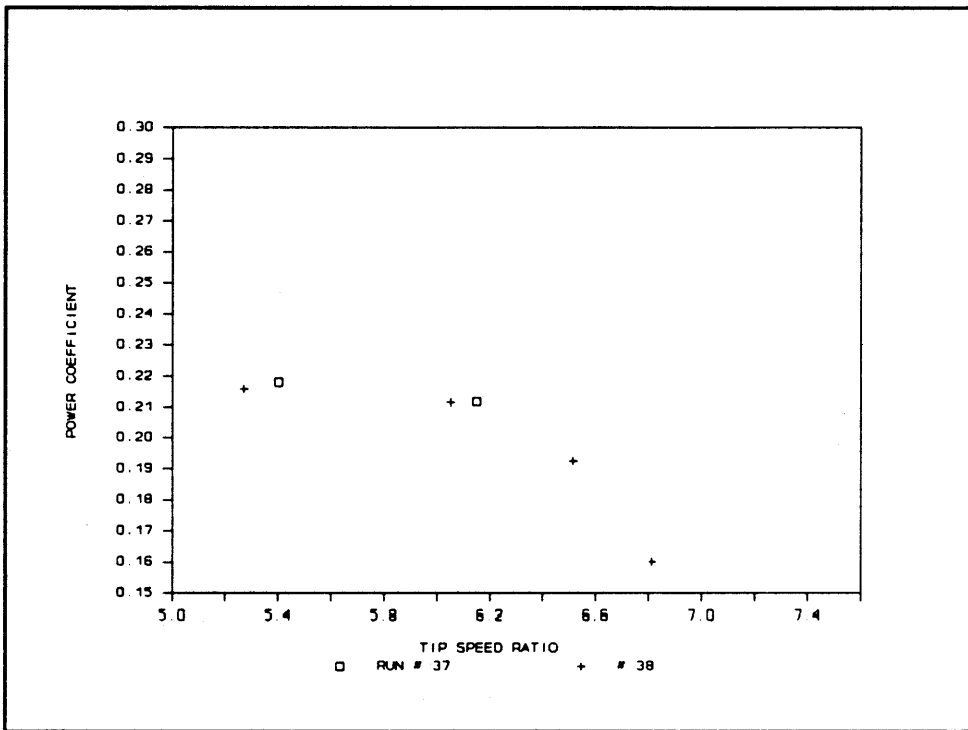


Figure 67 Multiple Turbine Power Interaction: Power Coefficient vs. Tip Speed Ratio for Run Numbers 37, 38

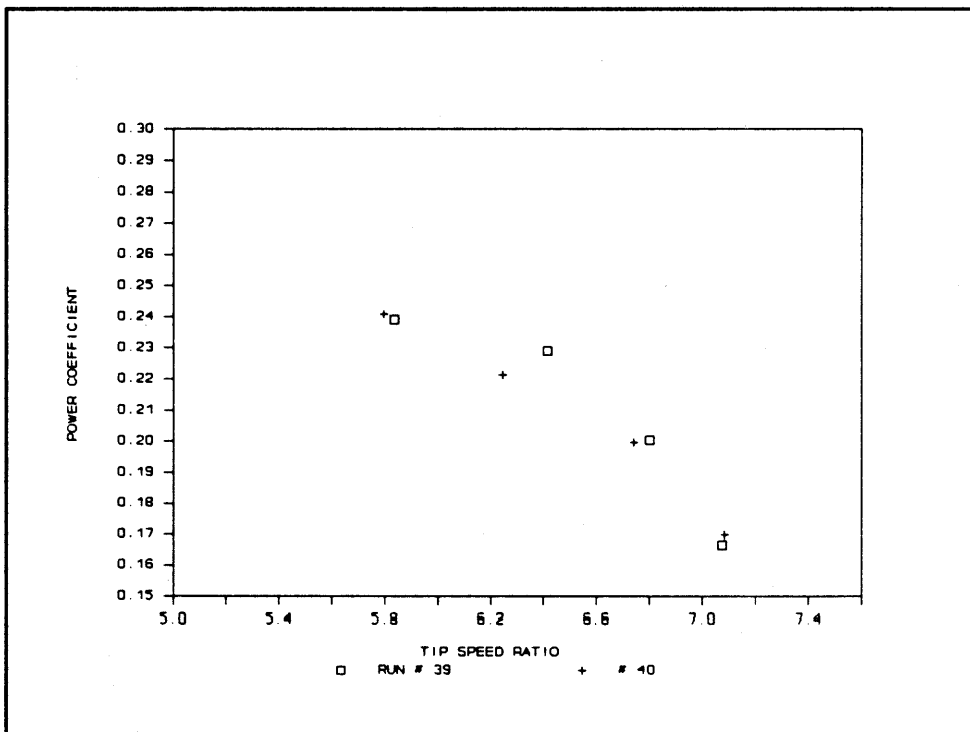


Figure 68 Multiple Turbine Power Interaction: Power Coefficient vs. Tip Speed Ratio for Run Numbers 39, 40

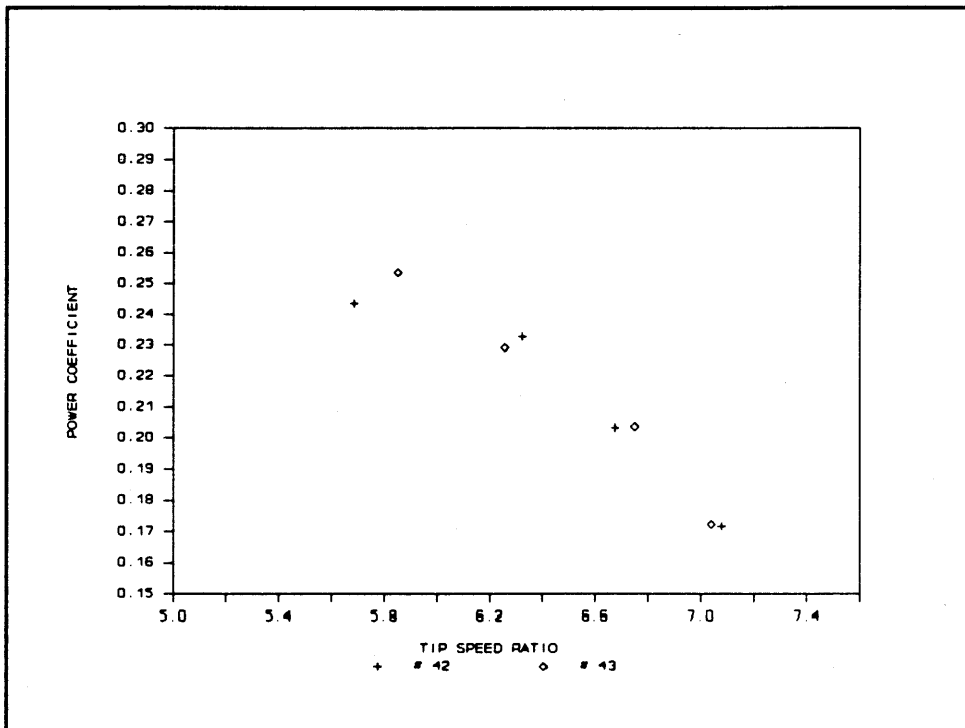


Figure 69 Multiple Turbine Power Interaction: Power Coefficient vs. Tip Speed Ratio for Run Numbers 42, 43

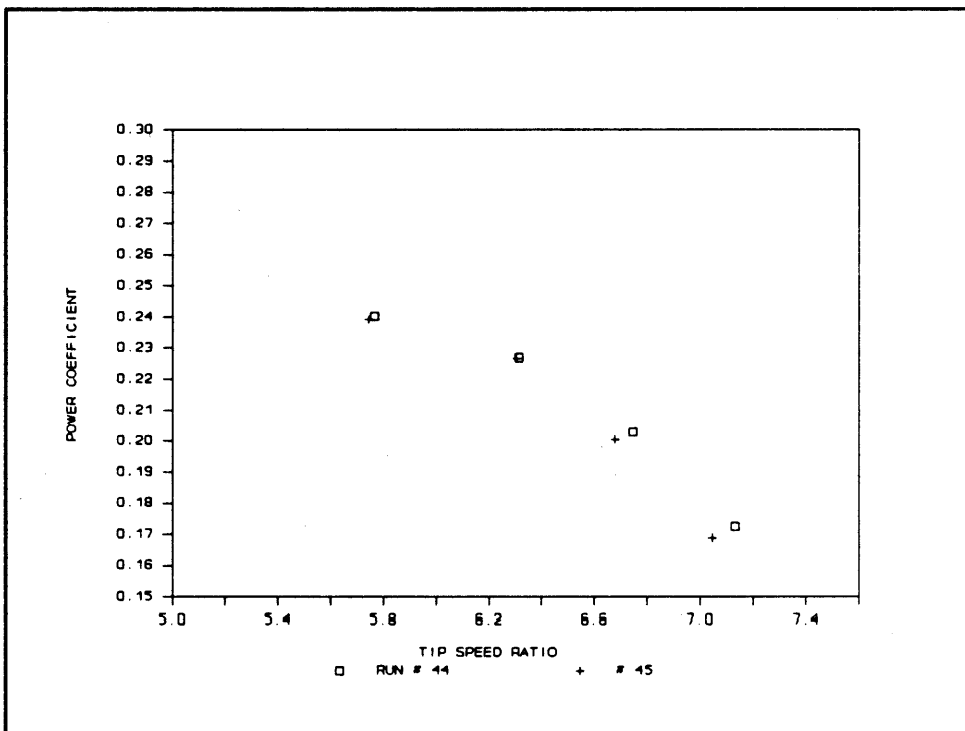


Figure 70 Multiple Turbine Power Interaction: Power Coefficient vs. Tip Speed Ratio for Run Numbers 44, 45

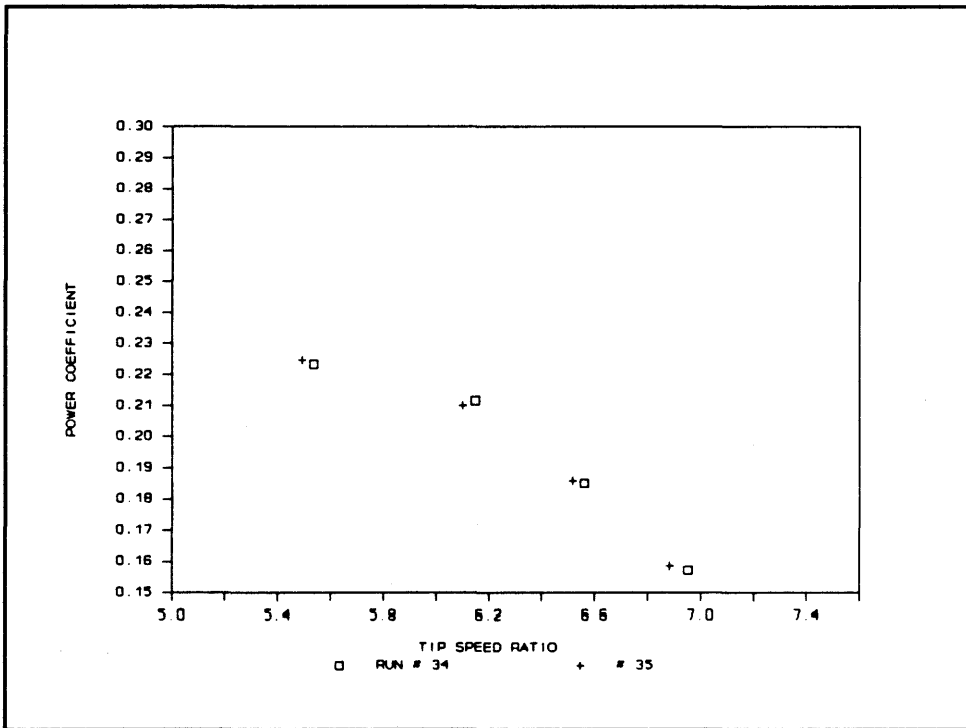


Figure 71 Multiple Turbine Power Interaction : Power Coefficient vs. Tip Speed Ratio for Run Numbers 46, 47

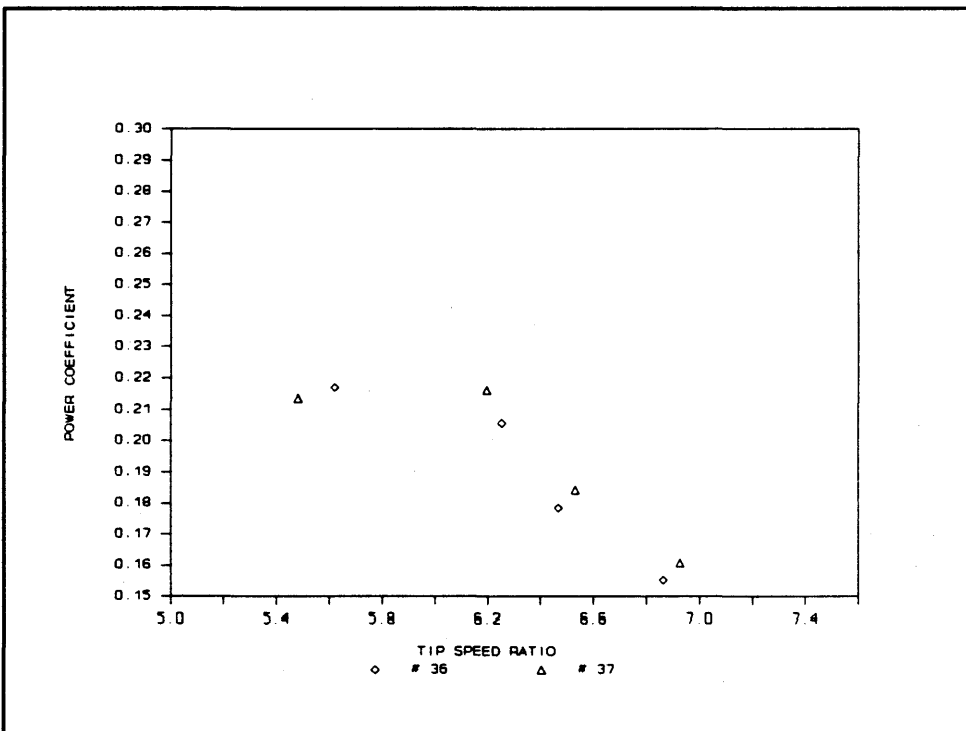


Figure 72 Multiple Turbine Power Interaction : Power Coefficient vs. Tip Speed Ratio for Run Numbers 48, 49